UNIVERSITY OF CALIFORNIA SAN DIEGO

Protein synthesis and transport dynamics in injury and disease

A dissertation submitted in partial satisfaction
of the requirements for the Doctor of Philosophy

in

Neurosciences

by

Sahil Hemant Shah

Committee in charge:

Professor Hollis Cline, Chair
Professor Binhai Zheng, Co-Chair
Professor Don Cleveland
Professor Jeffrey Goldberg
Professor Yishi Jin
Professor Samara Reck-Peterson

2019

The Dissertation of Sahil Hemant Shah is approved, and it is acceptable in quality and form for publication on microfilm and electronically:

_____

_____

_____

_____

_____

_____
Co-Chair

_____
Chair

University of California San Diego

2019

TABLE OF CONTENTS

LIST OF FIGURES

ACKNOWLEDGEMENTS

I would like to acknowledge members of both the Goldberg and Cline labs, whose support allowed me seamless transitions through 3 institutions over the last 5 years. I am first and foremost grateful for the mentorship by both Drs. Goldberg and Cline, whose complementary styles taught me to approach broad questions in a direct manner, to learn from and build upon established literature, and to communicate ideas effectively in both written and oral presentations. I want to thank Lucio Schiapparelli, my collaborator for all the following chapters, for teaching me biochemistry and proteomics. Geoff Weiner gave helpful advice on asking scientific questions and has been a great resource for navigating graduate and medical school. Joana Galvao and Evan Cameron have been invaluable as postdocs in the lab giving their input on both experimental techniques and new questions to explore. I am grateful for the help provided by several undergraduates and technicians in both Cline and Goldberg labs: Sarah Saturday, Melissa Atkins, Catalina Sun, and Cara Knasel. Finally I would like to thank lab managers Kristina Russano and Nancy Wentworth for handling the rodent colonies, ordering all reagents and equipment, navigating administrative matters, and allowing me to primarily focus on research.

This introduction, in full, is a reprint of the material as it appears in Shah SH, Goldberg JL. (2018) The Role of Axon Transport in Neuroprotection and Regeneration. *Developmental Neurobiology, 78*(10) 998-1010. The dissertation author was the primary investigator and author of this paper.

Chapter 1, in part, has been submitted for publication of the material as it currently appears in: Schiapparelli LM*, Shah SH*, McClatchy D, Ma Y, Sharma P, Yates III JR, Goldberg JL, Cline HT. “Retinal ganglion cell transportome identifies proteins transported to axons and presynaptic compartments in the visual system in vivo”. The dissertation author was a primary investigator and author of this paper.

Chapter 2, in part, is currently being prepared for submission for publication of the material. Shah SH*, Schiapparelli LM*, Ma Y, Atkins M, Xia X, Saturday S, Sun C, Knasel C, Yates III JR, Cline HT, Goldberg JL. “Quantitative transportomics identifies Kif5a as a major regulator of neurodegeneration”. The dissertation author was a primary investigator and author of this paper.

Chapter 3, in part, is currently being prepared for submission for publication of the material. Shah SH, Schiapparelli LM, Yakota S, Ma Y, Xia X, Saturday S, Sun C, Yates III JR, Cline HT, Goldberg JL. “Quantitative protein synthesis changes in the visual system after optic nerve injury”. The dissertation author was a primary investigator and author of this paper.

VITA

2012 Bachelor of Science, University of Maryland, College Park

2019 Doctor of Philosophy, University of California San Diego

PUBLICATIONS

Shah SH, Goldberg JL. (2018) The Role of Axon Transport in Neuroprotection and Regeneration. Developmental Neurobiology, 78(10) 998-1010.

Carr CE, Shah SH, McColgan T, Ashida G, Kuokkanen P, Brill S, Kempter R, Wagner H. (2015) Maps of Interaural delay in the owl's nucleus laminaris. Journal of Neurophysiology.

McColgan T, Shah SH, Koppl C, Carr CE, Wagner H. (2014). A Functional Circuit Model of Interaural Time Difference Processing. Journal of Neurophysiology.

ABSTRACT OF THE DISSERTATION

Protein synthesis and transport dynamics in injury and disease

by

Sahil Hemant Shah

Doctor of Philosophy in Neurosciences

University of California San Diego, 2019

Professor Hollis Cline, Chair
Professor Binhai Zheng, Co-Chair

Central nervous system neurons, like retinal ganglion cells, often fail to regenerate their axons and die following axonal injury. A complete understanding of cellular dynamics in injured neurons is necessary to identify critical regulators of degeneration and to develop therapies for survival and regeneration. Although extensive efforts have been made to dissect the transcriptomic and genetic changes in these neurons, less headway has been made into understanding protein dynamics, the effectors of cellular responses.

In this dissertation, I begin by reviewing the literature of regulators of neuronal regeneration and mechanisms underlying regenerative failure. Insights from disease point towards axonal transport failure as a unifying hypothesis underlying a portion of degenerative disease, yet methods of detecting protein transport are unsatisfactory. In fact, physiological protein transport in the central nervous system *in vivo* was not well understood, surprising given the importance of protein transport for pre-synaptic regulation. Therefore we first developed a

mass spectrometry-compatible methodology for detecting axonally-transported proteins (the "transportome"), using it to first catalogue the RGC transportome and then to probe why different sub-cortical RGC targets transduce different signal across their synapses. I next adapt this methodology to quantify changes in protein transport to the optic nerve after injury, identifying a significant reduction in transport of Kif5a, a protein necessary for RGC survival. I next adapt a method for quantifying new protein synthesis to the retina in two time points following optic nerve injury, generating candidate proteins for neurite outgrowth *in vitro* and RGC survival after injury *in vivo*. I conclude that the successful integration of multiple modalities of cellular response across time points after injury, including ChIP-sequencing, RNA-sequencing, protein synthesis, degradation, transport, and maintenance, will give a more complete understanding of dynamic cellular regulation in degeneration and provide key therapeutic targets for survival and axon regeneration.

INTRODUCTION

Like most other mature neurons in the central nervous system (CNS), retinal ganglion cells (RGCs) cannot regenerate their axons in disease and after injury. In the visual system, RGCs carry visual information along their axons down the optic nerve to the superior colliculus (SC) and the lateral geniculate nucleus (LGN) of the thalamus, among other important brain targets. Therapies to protect or restore vision after axon insult must address RGC survival and axon regeneration, and re-integration of the RGC axons into the appropriate visual circuitry. To combat regenerative failure, many strategies have been devised both alone and in combination to allow partial regeneration of injured RGCs to their visual targets. Over the last 30 years, to understand why adult, mammalian RGCs and other CNS neurons do not regenerate after injury, and convert them into neurons that do regenerate, many groups have asked what are the molecular differences between adult, mammalian CNS neurons and 1) “immature” mammalian CNS neurons, which have a higher intrinsic growth capacity; 2) adult peripheral nervous system (PNS) neurons, which do regenerate their axons after injury; and 3) CNS neurons from other species that do show regenerative capacity? Here we review advances in these parallel strategies, and then discuss a hypothesis that links prior work into a unified model for the role of axon transport in regenerative failure, as well as a new way to target approaches to promote regeneration.

Immature CNS Neurons Have a High Regenerative Potential

Developing mammalian CNS neurons have a high growth potential that is lost by adulthood. In fact, isolated RGCs from embryonic mice have a far greater *in vitro* growth potential than RGCs isolated from early postnatal mice (Goldberg et al., 2002a). Manipulating growth regulation pathways in mature neurons may promote regeneration, by increasing intrinsic growth factor-driven signaling pathways such as mTOR, cAMP, suppressors of cytokine signaling (e.g. SOCS3) and mitogen-activated protein kinases (Cai et al., 1999; Kurimoto et al., 2010; Leaver et al., 2006; Park et al., 2010; Smith et al., 2009; Zhou et al., 2005), manipulating

responsiveness to extrinsic inhibitory factors such as by blocking Nogo receptor expression or activation (Chen et al., 2000; Fischer et al., 2004; GrandPré et al., 2000), and decreasing transcriptional inhibitors of axon growth such as Krüppel-like family transcription factors (KLFs) (Moore et al., 2009, 2011). Identifying genes or pathways whose pattern of expression in immature, highly regenerative CNS neurons are drastically altered after maturation may lead to candidate regulators of intrinsic growth potential. In the case of KLFs, where developmental upregulation of KLF9 and KLF4 and downregulation of KLF6 and KLF7 are coincident with the reduction of intrinsic regenerative capacity of RGCs, reversing these expression patterns in adult RGCs or in other CNS neuron pathways after injury allows sprouting or long-distance regeneration (Apara et al., 2017; Blackmore et al., 2012; Moore et al., 2009; Wang et al., 2017). Exploring the molecular mechanisms of the KLFs further, identification of co-factors such as JNK3 and STAT3, and downstream targets such as serotonin receptors and dual-specificity phosphatase 14 (DUSP14) (Apara et al., 2017; Galvao et al., 2018; Qin et al., 2013; Trakhtenberg et al., 2017) have led to broader understanding of the biology of intrinsic capacity for axon growth. What other molecular targets do KLF family transcription factors and other intrinsic regulators of axon growth affect? Advances in sequencing and mass spectrometry technologies can uncover a more complete understanding of the cellular and molecular changes underlying the developmental loss of regenerative capacity.

Beyond transcriptional regulation, immature and mature CNS neurons have differential axonal transport. In embryonic cortical neurons *in vitro*, axonal transport included integrins important for axonal growth and elongation; in mature cortical neurons, this transport is lost. While most molecular transport is dependent on motor trafficking, axonal integrin transport has some specificity to a specific kinesin KIF4A (Heintz et al., 2014). It is particularly noteworthy that axonal transport of integrins in mature neurons switches from an anterograde to mainly retrograde transport (Franssen et al., 2015).

These findings present a clear opportunity for future research into the axonal transport changes after optic nerve injury. Does integrin transport change more and less than other proteins after injury? Are all kinesin-transported proteins affected the same by injury, or are there kinesin isoform responses specific to different injuries or insults? While not a direct link, these examples underline how developmental changes in gene expression and axonal transport parallel developmental changes in intrinsic axon growth ability—and a ripe avenue for future regeneration research.

Electrical Stimulation After RGC Injury

An additional element to consider beyond molecular signaling pathways is the functionality of RGCs: electrical activity is critical for transmission of action potentials and visual information, but it turns out it is also beneficial for RGC and other CNS neurons' responsiveness to survival and growth signals. It has previously been shown that electrical activity regulates mitochondrial localization and motility from the cell body in myelinated axons (Ohno et al., 2011). In addition, electrical modulation through eye-opening, brain-derived neurotrophic factor (BDNF), or tetrodotoxin administration *in vivo* during development greatly impact mitochondrial function and trafficking in RGC axons (our unpublished data), demonstrating a direct connection between activity and transport. RGCs extend longer neurites with concurrent electrical stimulation and growth factor administration *in vitro* (Goldberg et al., 2002b) and *in vivo* (Lim et al., 2016). Increasing conduction in regenerating axons with a voltage-gated potassium channel blocker enhances visual recovery measured at the level of behavior (Bei et al., 2016). This electrical stimulation pathway acts at least in part through activation of adenylate cyclases, and specifically the calcium-sensitive, soluble adenylate cyclase (sAC) *in vitro* and *in vivo* (Corredor et al., 2012; Martinez et al., 2014). Complicating the story, however, is that excessive calcium influx into the axon after injury is a primary step in acute axon degeneration (Knoferle et al., 2010). Pre-loading RGCs with calcium channel blockers before optic nerve crush results in improved survival and regeneration of RGCs (Ribas et al., 2017). How are calcium or

downstream cAMP signaling compartmentalized to regulate complex cellular responses? Is there anterograde or retrograde effector transport responsible for long-distance communication? Further work dissecting timing, compartmentalization, and localization of these pathways will be needed to reconcile these data.

PNS Neuronal Regeneration Informs CNS Regeneration

Early experiments showing that PNS neuronal grafts can induce CNS axon elongation started a field of comparative work of PNS and CNS neurons, and the glial environments they must regenerate through (Benfey and Aguayo, 1982; David and Aguayo, 1981; Richardson et al., 1980). Exploring differences in the molecular characteristics of the regenerative response after injury between PNS and CNS has uncovered several networks that all could contribute towards inducing RGC regeneration (Chandran et al., 2016; Smith et al., 2011).

For example, cytokines, such as gp130 family members like interleukin-6, are differentially activated after PNS injury as compared to CNS injury (Cafferty et al., 2001). Further studies expanded on the subsequent activation of the JAK/STAT pathway, showing a correlation with enhanced PNS regeneration (Miao et al., 2006). Removing SOCS3, an inhibitor of the JAK/STAT pathway present in high levels following injury in CNS neurons, promotes RGC regeneration (Smith et al., 2009). Surprisingly, STAT3-dependent gene expression is directly inhibited by KLF family member KLF4 after cytokine activation, potentially explaining one mechanism by which KLF4 deletion promotes RGC regeneration (Qin et al., 2013).

Through differential proteomics and bioinformatic network analysis, c-Myc was identified as a hub protein that was downregulated in RGCs but not in dorsal root ganglion PNS neurons after injury (Belin et al., 2015). Furthermore, overexpression of this protein increased survival and regeneration. As another example, the transcription factor SOX11 was first identified as a modulator of regeneration in the PNS (Jankowski et al., 2009). This was extended to the CNS, showing that SOX11 underlies DLK/LZK-mediated cell death, and that overexpression of Sox11 can induce regeneration of some subtypes of RGCs, although also leading to cell death of other

RGC subtypes (Norsworthy et al., 2017; Welsbie et al., 2017). This unveiling of factors that differentially promote survival or regeneration depending on the subtype of neuron was also seen with osteopontin and IGF1, which improved survival and regeneration of the alpha-RGCs that preferentially express the relevant receptors (Duan et al., 2015). As more details emerge about not only CNS-PNS differences but also about the heterogeneity of CNS neuron subtypes and their responses to injury, more work will be needed to fine-tune individualized therapies for regeneration.

Intrinsically Regenerative Species

Regenerative failure of the CNS is not a universally conserved phenomenon: in fact, diverse phyla and classes like nematodes (Yanik et al., 2004), fruitflies (Soares et al., 2014), zebrafish (Cameron, 2000; Sherpa et al., 2007), and reptiles (Lang et al., 1998), demonstrate at least partial neural regeneration after injury. In *C. elegans*, DLK-1 was first shown to promote and regulate adult axon regeneration, regulating the cells to respond to injury, partially through mRNA stabilization, discussed further below (Hammarlund et al., 2009; Yan et al., 2009). This finding was also seen in peripheral nerve regeneration in mice, with DLK required for retrograde transport of phosphorylated STAT3 to the cell body from the damaged axon (Shin et al., 2012). In one study of Drosophila wing regeneration after injury, transgenic screening highlighted JNK pathway inhibition as pro-growth, a finding conserved in mammalian RGCs after injury (Apara et al., 2017; Soares et al., 2014; Welsbie et al., 2013). In fact it seems the DLK/JNK pathway underlies cellular responsiveness to injury in intrinsically regenerative species, regenerative PNS neurons, and non-regenerative neurons even in humans, either pro-growth or pro-apoptotic depending on the neuronal context (Le Pichon et al., 2017).

In zebrafish, KLF6a and KLF7a together are necessary for RGC regeneration after optic nerve crush, and similarly promote axon growth and regeneration in rodent RGCs and corticospinal neurons (Blackmore et al., 2012; Moore et al., 2009; Veldman et al., 2007). However, a downstream target in zebrafish was identified as *tuba1a*, a key protein for

regeneration in fish that has not been found to be relevant for regeneration in mammals (Veldman et al., 2010). Thus exploring conserved and divergent molecular pathways and functions has helped to understand differences in regenerative capacity between mammals and other species and has led to candidate approaches for promoting regeneration.

Combining Therapies to Enhance Regeneration

As many of these regenerative therapies target different pathways, the combination of cell intrinsic and cell extrinsic approaches has led to novel insights and improvements in survival and regeneration of ganglion cells. For example, while the deletion of *PTEN* or *SOCS3* independently lead to extensive RGC regeneration, the co-deletion of *PTEN* and *SOCS3* had a synergistic effect for robust, sustained axon regeneration (Sun et al., 2011). Recently, the combination of KLF9 knockdown with zinc chelation by TPEN was shown to lead to more enhanced regeneration and cell survival than either therapy alone (Trakhtenberg et al., 2018). Visual or electrical stimulation also elicits more profound effects in combination with neurotrophic factors or with manipulation of pro-growth signaling pathways in neurons such as RGCs (Goldberg et al., 2002b; Lim et al., 2016). However, despite the best combinations of transcription factors and growth pathways, relatively few RGC axon reach their target regions. It is likely that a cocktail approach manipulating several factors together may enhance regeneration and indeed be necessary for full visual recovery.

Indeed, we must now ask how regenerated RGC synapses compare to those established during development. Do they have adequate transport of pre-synaptic machinery to maintain synaptic connections? Is exogenous expression of guidance molecules necessary for axon targeting? The answers to these questions and more form the next frontier of visual regeneration research. Despite these advances, limited visual recovery has been seen, underscoring the need for a deeper understanding of cellular changes in injury and disease. Many of the regenerative factors discussed above were hypothesized as candidate therapies due to differential expression in regenerative and non-regenerative neurons. Similarly,

differential expression of factors in degenerative and non-degenerative neurons can highlight candidates for survival and maintenance of axons, which when combined with regenerative therapy, will lead to enhanced therapeutic response. Indeed the link between degenerative molecular pathways and those failing to promote regenerative response may be one fertile area to focus on. With that in mind, insights from degenerative changes seen in conditions like glaucoma may suggest new avenues for vision restoration research.

Axon Transport in Glaucoma and Other Neurodegenerative Diseases

Glaucoma is the leading cause of irreversible blindness worldwide and is predicted to affect 80 million people by 2020 (Quigley and Broman, 2006). The biggest risk factor is age; increased intraocular pressure (IOP) is currently the only modifiable risk factor. Vision loss occurs due to dysfunction and death of RGCs and their axons. Furthermore, widespread damage can be seen throughout the visual system, with degenerative changes in the LGN and the visual cortex (Yucel et al., 2000). The molecular pathophysiology of glaucoma is still poorly understood, but increasing evidence implicates interference with axonal transport mechanisms.

Decreased axoplasmic flow between the RGC cell bodies and their axon terminals in the SC or LGN in the face of increased IOP remains one of longest-standing hypotheses for pathophysiologic mechanism in this disease. Since the 1970s, studies into axoplasmic transport in glaucomatous degeneration have shown an association between increased IOP and decreased anterograde and retrograde protein transport (Anderson and Hendrickson, 1974, 1977; Crish et al., 2010; Minckler et al., 1977; Quigley and Anderson, 1977; Quigley et al., 1979). Indeed there is a strong link between many neurodegenerative diseases and dysfunctional axon transport (Appel, 1981). Causative mutations in genes that directly or indirectly lead to axon transport deficits may underlie at least a portion of the neuronal death seen in Huntington's disease (Trushina et al., 2004), amyotrophic lateral sclerosis (ALS) (Nicolas et al., 2018; Pasinelli and Brown, 2006), Parkinson's disease (Saha et al., 2004), and Alzheimer's disease (Wu et al., 2009; Zhang et al., 2004). Specifically, decreases in axonal

transport precede and possibly contribute to axonal and microtubule, and then somatic, degeneration (Morfini et al., 2009; Stokin et al., 2005).

What mechanistic insights can be derived from such consistent, distal-to-proximal cellular neurodegeneration? Identifying the molecular cargoes of bidirectional cellular transport mechanisms and ensuring adequate transport of these molecules to their targets may be a key component to achieving long-distance regeneration and re-innervation of RGCs to the brain.

Dendritic and Synaptic Degeneration and Transport in Glaucoma

RGCs require functional connections with pre-synaptic neurons in the retina and post-synaptic neurons in the brain to maintain transmission of visual information, and re-establishing and maintaining synaptic communication is vital to survival of RGCs (Della Santina et al., 2013). In different glaucoma models, the DBA/2J mouse and a microbead injection-induced IOP model of glaucoma, axon transport fails early, with synaptic transmission and axon and dendritic dysfunction preceding the eventual RGC death, implicating axon transport in disease pathology (Buckingham et al., 2008; Ou et al., 2012; Sappington et al., 2010; Ward et al., 2014). Additional work has also highlighted early dendritic field reorganization in different RGC subtypes, before measurable axonal degeneration, and well before cell death (El-Danaf and Huberman, 2015; Della Santina et al., 2013). Thus failure of long-distance transport down axonal or dendritic neurites may underlie early phases of degeneration.

Molecular Motors Underlying Transport Are Linked to Neurodegenerative Disease

In neurons, microtubule motor proteins, dyneins and kinesins, drive organelle and molecular axonal transport (Hirokawa, 1998; Hirokawa et al., 2009; Teng et al., 2005; Vale et al., 1985). Given the importance of axon transport in the homeostatic maintenance of neuronal survival, disruptions to these motor proteins underlies a variety of neurological diseases. For example, Charcot-Marie-Tooth disease type 2A can be caused by mutations in KIF1B1, and congenital fibrosis of the extraocular muscles (which is a neuropathy, not a myopathy) can be caused by mutations in KIF21A (Yamada et al., 2003; Zhao et al., 2001). Kinesins can form

axonal aggregates in some neurodegenerative conditions like Alzheimer's disease, especially in cases with certain amyloid precursor protein (APP) mutants, with blockages occurring before the characteristic amyloid plaque accumulations (Stokin et al., 2005). A loss-of-function mutation in KIF5A results in hereditary spastic paraplegia, characterized by a progressive loss of function and degeneration of upper motor neurons, starting with synaptic degradation (Morfini et al., 2009; Reid, 2003; Xia et al., 2003). Different loss-of-function mutations in KIF5A, all affecting the cargo binding domain, are causative in some cases of ALS (Nicolas et al., 2018). Charcot-Marie-Tooth syndromes can include optic atrophy among the peripheral neuropathies that define the disease, supporting the premise of shared axon transport-related pathophysiologies among axonopathies. The vital role of molecular transport in injury and disease, and their corresponding variety of mRNA, protein, and mitochondrial cargoes, highlight the necessity of addressing axonal transport when attempting to regenerate and re-innervate CNS neurons.

Does neurodegeneration follow a general decline in transport, or is the transport of specific, key cargoes causative in these different diseases. In the last few decades, increasing evidence has shown that kinesin subtypes and adaptor proteins have at least partial cargo specificity (Chevalier-Larsen and Holzbaur, 2006). For example, KIF1A and KIF1B of the Kinesin 3 family transport synaptic vesicle precursors synaptophysin and synaptotagmin, but do not transport syntaxin 1A or SNAP25 (Okada et al., 1995), whereas KIF5 motors do transport syntaxin 1A and SNAP25, and also transport synaptotagmin (Toda et al., 2008). The physiologic relevance of this partial specificity and partial redundancy is not fully elucidated but could reflect compensatory mechanisms for vital cargo to maintain cellular function and survival.

Regulation of these motors' active state and specific cargoes also depends on cell signaling cascades and post-translational modifications such as phosphorylation and changes in adaptor proteins. For KIF5 motors, protein kinase A phosphorylation inhibits the binding of synaptic vesicles and glycogen synthase kinase-3 phosphorylation inhibits the binding of

membrane organelles (Morfini et al., 2002; Sato-Yoshitake et al., 1992). In mitochondrial trafficking, the adaptor proteins Milton and Miro bridge KIF5 motors to the mitochondria in a calcium dependent manner (Glater et al., 2006; MacAskill et al., 2009). The wide heterogeneity of these identified cargoes leads directly to the question of how specificity is effected, if they form functional groups, and how they change after injury or during regeneration. What are the key molecules and organelles transported in axons? And, which are affected in RGC axons in optic neuropathies like glaucoma with associated axon transport loss?

Axonal Transport of Mitochondria

Mitochondria are perhaps the most-studied organelle being shuttled up and down the axon by motor proteins. Mitochondria are responsible for ATP generation by oxidative phosphorylation, generation of reactive oxygen species, calcium buffering, amongst many other functions (Werth and Thayer, 1994). Dysregulation of mitochondria and mitochondrial distribution can lead to apoptotic cell death. Mitochondrial trafficking is essential for neurite outgrowth *in vitro* (Morris and Hollenbeck, 1993), and *in vivo* transport of mitochondria after injury has recently been more appreciated. *In vivo* imaging of mitochondria in the retina has shown a general decrease in motility and transport in aged mice compared to adult mice, as well as a reduced number of transported mitochondria in a glaucoma model (Takihara et al., 2015). Interestingly, aged mice are more susceptible to the mitochondrial transport disruption of glaucoma compared to younger adult mice, correlating with the increased incidence of glaucoma as humans age. Mitochondria traffic to injured axons in *C. elegans* is required for normal regeneration (Han et al., 2016). Similarly, after optic nerve crush in mice, the mitochondrial protein Armcx1 is upregulated during injury in a regenerative condition, and further overexpression enhances both survival and regeneration of RGCs. This effect is hypothesized to be due to an increased in mobilization of mitochondria after injury, consistent with the results seen in *C. elegans* and in the mammalian sciatic nerve (Cartoni et al., 2016; Han et al., 2016; Zhou et al., 2016). Thus promoting increased mitochondrial transport promotes

regenerative responses in the mammalian optic nerve, although it is not yet understood how regulation of this mitochondrial re-distribution and energetics modulation contributes to survival and regeneration.

Axonal Transport of mRNA

Effectors from the cell body arrive at pre-synaptic terminals, growth cones, dendrites and sites of injury by two methods: local axonal translation after transport of mRNA, and direct long-distance transport of proteins. Before the detection of mRNA transport into mammalian axons, local translation was predicted based on an efficiency hypothesis: over long distances, transport of few mRNA molecules that could be translated many times over at the desired location conserves energy over synthesizing these proteins at the cell body and transporting them (Spaulding and Burgess, 2017). Evidence for local translation in PNS neurons has first been shown through radioactive protein synthesis labelling *in vitro* and *in vivo*, followed by microscopic evidence of ribosomes *in vivo* (Bleher and Martin, 2001; Eng et al., 1999; Koenig, 1991). The presence of ribosomes and mRNA in the axons of mature CNS neurons is a pre-requisite for local translation. PolyA and rRNA are seen in developing hippocampal neurons *in vitro*, and axonal protein synthesis contributes to growth cone stabilization in isolated, regenerating DRG neurons *in vivo* (Kleiman et al., 1994; Zheng et al., 2001). Furthermore, specific mRNA molecules whose transport is increased after injury have been seen in both PNS and CNS axons *in vivo.* (Hanz et al., 2003; Willis et al., 2011). RNA-binding proteins and ribosomes for local translation have been found in peripheral neurons (Spillane et al., 2013; Zheng et al., 2001), and bound to mitochondria in RGC axons *in vitro* (our unpublished data). Isolated mRNA from purified axons of cortical neurons using a specialized microfluidic chamber also revealed many transcripts related to RNA translation machinery and transport (Taylor et al., 2009). Indeed even with these data in CNS neurons, having less translation machinery in CNS axons than PNS axons (Verma et al., 2005) may contribute to the differential regenerative capacities between these two populations. Is a relative lack of mRNA transport and/or locally

translated effector proteins a fundamental reason for regenerative failure? While further work in this field is necessary to determine if increased translation after injury in RGC axons can improve regeneration, progress has been made in identifying and targeting specific mRNA transport pathways.

Are there links between mRNA transport and molecular pathways implicated in neuroprotection or regeneration? One strong example involves the dual leucine zipper kinase (DLK-1) pathway, which was first shown to lead to *cebp-1* mRNA stabilization and local translation in *C. elegans* (Yan et al., 2009), and later tied to RGC survival in mice (Watkins et al., 2013; Welsbie et al., 2013). In a high throughput siRNA assay, DLK inhibition was seen to be pro-survival in primary RGCs given an axonal injury. Similarly, inhibition of leucine zipper kinase (LZK), whose *C. elegans* homolog is DLK-1, in conjunction with DLK knockdown, more completely prevents RGC death both *in vitro* and *in vivo* (Welsbie et al., 2017). Downstream effectors of this pathway have been identified, including SOX11, MEF2A, JUN, and ATF2, and a number of these also affect RGC survival and optic nerve regeneration. It is not known, however, whether DLK or these DLK/LZK pathway effectors lead to mRNA stabilization and local translation or transport changes in mammalian axons, similar to DLK's mechanism of action in *C. elegans.*

Even more broadly, how can we discover the identities of these pools of mRNA that are actively being translated in RGC axons? Ribotrap techniques to isolate actively translating RNA in the visual system, and identifying them with RNA-Seq, takes this exploration of *in vivo* axonal translation a step further (Shigeoka et al., 2016). Briefly, affinity-tagged ribosomes are expressed in a cell-specific manner, cross-linked, and isolated. The bound mRNA to these ribosomes, the "translatome", gives insight into actively translating mRNA in a specific cell type. In neurons with spatial separation of compartments, such as RGCs, optic nerve and synaptic terminals can be isolated to identify locally translating axonal proteins. Quantifying changes of intra-axonal protein synthesis in the normal, injured, and regenerating optic nerves as compared

to intrinsically regenerating axons will identify aspects of the translatome most relevant to neuro-regeneration.

Axonal Transport of Proteins

Directly transported proteins have been identified and studied in glaucoma and acute optic nerve injury, with an experimental focus on strong candidates for involvement in neurodegeneration, such as the transport of brain-derived neurotrophic factor (BDNF) (Pease et al., 2000). To truly appreciate the complement of proteins transported normally or disrupted in glaucoma or other insults, unbiased methods are needed for broad identification. Mass spectrometry for proteins and lipids continue to show the most promise for tackling such questions. As these technologies continue to advance, methods for subdividing these pools, including time resolution for synthesis and degradation of these molecules and compartmentalized sequencing, will provide a clearer picture of molecular interactions.

Historically, studies in goldfish (Benowitz et al., 1981; Perry et al., 1985), tadpoles (Szaro et al., 1984), toads (Skene and Willard, 1981), and mammals (McKerracher et al., 1990) using radiolabeled amino acids have shown that there is a global loss of axonal transport following nerve injury, with selective increases in proteins of certain molecular weights. In non-regenerating mammalian RGCs, there is a preferential loss of slow compared to fast axonal transport, which may underlie some of the differences in regenerative potential between species. Studies that try to dissect the identities of axonal proteins and protein changes are confounded by proteins originating from non-axonal sources, such as glia (Perry et al., 1985). Approaches to separate axonal from glial proteins have included isolating axoplasm e.g. from ligated sciatic nerves with or without injury; however biological variability limited attempts to quantify protein differences even when using clustering methods to correlate and group transport machinery to a set of proteins (Michaelevski et al., 2010). Nonetheless, there is evidence of increased anterograde transport of structural components of translation machinery and mRNAs in PNS neurons that may not occur in CNS neurons after injury or in degenerative

disease. Together these findings paint a picture of a coordinated cellular response to injury that relies on transporting both formed proteins and the machinery to synthesize new proteins (See Figure 1).

Even better than such indirect, bioinformatics-based approaches to identify and separate axonally transported proteins from glial proteins after injury would be direct detection of anterogradely or retrogradely transported proteins *in vivo.* This has been challenging, primarily due to the low proportion of transported axonal proteins compared to those from the surrounding white matter milieu. Are regenerated RGCs able to adequately transport synaptic proteins and mRNA for local translation from the cell body? In fact, what proteins make up the pre-synaptic compartment in RGCs, and do these differ by RGC subtype or target region? While synaptosomal proteomics have improved with novel compartment labelling techniques (Ting et al., 2016), these have for the most part been restricted to cell culture.

Recent advances in mass spectrometry-compatible signal detection *in vivo* have allowed a re-evaluation of this open question in transport biology (Schiapparelli et al., 2014), to the point that we can now directly detect changes in CNS axoplasmic protein transport in injury and disease. Labelling a group of proteins with an affinity tag, such as biotin, is a common method of separating proteins of interest from the background. In such paradigms, these labelled proteins are enriched with streptavidin pulldown, and once isolated, trypsinized and identified with mass spectrometry. This technique has mostly been limited to situations where labelled proteins are a large portion of total proteins, as can be controlled in cell culture, but is a challenge when labelled proteins are only a small fraction of total proteins. *In vivo*, the percentage of proteins transported from a cell body to the axon is low compared to all the proteins found in the optic nerve, resulting in a high false-positive rate of contaminating unlabeled proteins. To overcome this limitation, reversing the order of the technique, trypsinizing all protein and then pulling down and searching by mass spec for only the biotinylated peptides can now allow direct detection and high specificity even in rare samples (Schiapparelli et al., 2014). A second technical

improvement is the ability to multiplex tags with slightly different molecular weight biotin groups, similar to tandem mass tagging, allowing for quantitative differences in protein abundance between conditions (Thompson et al., 2003). We have been exploring these approaches in optic nerve injury and regeneration, and our early findings suggest feasibility of the technique and identification of promising candidates.

Figure 1

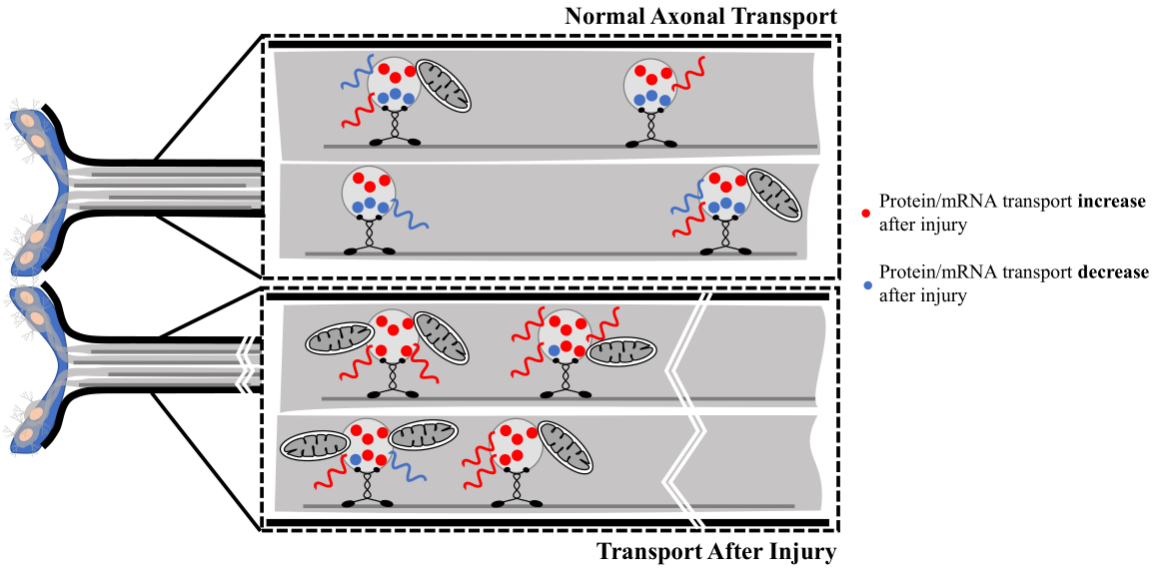

Figure 0.1. After axonal injury, anterograde transport of mitochondria, mRNA, and proteins are all affected. Certain proteins and mRNA decrease in transport, while the transport of other specific transcripts, proteins, and mitochondria towards the injury site may increase.

Could Axon Transport Be One Universal Effector Regulating Regenerative Failure or Success?

Re-examining recent advances in regeneration with a renewed and technically improved focus on axonal transport underscores that many of these strategies may depend or be enhanced by functioning molecular motor networks. For example, KLF4 has been directly linked to mitochondrial biogenesis and autophagy in non-neuronal cells, and proper translocation of mitochondrial to the site of injury is critical for axon growth (Jang and Arany, 2015). While KLF4 deletion promotes partial RGC regeneration, could negative regulation of mitochondrial translocation limit the effectiveness of this therapy? Dissection of the KLF9-Dusp14 link in RGC regeneration may potentially unveil a direct link between nuclear gene expression changes and the transport of signals sent to the RGC axon. As discussed above, the DLK/LZK pathway, which ties in upstream to the role of Sox11 in RGC survival and regeneration, is also known to affect mRNA stabilization and translation in other species. Could transport failure after injury be a cause of incomplete regeneration with visual recovery seen in each of these studies?

As mentioned previously, functional axonal transport depends on multiple kinesins and dynein. How are these motors, and their respective cargoes, differentially expressed and regulated after injury? What is the redundancy and specificity of cargo transport between motors? In uninjured neurons, loss of KIF4a reduces integrin trafficking, but overexpression is not able to increase integrin transport to the axonal compartment (Heintz et al., 2014). Approaching this problem from the opposite side, how do known regenerative or survival therapies affect kinesin expression, and protein translocation? Identifying the upstream regulators of transport through comparisons between regenerative and nonregenerative neurons, and specifically targeting them, may unmask the intrinsic growth capacities of adult CNS neurons.

In summary, recent large-scale ‘omics studies, both transcriptomic and proteomic, have opened up the ability to quantitatively probe all changes in the neuronal cell body—which may

generate a deluge of differentially expressed candidates—and now changes in transport to other compartments, like the axon, which may narrow such molecular candidates to those most relevant for axonal degeneration and regeneration. Indeed probing these together may suggest a mechanistic link between gene transcription, protein expression, and molecular transport to affected axons. We hypothesize that understanding such mechanistic links will not only impact axon regeneration approaches, but also address myelination in regenerating fibers, electrophysiology and axon conductance of action potentials, and formation of synapses, all key to restoring the diversity of visual responses and behavior.

This introduction, in full, is a reprint of the material as it appears in Shah SH, Goldberg JL. (2018) The Role of Axon Transport in Neuroprotection and Regeneration. *Developmental Neurobiology, 78*(10), 998-1010. The dissertation author was the primary investigator and author of this paper.

References

Anderson, D.R., and Hendrickson, A. (1974). Effect of intraocular pressure on rapid axoplasmic transport in monkey optic nerve. Investig. Ophthalmol. Vis. Sci.

Anderson, D.R., and Hendrickson, A.E. (1977). Failure of increased intracranial pressure to affect rapid axonal transport at the optic nerve head. Investig. Ophthalmol. Vis. Sci. 423–426.

Apara, A., Galvao, J., Wang, Y., Blackmore, M., Trillo, A., Iwao, K., Brown, D.P., Fernandes, K.A., Huang, A., Nguyen, T., Ashouri, M., Zhang, X., Shaw, P.X., Kunzevitzky, N.J., Moore, D.L., Libby, R.T., and Goldberg, J.L. (2017). KLF9 and JNK3 Interact to Suppress Axon Regeneration in the Adult CNS. J. Neurosci. *37*, 9632–9644.

Appel, S.H. (1981). A unifying hypothesis for the cause of amyotrophic lateral sclerosis, parkinsonism, and alzheimer disease. Ann. Neurol. *10*, 499–505.

Bei, F., Lee, H.H.C., Liu, X., Gunner, G., Jin, H., Ma, L., Wang, C., Hou, L., Hensch, T.K., Frank, E., Sanes, J.R., Chen, C., Fagiolini, M., and He, Z. (2016). Restoration of Visual Function by Enhancing Conduction in Regenerated Axons. Cell *164*, 219–232.

Belin, S., Nawabi, H., Wang, C., Tang, S., Latremoliere, A., Warren, P., Schorle, H., Uncu, C., Woolf, C.J., He, Z., and Steen, J.A. (2015). Injury-Induced Decline of Intrinsic Regenerative Ability Revealed by Quantitative Proteomics. Neuron *86*, 1000–1014.

Benfey, M., and Aguayo, A.J. (1982). Extensive elongation of axons from rat brain into peripheral nerve grafts. Nature *296*, 150–152.

Benowitz, L.I., Shashoua, V.E., and Yoon, M.G. (1981). Specific changes in rapidly transported proteins during regeneration of the goldfish optic nerve. J. Neurosci. *1*, 300–307.

Blackmore, M.G., Wang, Z., Lerch, J.K., Motti, D., Zhang, Y.P., Shields, C.B., Lee, J.K., Goldberg, J.L., Lemmon, V.P., and Bixby, J.L. (2012). Kruppel-like Factor 7 engineered for transcriptional activation promotes axon regeneration in the adult corticospinal tract. Proc. Natl. Acad. Sci. *109*, 7517–7522.

Bleher, R., and Martin, R. (2001). Ribosomes in the Squid Giant Axon. Neuroscience *107*, 527–534.

Buckingham, B.P., Inman, D.M., Lambert, W., Oglesby, E., Calkins, D.J., Steele, M.R., Vetter, M.L., Marsh-Armstrong, N., and Horner, P.J. (2008). Progressive ganglion cell degeneration precedes neuronal loss in a mouse model of glaucoma. J. Neurosci. *28*, 2735–2744.

Cafferty, W.B.J., Gardiner, N.J., Gavazzi, I., Powell, J., Mcmahon, S.B., Heath, J.K., Munson, J., Cohen, J., and Thompson, S.W.N. (2001). Leukemia Inhibitory Factor Determines the Growth Status of Injured Adult Sensory Neurons. J. Neurosci. *21*, 7161–7170.

Cai, D., Yingjing, S., De Bellard, M.E., Tang, S., and Filbin, M.T. (1999). Prior exposure to neurotrophins blocks inhibition of axonal regeneration by MAG and myelin via a cAMP-dependent mechanism. Neuron *22*, 89–101.

Cameron, D.A. (2000). Cellular proliferation and neurogenesis in the injured retina of adult zebrafish. Vis. Neurosci. *17*, 789–797.

Cartoni, R., Norsworthy, M.W., Bei, F., Wang, C., Li, S., Zhang, Y., Gabel, C. V., Schwarz, T.L., and He, Z. (2016). The Mammalian-Specific Protein Armcx1 Regulates Mitochondrial

Transport during Axon Regeneration. Neuron *94*, 689.

Chandran, V., Coppola, G., Nawabi, H., Omura, T., Versano, R., Huebner, E.A., Zhang, A., Costigan, M., Yekkirala, A., Barrett, L., Blesch, A., Michaelevski, I., Davis-Turak, J., Gao, F., Langfelder, P., Horvath, S., He, Z., Benowitz, L., Fainzilber, M., Tuszynski, M., Woolf, C.J., and Geschwind, D.H. (2016). A Systems-Level Analysis of the Peripheral Nerve Intrinsic Axonal Growth Program. Neuron *89*, 956–970.

Chen, M.S., Huber, A.B., Van Der Haar, M.E.D., Frank, M., Schnell, L., Spillmann, A.A., Christ, F., and Schwab, M.E. (2000). Nogo-A is a myelin-associated neurite outgrowth inhibitor and an antigen for monoclonal antibody IN-1. Nature *403*, 434–439.

Chevalier-Larsen, E., and Holzbaur, E.L.F. (2006). Axonal transport and neurodegenerative disease. Biochim. Biophys. Acta *1762*, 1094–1108.

Corredor, R.G., Trakhtenberg, E.F., Pita-Thomas, W., Jin, X., Hu, Y., and Goldberg, J.L. (2012). Soluble Adenylyl Cyclase Activity Is Necessary for Retinal Ganglion Cell Survival and Axon Growth. J. Neurosci. *32*, 7734–7744.

Crish, S.D., Sappington, R.M., Inman, D.M., Horner, P.J., and Calkins, D.J. (2010). Distal axonopathy with structural persistence in glaucomatous neurodegeneration. Proc. Natl. Acad. Sci. *107*, 5196–5201.

David, S., and Aguayo, A.J. (1981). Axonal Elongation into Peripheral Nervous System "Bridges" after Central Nervous System Injury in Adult Rats. Science (80-.). *214*, 931–933.

Duan, X., Qiao, M., Bei, F., Kim, I.J., He, Z., and Sanes, J.R. (2015). Subtype-Specific regeneration of retinal ganglion cells following axotomy: Effects of osteopontin and mtor signaling. Neuron *85*, 1244–1256.

El-Danaf, R.N., and Huberman, a. D. (2015). Characteristic Patterns of Dendritic Remodeling in Early-Stage Glaucoma: Evidence from Genetically Identified Retinal Ganglion Cell Types. J. Neurosci. *35*, 2329–2343.

Eng, H., Lund, K., and Campenot, R.B. (1999). Synthesis of B-Tubulin, Actin, and Other Proteins in Axons of Sympathetic Neurons in Compartmented Cultures. J. Neurosci. *19*, 1–9.

Fischer, D., He, Z., and Benowitz, L.I. (2004). Counteracting the Nogo receptor enhances optic nerve regeneration if retinal ganglion cells are in an active growth state. J. Neurosci. *24*, 1646–1651.

Franssen, E.H.P., Zhao, R.-R., Koseki, H., Kanamarlapudi, V., Hoogenraad, C.C., Eva, R., and Fawcett, J.W. (2015). Exclusion of Integrins from CNS Axons Is Regulated by Arf6 Activation and the AIS. J. Neurosci. *35*, 8359–8375.

Galvao, J., Iwao, K., Apara, A., Wang, Y., Ashouri, M., Shah, N., Blackmore, M., Kunzevitzky, N.J., Moore, D.L., and Goldberg, J.L. (2018). The Kruppel-Like Factor Gene Target Dusp14 Regulates Axon Growth and Regeneration. Investig. Ophthalmol. Vis. Sci. *59*.

Glater, E.E., Megeath, L.J., Stowers, R.S., and Schwarz, T.L. (2006). Axonal transport of mitochondria requires milton to recruit kinesin heavy chain and is light chain independent. J. Cell Biol. *173*, 545–557.

Goldberg, J.L., Klassen, M.P., Hua, Y., and Barres, B.A. (2002a). Amacrine-Signaled Loss of

Intrinsic Axon Growth Ability by Retinal Ganglion Cells. Science (80-.). *296*, 1860–1865.

Goldberg, J.L., Espinosa, J.S., Xu, Y., Davidson, N., Kovacs, G.T., and Barres, B.A. (2002b). Retinal Ganglion Cells Do Not Extend Axons by Default. Neuron *33*, 689–702.

GrandPré, T., Nakamura, F., Vartanlan, T., and Strittmatter, S.M. (2000). Identification of the Nogo inhibitor of axon regeneration as a Reticulon protein. Nature *403*, 439–444.

Hammarlund, M., Nix, P., Hauth, L., Jorgensen, E.M., and Bastiani, M. (2009). Axon Regeneration Requires a Conserved MAP Kinase Pathway. Science (80-.). *323*.

Han, S.M., Baig, H.S., and Hammarlund, M. (2016). Mitochondria Localize to Injured Axons to Support Regeneration. Neuron *92*, 1308–1323.

Hanz, S., Perlson, E., Willis, D., Zheng, J.Q., Massarwa, R., Huerta, J.J., Koltzenburg, M., Kohler, M., Van-Minnen, J., Twiss, J.L., and Fainzilber, M. (2003). Axoplasmic importins enable retrograde injury signaling in lesioned nerve. Neuron *40*, 1095–1104.

Heintz, T.G., Heller, J.P., Zhao, R., Caceres, A., Eva, R., and Fawcett, J.W. (2014). Kinesin KIF4A transports integrin β1 in developing axons of cortical neurons. Mol. Cell. Neurosci. *63*, 60–71.

Hirokawa, N. (1998). Kinesin and Dynein Superfamily Proteins and the Mechanism of Organelle Transport. Science (80-.). *279*, 519–526.

Hirokawa, N., Noda, Y., Tanaka, Y., and Niwa, S. (2009). Kinesin superfamily motor proteins and intracellular transport. Nat. Rev. Mol. Cell Biol. *10*, 682–696.

Jang, C., and Arany, Z. (2015). Mitochondria Cripple without Krüppel. Trends Endocrinol. Metab. *26*, 587–589.

Jankowski, M.P., McIlwrath, S.L., Jing, X., Cornuet, P.K., Salerno, K.M., Koerber, H.R., and Albers, K.M. (2009). Sox11 transcription factor modulates peripheral nerve regeneration in adult mice. Brain Res. *1256*, 43–54.

Kleiman, R., Banker, G., and Steward, O. (1994). Development of subcellular mRNA compartmentation in hippocampal neurons in culture. J. Neurosci. *14*, 1130–1140.

Knoferle, J., Koch, J.C., Ostendorf, T., Michel, U., Planchamp, V., Vutova, P., Tonges, L., Stadelmann, C., Bruck, W., Bahr, M., and Lingor, P. (2010). Mechanisms of acute axonal degeneration in the optic nerve in vivo. Proc. Natl. Acad. Sci. *107*, 6064–6069.

Koenig, E. (1991). Evaluation of Local Synthesis of Axonal Proteins in the Goldfish Mauthner Cell Axon and Axons of Dorsal and Ventral Roots of the Rat in vitro. Mol. Cell. Neurosci. *2*, 384–394.

Kurimoto, T., Yin, Y., Omura, K., Gilbert, H., Kim, D., Cen, L.-P., Moko, L., Kügler, S., and Benowitz, L.I. (2010). Long-distance axon regeneration in the mature optic nerve: contributions of oncomodulin, cAMP, and pten gene deletion. J. Neurosci. *30*, 15654–15663.

Lang, D.M., Monzón-Mayor, M., Bandtlow, C.E., and Stuermer, C.A.O. (1998). Retinal axon regeneration in the lizard Gallotia galloti in the presence of CNS myelin and oligodendrocytes. Glia *23*, 61–74.

Leaver, S.G., Cui, Q., Plant, G.W., Arulpragasam, A., Hisheh, S., Verhaagen, J., and Harvey, a R. (2006). AAV-mediated expression of CNTF promotes long-term survival and

regeneration of adult rat retinal ganglion cells. Gene Ther. *13*, 1328–1341.

Lim, J.-H.A., Stafford, B.K., Nguyen, P.L., Lien, B. V, Wang, C., Zukor, K., He, Z., and Huberman, A.D. (2016). Neural activity promotes long-distance, target-specific regeneration of adult retinal axons. Nat. Neurosci. *19*.

MacAskill, A.F., Rinholm, J.E., Twelvetrees, A.E., Arancibia-Carcamo, I.L., Muir, J., Fransson, A., Aspenstrom, P., Attwell, D., and Kittler, J.T. (2009). Miro1 Is a Calcium Sensor for Glutamate Receptor-Dependent Localization of Mitochondria at Synapses. Neuron *61*, 541–555.

Martinez, J., Stessin, A.M., Campana, A., Hou, J., Nikulina, E., Buck, J., Levin, L.R., and Filbin, M.T. (2014). Soluble adenylyl cyclase is necessary and sufficient to overcome the block of axonal growth by myelin-associated factors. J. Neurosci. *34*, 9281–9289.

McKerracher, L., Vidal-Sanz, M., Essagian, C., and Aguayo, A.J. (1990). Selective impairment of slow axonal transport after optic nerve injury in adult rats. J. Neurosci. *10*, 2834–2841.

Miao, T., Wu, D., Zhang, Y., Bo, X., Subang, M.C., Wang, P., and Richardson, P.M. (2006). Suppressor of Cytokine Signaling-3 Suppresses the Ability of Activated Signal Transducer and Activator of Transcription-3 to Stimulate Neurite Growth in Rat Primary Sensory Neurons. J. Neurosci. *26*, 9512–9519.

Michaelevski, I., Medzihradszky, K.F., Lynn, A., Burlingame, A.L., and Fainzilber, M. (2010). Axonal transport proteomics reveals mobilization of translation machinery to the lesion site in injured sciatic nerve. Mol. Cell. Proteomics *9*, 976–987.

Minckler, D.S., Bunt, A.H., and Johanson, G.W. (1977). Orthograde and retrograde axoplasmic transport during acute ocular hypertension in the monkey. Investig. Ophthalmol. Vis. Sci. *16*, 426–441.

Moore, D.L., Blackmore, M.G., Hu, Y., Kaestner, K.H., Bixby, J.L., Lemmon, V.P., and Goldberg, J.L. (2009). KLF Family Members Regulate Intrinsic Axon Regeneration Ability. Science (80-.). *326*, 298–301.

Moore, D.L., Apara, A., and Goldberg, J.L. (2011). Krüppel-like transcription factors in the nervous system: Novel players in neurite outgrowth and axon regeneration. Mol. Cell. Neurosci. *47*, 233–243.

Morfini, G., Pigino, G., Beffert, U., Busciglio, J., and Brady, S.T. (2002). Fast axonal transport misregulation and Alzheimer's disease. Neuromolecular Med. *2*, 89–99.

Morfini, G.A., Burns, M., Binder, L.I., Kanaan, N.M., LaPointe, N., Bosco, D.A., Brown, R.H., Brown, H., Tiwari, A., Hayward, L., Edgar, J., Nave, K.-A., Garberrn, J., Atagi, Y., Song, Y., Pigino, G., and Brady, S.T. (2009). Axonal transport defects in neurodegenerative diseases. J. Neurosci. *29*, 12776–12786.

Morris, R.L., and Hollenbeck, P.J. (1993). The regulation of bidirectional mitochondrial transport is coordinated with axonal outgrowth. J. Cell Sci. *104 (Pt 3*, 917–927.

Nicolas, A., Kenna, K.P., Renton, A.E., Ticozzi, N., Faghri, F., Chia, R., Dominov, J.A., Kenna, B.J., Nalls, M.A., Keagle, P., Rivera, A.M., Rheenen, W. van, Murphy, N.A., Vugt, J.J.F.A. van, Geiger, J.T., Spek, R.A. Van der, Pliner, H.A., Shankaracharya, Smith, B.N., Marangi, G., Topp, S.D., Abramzon, Y., Gkazi, A.S., Eicher, J.D., Kenna, A., Logullo, F.O., Simone, I., Logroscino, G., Salvi, F., Bartolomei, I., Borghero, G., Murru, M.R., Costantino, E., Pani, C., Puddu, R., Caredda, C., Piras, V., Tranquilli, S., Cuccu,

S., Corongiu, D., Melis, M., Milia, A., Marrosu, F., Marrosu, M.G., Floris, G., Cannas, A., Tranquilli, S., Capasso, M., Caponnetto, C., Mancardi, G., Origone, P., Mandich, P., Conforti, F.L., Cavallaro, S., Mora, G., Marinou, K., Sideri, R., Penco, S., Mosca, L., Lunetta, C., Pinter, G.L., Corbo, M., Riva, N., Carrera, P., Volanti, P., Mandrioli, J., Fini, N., Fasano, A., Tremolizzo, L., Arosio, A., Ferrarese, C., Trojsi, F., Tedeschi, G., Monsurrò, M.R., Piccirillo, G., Femiano, C., Ticca, A., Ortu, E., Bella, V. La, Spataro, R., Colletti, T., Sabatelli, M., Zollino, M., Conte, A., Luigetti, M., Lattante, S., Marangi, G., Santarelli, M., Petrucci, A., Pugliatti, M., Pirisi, A., Parish, L.D., Occhineri, P., Giannini, F., Battistini, S., Ricci, C., Benigni, M., Cau, T.B., Loi, D., Calvo, A., Moglia, C., Brunetti, M., Barberis, M., Restagno, G., Casale, F., Marrali, G., Fuda, G., Ossola, I., Cammarosano, S., Canosa, A., Ilardi, A., Manera, U., Grassano, M., Tanel, R., Pisano, F., Mora, G., Calvo, A., Mazzini, L., Riva, N., Mandrioli, J., Caponnetto, C., Battistini, S., Volanti, P., Bella, V. La, Conforti, F.L., Borghero, G., Messina, S., Simone, I.L., Trojsi, F., Salvi, F., Logullo, F.O., D'Alfonso, S., Corrado, L., Capasso, M., Ferrucci, L., Harms, M.B., Goldstein, D.B., Shneider, N.A., Goutman, S., Simmons, Z., Miller, T.M., Chandran, S., Pal, S., Manousakis, G., Appel, S.H., Simpson, E., Wang, L., Baloh, R.H., Gibson, S., Bedlack, R., Lacomis, D., Sareen, D., Sherman, A., Bruijn, L., Penny, M., Moreno, C. de A.M., Kamalakaran, S., Goldstein, D.B., Allen, A.S., Appel, S., Baloh, R.H., Bedlack, R.S., Boone, B.E., Brown, R., Carulli, J.P., Chesi, A., Chung, W.K., Cirulli, E.T., Cooper, G.M., Couthouis, J., Day-Williams, A.G., Dion, P.A., Gibson, S., Gitler, A.D., Glass, J.D., Goldstein, D.B., Han, Y., Harms, M.B., Harris, T., Hayes, S.D., Jones, A.L., Keebler, J., Krueger, B.J., Lasseigne, B.N., Levy, S.E., Lu, Y.-F., Maniatis, T., McKenna-Yasek, D., Miller, T.M., Myers, R.M., Petrovski, S., Pulst, S.M., Raphael, A.R., Ravits, J.M., Ren, Z., Rouleau, G.A., Sapp, P.C., Shneider, N.A., Simpson, E., Sims, K.B., Staropoli, J.F., Waite, L.L., Wang, Q., Wimbish, J.R., Xin, W.W., Gitler, A.D., Harris, T., Myers, R.M., Phatnani, H., Kwan, J., Sareen, D., Broach, J.R., Simmons, Z., Arcila-Londono, X., Lee, E.B., Deerlin, V.M. Van, Shneider, N.A., Fraenkel, E., Ostrow, L.W., Baas, F., Zaitlen, N., Berry, J.D., Malaspina, A., Fratta, P., Cox, G.A., Thompson, L.M., Finkbeiner, S., Dardiotis, E., Miller, T.M., Chandran, S., Pal, S., Hornstein, E., MacGowan, D.J., Heiman-Patterson, T., Hammell, M.G., Patsopoulos, N.A., Dubnau, J., Nath, A., Phatnani, H., Musunuri, R.L., Evani, U.S., Abhyankar, A., Zody, M.C., Kaye, J., Finkbeiner, S., Wyman, S., LeNail, A., Lima, L., Fraenkel, E., Rothstein, J.D., Svendsen, C.N., Thompson, L.M., Eyk, J. Van, Maragakis, N.J., Berry, J.D., Glass, J.D., Miller, T.M., Kolb, S.J., Baloh, R.H., Cudkowicz, M., Baxi, E., Kaye, J., Finkbeiner, S., Wyman, S.K., LeNail, A., Lima, L., Fraenkel, E., Svendsen, C.N., Thompson, L.M., Eyk, J.E. Van, Berry, J.D., Miller, T.M., Kolb, S.J., Cudkowicz, M., Baxi, E., Benatar, M., Taylor, J.P., Wu, G., Rampersaud, E., Wuu, J., Rademakers, R., Züchner, S., Schule, R., McCauley, J., Hussain, S., Cooley, A., Wallace, M., Clayman, C., Barohn, R., Statland, J., Ravits, J., Swenson, A., Jackson, C., Trivedi, J., Khan, S., Katz, J., Jenkins, L., Burns, T., Gwathmey, K., Caress, J., McMillan, C., Elman, L., Pioro, E., Heckmann, J., So, Y., Walk, D., Maiser, S., Zhang, J., Benatar, M., Taylor, J.P., Rampersaud, E., Wu, G., Wuu, J., Silani, V., Ticozzi, N., Gellera, C., Ratti, A., Taroni, F., Lauria, G., Verde, F., Fogh, I., Tiloca, C., Comi, G.P., Sorarù, G., Cereda, C., D'Alfonso, S., Corrado, L., Marchi, F. De, Corti, S., Ceroni, M., Mazzini, L., Siciliano, G., Filosto, M., Inghilleri, M., Peverelli, S., Colombrita, C., Poletti, B., Maderna, L., Bo, R. Del, Gagliardi, S., Querin, G., Bertolin, C., Pensato, V., Castellotti, B., Lauria, G., Verde, F., Fogh, I., Tiloca, C., Comi, G.P., Sorarù, G., Cereda, C., Camu, W., Mouzat, K., Lumbroso, S., Corcia, P., Meininger, V., Besson, G., Lagrange, E., Clavelou, P., Guy, N., Couratier, P., Vourch, P., Danel, V., Bernard, E., Lemasson, G., Corcia, P., Laaksovirta, H., Myllykangas, L., Jansson, L., Valori, M., Ealing, J., Hamdalla, H., Rollinson, S., Pickering-Brown, S., Orrell, R.W., Sidle, K.C., Malaspina, A., Hardy, J., Singleton, A.B., Johnson, J.O., Arepalli, S., Sapp, P.C.,

McKenna-Yasek, D., Polak, M., Asress, S., Al-Sarraj, S., King, A., Troakes, C., Vance, C., Belleroche, J. de, Baas, F., Asbroek, A.L.M.A. ten, Muñoz-Blanco, J.L., Hernandez, D.G., Ding, J., Gibbs, J.R., Scholz, S.W., Floeter, M.K., Campbell, R.H., Landi, F., Bowser, R., Pulst, S.M., Ravits, J.M., MacGowan, D.J.L., Kirby, J., Pioro, E.P., Pamphlett, R., Broach, J., Gerhard, G., Dunckley, T.L., Brady, C.B., Kowall, N.W., Troncoso, J.C., Ber, I. Le, Mouzat, K., Lumbroso, S., Heiman-Patterson, T.D., Kamel, F., Bosch, L. Van Den, Baloh, R.H., Strom, T.M., Meitinger, T., Shatunov, A., Eijk, K.R. Van, Carvalho, M. de, Kooyman, M., Middelkoop, B., Moisse, M., McLaughlin, R.L., Es, M.A. Van, Weber, M., Boylan, K.B., Blitterswijk, M. Van, Rademakers, R., Morrison, K.E., Basak, A.N., Mora, J.S., Drory, V.E., Shaw, P.J., Turner, M.R., Talbot, K., Hardiman, O., Williams, K.L., Fifita, J.A., Nicholson, G.A., Blair, I.P., Rouleau, G.A., Esteban-Pérez, J., García-Redondo, A., Al-Chalabi, A., Kheifat, A. Al, Al-Chalabi, A., Andersen, P., Basak, A.N., Blair, I.P., Chio, A., Cooper-Knock, J., Corcia, P., Couratier, P., Carvalho, M. de, Dekker, A., Drory, V., Redondo, A.G., Gotkine, M., Hardiman, O., Hide, W., Iacoangeli, A., Glass, J., Kenna, K., Kiernan, M., Kooyman, M., Landers, J., McLaughlin, R., Middelkoop, B., Mill, J., Neto, M.M., Moisse, M., Pardina, J.M., Morrison, K., Newhouse, S., Pinto, S., Pulit, S., Robberecht, W., Shatunov, A., Shaw, P., Shaw, C., Silani, V., Sproviero, W., Tazelaar, G., Ticozzi, N., Damme, P. van, Berg, L. van den, Spek, R. van der, Eijk, K. van, Es, M. van, Rheenen, W. van, Vugt, J. van, Veldink, J., Weber, M., Williams, K.L., Zatz, M., Bauer, D.C., Twine, N.A., Rogaeva, E., Zinman, L., Ostrow, L.W., Maragakis, N.J., Rothstein, J.D., Simmons, Z., Cooper-Knock, J., Brice, A., Goutman, S.A., Feldman, E.L., Gibson, S.B., Taroni, F., Ratti, A., Gellera, C., Damme, P. Van, Robberecht, W., Fratta, P., Sabatelli, M., Lunetta, C., Ludolph, A.C., Andersen, P.M., Weishaupt, J.H., Camu, W., Trojanowski, J.Q., Deerlin, V.M. Van, Brown, R.H., Berg, L.H. van den, Veldink, J.H., Harms, M.B., Glass, J.D., Stone, D.J., Tienari, P., Silani, V., Chiò, A., Shaw, C.E., Traynor, B.J., and Landers, J.E. (2018). Genome-wide Analyses Identify KIF5A as a Novel ALS Gene. Neuron *97*, 1268–1283.e6.

Norsworthy, M.W., Bei, F., Kawaguchi, R., Wang, Q., Tran, N.M., Li, Y., Brommer, B., Zhang, Y., Wang, C., Sanes, J.R., Coppola, G., and He, Z. (2017). Sox11 Expression Promotes Regeneration of Some Retinal Ganglion Cell Types but Kills Others. Neuron *94*, 1112–1120.e4.

Ohno, N., Kidd, G.J., Mahad, D., Kiryu-seo, S., Avishai, A., Komuro, H., and Trapp, B.D. (2011). Myelination and Axonal Electrical Activity Modulate the Distribution and Motility of Mitochondria at CNS Nodes of Ranvier. J. Neurosci. *31*, 7249–7258.

Okada, Y., Yamazaki, H., Sekine-Aizawa, Y., and Hirokawa, N. (1995). The neuron-specific kinesin superfamily protein KIF1A is a uniqye monomeric motor for anterograde axonal transport of synaptic vesicle precursors. Cell *81*, 769–780.

Ou, Y., Lopez, E.R., Sretavan, D.W., and Ullian, E.M. (2012). Retinal Ganglion Cell Synapse Loss in a Mouse Model of Ocular Hypertension. Investig. Ophthalmol. Vis. Sci.

Park, K.K., Liu, K., Hu, Y., Kanter, J.L., and He, Z. (2010). PTEN/mTOR and axon regeneration. Exp. Neurol. *223*, 45–50.

Pasinelli, P., and Brown, R.H. (2006). Molecular biology of amyotrophic lateral sclerosis: insights from genetics. Nat. Rev. Neurosci. *7*, 710–723.

Pease, M.E., McKinnon, S.J., Quigley, H.A., Kerrigan-Baumrind, L.A., and Zack, D.J. (2000). Obstructed axonal transport of BDNF and its receptor TrkB in experimental glaucoma. Investig. Ophthalmol. Vis. Sci. *41*, 764–774.

Perry, G.W., Burmeister, D.W., and Grafstein, B. (1985). Changes in protein content of goldfish optic nerve during degeneration and regeneration following nerve crush. J Neurochem *44*, 1142–1151.

Le Pichon, C.E., Meilandt, W.J., Dominguez, S., Solanoy, H., Lin, H., Ngu, H., Gogineni, A., Sengupta Ghosh, A., Jiang, Z., Lee, S.-H., Maloney, J., Gandham, V.D., Pozniak, C.D., Wang, B., Lee, S., Siu, M., Patel, S., Modrusan, Z., Liu, X., Rudhard, Y., Baca, M., Gustafson, A., Kaminker, J., Carano, R.A.D., Huang, E.J., Foreman, O., Weimer, R., Scearce-Levie, K., and Lewcock, J.W. (2017). Loss of dual leucine zipper kinase signaling is protective in animal models of neurodegenerative disease. Sci. Transl. Med. *9*, eaag0394.

Qin, S., Zou, Y., and Zhang, C.L. (2013). Cross-talk between klf4 and stat3 regulates axon regeneration. Nat. Commun. *4*, 1–9.

Quigley, H., and Broman, A.T. (2006). The number of people with glaucoma worldwide in 2010 and 2020. Br. J. Ophthalmol. *90*, 262–267.

Quigley, H.A., and Anderson, D.R. (1977). Distribution of axonal transport blockade by acute intraocular pressure elevation in the primate optic nerve head. Investig. Ophthalmol. Vis. Sci. *16*, 640–644.

Quigley, H.A., Guy, J., and Anderson, D.R. (1979). Blockade of Rapid Axonal Transport: Effect of Intraocular Pressure Elevation in Primate Optic Nerve. Arch. Ophthalmol. *97*, 525–531.

Reid, E. (2003). Science in motion: common molecular pathological themes emerge in the hereditary spastic paraplegias. J. Med. Genet. *40*, 81–86.

Ribas, V.T., Koch, J.C., Michel, U., Bähr, M., and Lingor, P. (2017). Attenuation of Axonal Degeneration by Calcium Channel Inhibitors Improves Retinal Ganglion Cell Survival and Regeneration After Optic Nerve Crush. Mol. Neurobiol. *54*, 72–86.

Richardson, P.M., McGuinness, U.M., and Aguayo, A.J. (1980). Axons from CNS neurones regenerate into PNS grafts. Nature *284*, 264–265.

Saha, A.R., Hill, J., Utton, M.A., Asuni, A.A., Ackerley, S., Grierson, A.J., Miller, C.C., Davies, A.M., Buchman, V.L., Anderton, B.H., and Hanger, D.P. (2004). Parkinson's disease alpha-synuclein mutations exhibit defective axonal transport in cultured neurons. J. Cell Sci. *117*, 1017–1024.

Della Santina, L., Inman, D.M., Lupien, C.B., Horner, P.J., and Wong, R.O.L. (2013). Differential Progression of Structural and Functional Alterations in Distinct Retinal Ganglion Cell Types in a Mouse Model of Glaucoma. J. Neurosci. *33*, 17444–17457.

Sappington, R.M., Carlson, B.J., Crish, S.D., and Calkins, D.J. (2010). The microbead occlusion model: a paradigm for induced ocular hypertension in rats and mice. Investig. Ophthalmol. Vis. Sci. *51*, 207–216.

Sato-Yoshitake, R., Yorifuji, H., Inagaki, M., and Hirokawa, N. (1992). The phosphorylation of kinesin regulates its binding to synaptic vesicles. J Biol Chem *267*, 23930–23936.

Schiapparelli, L.M., Mcclatchy, D.B., Liu, H., Sharma, P., Yates, J.R., and Cline, H.T. (2014). Direct Detection of Biotinylated Proteins by Mass Spectrometry. J. Proteome Res. *13*, 3966–3978.

Sherpa, T., Fimbel, S.M., Mallory, D.E., Maaswinkel, H., Spritzer, S.D., Sand, J.A., Li, L., Hyde, D.R., and Stenkamp, D.L. (2007). Ganglion Cell Regeneration Following Whole-Retina Destruction in Zebrafish. Dev. Neurobiol. 166–181.

Shigeoka, T., Jung, H., Jung, J., Turner-Bridger, B., Ohk, J., Lin, J.Q., Amieux, P.S., and Holt, C.E. (2016). Dynamic Axonal Translation in Developing and Mature Visual Circuits. Cell *166*, 181–192.

Shin, J.E., Cho, Y., Beirowski, B., Milbrandt, J., Cavalli, V., and Diantonio, A. (2012). Dual Leucine Zipper Kinase Is Required for Retrograde Injury Signaling and Axonal Regeneration. Neuron *74*, 1015–1022.

Skene, J.H.P., and Willard, M. (1981). Changes in axonally transported proteins during axon regeneration in toad retinal ganglion cells. J. Cell Biol. *89*, 86–95.

Smith, P.D., Sun, F., Park, K.K., Cai, B., Wang, C., Kuwako, K., Martinez-Carrasco, I., Connolly, L., and He, Z. (2009). SOCS3 Deletion Promotes Optic Nerve Regeneration In Vivo. Neuron *64*, 617–623.

Smith, R.P., Lerch-Haner, J.K., Pardinas, J.R., Buchser, W.J., Bixby, J.L., and Lemmon, V.P. (2011). Transcriptional profiling of intrinsic PNS factors in the postnatal mouse. Mol. Cell. Neurosci. *46*, 32–44.

Soares, L., Parisi, M., and Bonini, N.M. (2014). Axon injury and regeneration in the adult drosophila. Sci. Rep. *4*.

Spaulding, E.L., and Burgess, R.W. (2017). Accumulating evidence for axonal translation in neuronal homeostasis. Front. Neurosci. *11*, 1–7.

Spillane, M., Ketschek, A., Merianda, T.T., Twiss, J.L., and Gallo, G. (2013). Mitochondria Coordinate Sites of Axon Branching through Localized Intra-axonal Protein Synthesis. Cell Rep. *5*, 1564–1575.

Stokin, G.B., Lillo, C., Falzone, T.L., Brusch, R.G., Rockenstein, E., Mount, S.L., Raman, R., Davies, P., Masliah, E., Williams, D.S., and Goldstein, L.S.B. (2005). Axonopathy and transport deficits early in the pathogenesis of Alzheimer's disease. Science (80-.). *307*, 1282–1288.

Sun, F., Park, K.K., Belin, S., Wang, D., Lu, T., Chen, G., Zhang, K., Yeung, C., Feng, G., Yankner, B.A., and He, Z. (2011). Sustained axon regeneration induced by co-deletion of PTEN and SOCS3. Nature *480*, 372–375.

Szaro, B.G., Faulkner, L.A., Kevin Hunt, R., and Peng Loh, Y. (1984). Axonal transport of [35S]Methionine labeled proteins in Xenopus optic nerve: Phases of transport and the effects of nerve crush on protein patterns. Brain Res. *297*, 337–355.

Takihara, Y., Inatani, M., Eto, K., Inoue, T., Kreymerman, A., Miyake, S., Ueno, S., Nagaya, M., Nakanishi, A., Iwao, K., Takamura, Y., Sakamoto, H., Satoh, K., Kondo, M., Sakamoto, T., Goldberg, J.L., Nabekura, J., and Tanihara, H. (2015). In vivo imaging of axonal transport of mitochondria in the diseased and aged mammalian CNS. Proc. Natl. Acad. Sci. *112*, 10515–10520.

Taylor, A.M., Berchtold, N.C., Perreau, V.M., Tu, C.H., Jeon, N.L., and Cotman, C.W. (2009). Axonal mRNA in Uninjured and Regenerating Cortical Mammalian Axons. J. Neurosci. *29*, 4697–4707.

Teng, J., Rai, T., Tanaka, Y., Takei, Y., Nakata, T., Hirasawa, M., Kulkarni, A.B., and Hirokawa, N. (2005). The KIF3 motor transports N-cadherin and organizes the developing neuroepithelium. Nat. Cell Biol. *7*, 474–482.

Thompson, A., Schäfer, J., Kuhn, K., Kienle, S., Schwarz, J., Schmidt, G., Neumann, T., and Hamon, C. (2003). Tandem mass tags: A novel quantification strategy for comparative analysis of complex protein mixtures by MS/MS. Anal. Chem. *75*, 1895–1904.

Ting, A.Y., Stawski, P.S., Draycott, A.S., Udeshi, N.D., Lehrman, E.K., Wilton, D.K., Svinkina, T., Deerinck, T.J., Ellisman, M.H., Stevens, B., Carr, S.A., and Ting, A.Y. (2016). Proteomic Analysis of Unbounded Cellular Compartments: Synaptic Clefts. Cell *166*, 1295–1307.e21.

Toda, H., Mochizuki, H., Flores, R., Josowitz, R., Krasieva, T.B., Lamorte, V.J., Suzuki, E., Gindhart, J.G., Furukubo-Tokunaga, K., and Tomoda, T. (2008). UNC-51/ATG1 kinase regulates axonal transport by mediating motor-cargo assembly. Genes Dev. *22*, 3292–3307.

Trakhtenberg, E.F., Pita-Thomas, W., Fernandez, S.G., Patel, K.H., Venugopalan, P., Shechter, J.M., Morkin, M.I., Galvao, J., Liu, X., Dombrowski, S.M., and Goldberg, J.L. (2017). Serotonin receptor 2C regulates neurite growth and is necessary for normal retinal processing of visual information. Dev. Neurobiol. *77*, 419–437.

Trakhtenberg, E.F., Li, Y., Feng, Q., Tso, J., Rosenberg, P.A., Goldberg, J.L., and Benowitz, L.I. (2018). Zinc chelation and Klf9 knockdown cooperatively promote axon regeneration after optic nerve injury. Exp. Neurol. *300*, 22–29.

Trushina, E., Dyer, R.B., Badger, J.D., Ure, D., Eide, L., Tran, D.D., Vrieze, B.T., Legendre-Guillemin, V., McPherson, P.S., Mandavilli, B.S., Van Houten, B., Zeitlin, S., McNiven, M., Aebersold, R., Hayden, M., Parisi, J.E., Seeberg, E., Dragatsis, I., Doyle, K., Bender, A., Chacko, C., and McMurray, C.T. (2004). Mutant huntingtin impairs axonal trafficking in mammalian neurons in vivo and in vitro. Mol. Cell. Biol. *24*, 8195–8209.

Vale, R.D., Reese, T.S., and Sheetz, M.P. (1985). Identification of a novel force-generating protein, kinesin, involved in microtubule-based motility. Cell *42*, 39–50.

Veldman, M.B., Bemben, M.A., Thompson, R.C., and Goldman, D. (2007). Gene expression analysis of zebrafish retinal ganglion cells during optic nerve regeneration identifies KLF6a and KLF7a as important regulators of axon regeneration. Dev. Biol. *312*, 596–612.

Veldman, M.B., Bemben, M.A., and Goldman, D. (2010). Tuba1a gene expression is regulated by KLF6/7 and is necessary for CNS development and regeneration in zebrafish. Mol. Cell. Neurosci. *43*, 370–383.

Verma, P., Chierzi, S., Codd, A.M., Campbell, D., Meyer, R., Holt, C.E., and Fawcett, J.W. (2005). Axonal Protein Synthesis and Degradation Are Necessary for Efficient Growth Cone Regeneration. J. Neurosci. *25*, 331–342.

Wang, Z., Winsor, K., Nienhaus, C., Hess, E., and Blackmore, M.G. (2017). Combined chondroitinase and KLF7 expression reduce net retraction of sensory and CST axons from sites of spinal injury. Neurobiol. Dis. *99*, 24–35.

Ward, N.J., Ho, K.W., Lambert, W.S., Weitlauf, C., and Calkins, D.J. (2014). Absence of transient receptor potential vanilloid-1 accelerates stress-induced axonopathy in the

optic projection. J. Neurosci. *34*, 3161–3170.

Watkins, T.A., Wang, B., Huntwork-Rodriguez, S., Yang, J., Jiang, Z., Eastham-Anderson, J., Modrusan, Z., Kaminker, J.S., Tessier-Lavigne, M., and Lewcock, J.W. (2013). DLK initiates a transcriptional program that couples apoptotic and regenerative responses to axonal injury. Proc. Natl. Acad. Sci. *110*, 4039–4044.

Welsbie, D.S., Yang, Z., Ge, Y., Mitchell, K.L., Zhou, X., Martin, S.E., Berlinicke, C.A., Hackler, L., Fuller, J., Fu, J., Cao, L. -h., Han, B., Auld, D., Xue, T., Hirai, S. -i., Germain, L., Simard-Bisson, C., Blouin, R., Nguyen, J. V., Davis, C. -h. O., Enke, R.A., Boye, S.L., Merbs, S.L., Marsh-Armstrong, N., Hauswirth, W.W., DiAntonio, A., Nickells, R.W., Inglese, J., Hanes, J., Yau, K.-W., Quigley, H.A., and Zack, D.J. (2013). Functional genomic screening identifies dual leucine zipper kinase as a key mediator of retinal ganglion cell death. Proc. Natl. Acad. Sci. *110*, 4045–4050.

Welsbie, D.S., Mitchell, K.L., Jaskula-Ranga, V., Sluch, V.M., Yang, Z., Kim, J., Buehler, E., Patel, A., Martin, S.E., Zhang, P.W., Ge, Y., Duan, Y., Fuller, J., Kim, B.J., Hamed, E., Chamling, X., Lei, L., Fraser, I.D.C., Ronai, Z.A., Berlinicke, C.A., and Zack, D.J. (2017). Enhanced Functional Genomic Screening Identifies Novel Mediators of Dual Leucine Zipper Kinase-Dependent Injury Signaling in Neurons. Neuron *94*, 1142–1154.e6.

Werth, J.L., and Thayer, S.A. (1994). Mitochondria buffer physiological calcium loads in cultured rat dorsal root ganglion neurons. J. Neurosci. *14*, 348–356.

Willis, D.E., Xu, M., Donnelly, C.J., Tep, C., Kendall, M., Erenstheyn, M., English, A.W., Schanen, N.C., Kirn-Safran, C.B., Yoon, S.O., Bassell, G.J., and Twiss, J.L. (2011). Axonal Localization of transgene mRNA in mature PNS and CNS neurons. J. Neurosci. *31*, 14481–14487.

Wu, C., Cui, B., He, L., Chen, L., and Mobley, W.C. (2009). The coming of age of axonal neurotrophin signaling endosomes. J. Proteomics *72*, 46–55.

Xia, C.-H., Roberts, E.A., Her, L.-S., Liu, X., Williams, D.S., Cleveland, D.W., and Goldstein, L.S.B. (2003). Abnormal neurofilament transport caused by targeted disruption of neuronal kinesin heavy chain KIF5A. J. Cell Biol. *161*, 55–66.

Yamada, K., Andrews, C., Chan, W.-M., McKeown, C.A., Magli, A., de Berardinis, T., Loewenstein, A., Lazar, M., O'Keefe, M., Letson, R., London, A., Ruttum, M., Matsumoto, N., Saito, N., Morris, L., Del Monte, M., Johnson, R.H., Uyama, E., Houtman, W.A., de Vries, B., Carlow, T.J., Hart, B.L., Krawiecki, N., Shoffner, J., Vogel, M.C., Katowitz, J., Goldstein, S.M., Levin, A. V, Sener, E.C., Ozturk, B.T., Akarsu, A.N., Brodsky, M.C., Hanisch, F., Cruse, R.P., Zubcov, A.A., Robb, R.M., Roggenkäemper, P., Gottlob, I., Kowal, L., Battu, R., Traboulsi, E.I., Franceschini, P., Newlin, A., Demer, J.L., and Engle, E.C. (2003). Heterozygous mutations of the kinesin KIF21A in congenital fibrosis of the extraocular muscles type 1 (CFEOM1). Nat. Genet. *35*, 318–321.

Yan, D., Wu, Z., Chisholm, A.D., and Jin, Y. (2009). The DLK-1 Kinase Promotes mRNA Stability and Local Translation in C. elegans Synapses and Axon Regeneration. Cell *138*, 1005–1018.

Yanik, M.F., Cinar, H., Cinar, H.N., Chisholm, A.D., Jin, Y., and Ben-Yakar, A. (2004). Functional regeneration after laser axotomy. Nature *432*, 822.

Yucel, Y.H., Zhang, Q., Gupta, N., Kaufman, P.L., and Weinreb, R.N. (2000). Loss of Neurons in Magnocellular and Parvocellular Layers of the Lateral Geniculate Nucleus in

Glaucoma. Arch. Ophthalmol. *118*, 378–384.

Zhang, B., Higuchi, M., Yoshiyama, Y., Ishihara, T., Forman, M.S., Martinez, D., Joyce, S., Trojanowski, J.Q., and Lee, V.M.-Y. (2004). Retarded axonal transport of R406W mutant tau in transgenic mice with a neurodegenerative tauopathy. J. Neurosci. *24*, 4657–4667.

Zhao, C., Takita, J., Tanaka, Y., Setou, M., Nakagawa, T., Takeda, S., Yang, H.W., Terada, S., Nakata, T., Takei, Y., Saito, M., Tsuji, S., Hayashi, Y., and Hirokawa, N. (2001). Charcot-Marie-Tooth disease type 2A caused by mutation in a microtubule motor KIF1Bbeta. Cell *105*, 587–597.

Zheng, J.Q., Kelly, T.K., Chang, B., Ryazantsev, S., Rajasekaran, a K., Martin, K.C., and Twiss, J.L. (2001). A functional role for intra-axonal protein synthesis during axonal regeneration from adult sensory neurons. J. Neurosci. *21*, 9291–9303.

Zhou, B., Yu, P., Lin, M.Y., Sun, T., Chen, Y., and Sheng, Z.H. (2016). Facilitation of axon regeneration by enhancing mitochondrial transport and rescuing energy deficits. J. Cell Biol. *214*, 103–119.

Zhou, Y., Pernet, V., Hauswirth, W.W., and Di Polo, A. (2005). Activation of the extracellular signal-regulated kinase 1/2 pathway by AAV gene transfer protects retinal ganglion cells in glaucoma. Mol. Ther. *12*, 402–412.

CHAPTER 1: Retinal ganglion cell transportome identifies proteins transported to axons and presynaptic compartments in the visual system *in vivo*

Abstract

The brain processes visual and other sensory information and generates cognitive and motor outputs through functions of spatially organized proteins in different types of neurons. Understanding the biochemical processes underlying brain function has been impeded by incomplete knowledge of proteins and their distributions within neuronal compartments in intact brain circuits. Here we apply a suite of methods based on unbiased *in vivo* protein labeling with intravitreal NHS-biotin for discovery and analysis of endogenous axonally-transported proteins in the visual system using tandem mass spectrometric proteomics, biochemistry and both light and electron microscopy. We identified ~1000 biotin-labeled proteins transported from retinal ganglion cells comprising the RGC transportome. Purification and proteomic analysis of biotin-labeled retinal proteins from complex mixtures of cell types and inputs in retinal targets identified 575 proteins from glutamatergic retinal inputs, including 360 proteins that are differentially transported to two retinal targets.

Introduction

The visual system is composed of a spatially distributed neuronal circuit in which the axons of retinal ganglion cells (RGCs), the outputs of the retina, project to diverse retinorecipient targets via the optic nerve. The localization of proteins throughout various cellular compartments is particularly important in the central nervous system (CNS), where neuronal structures are highly polarized and biochemical processes in dendrites, cell bodies, axons and presynaptic terminals are specialized. Anatomical and functional studies indicate that visual information processing differs among retinal targets in the brain; this could be effected by differences in local postsynaptic cells, in RGC presynaptic protein complement, or a combination. Although the different cellular identities among target cells, for example between

the superior colliculus (SC) and lateral geniculate nucleus of the thalamus (LGN), are easily understood to contain different synaptic protein complements that could support differential processing of incoming visual information, it's less clear if RGCs are differentially transporting presynaptic or other proteins from the retina to distinct targets. Indeed although understanding of circuit function depends on it, study of protein distribution within neuronal compartments in the intact CNS has been impeded by the lack of technical approaches to label and quantify transported proteins in an unbiased manner.

Thus we were interested in dissecting the proteome of RGC projections in the intact brain to determine what proteins are transported from RGC somata into their axons, and are RGC proteins transported to retinorecipient targets in a target-specific manner? To address these points, we combined *in vivo* intravitreal protein labeling with *N*-hydroxysuccinimidobiotin (NHS-biotin) and unbiased proteomic analysis of the population of transported proteins from RGCs into the optic nerve (ON) and two major retinal targets, the SC and the LGN. Mass spectrometry revealed ~1000 biotinylated proteins in the RGC transportome, of which ~360 were differentially transported to SC or LGN. Light and electron microscopy (EM) demonstrated the distribution of biotinylated proteins within axons in the ON and retinal targets showing enrichment at presynaptic terminals, matching differentially transported protein identities associated with glutamatergic synaptic function. These data identify for the first time axonally-transported proteins from RGCs *in vivo* and demonstrate differential distribution of RGC proteins to distinct retinal targets.

Results

***In vivo* intravitreal NHS-biotin injection labels retinal proteins transported into the visual pathway**

To identify proteins that are transported from RGC somata into axons and synaptic targets *in vivo*, we studied the visual circuit in adult rats. We labeled proteins in the retina using

intravitreal injections of NHS-biotin and analyzed biotinylated proteins harvested from throughout the visual system. *In vivo* protein biotinylation with NHS-biotin has many advantages: It binds covalently to lysines and N-terminal amino acids of proteins, resulting in extensive protein labeling. NHS-biotin cannot be reincorporated after protein degradation because the succinimide group is quenched after reacting with amino groups. Furthermore, after degradation of biotinylated proteins, the resulting biotin-tagged amino acids, such as biotinyl-lysine, cannot be incorporated into newly synthesized proteins by endogenous protein synthesis machinery (Gallivan et al., 1997; Watanabe et al., 2007). We harvested tissue after 7 days from retinas, ON, SC, LGN, and frontal cortex (FC, a non-visual control area), for analysis using biochemistry, proteomics and histology (Fig 1a, b). To confirm intravitreal injections of NHS-biotin labelled retinal proteins, we created retinal cross sections from biotin and vehicle-injected eyes. Biotinylated proteins were visualized only in the NHS-biotin eyes using tyramide signal amplification conjugated to an Alexa fluorophore (Figure 1a). Through biochemical techniques, biotinylated proteins over a wide range of molecular weights were recovered from retina, ON, LGN and SC, whereas only endogenously biotinylated carboxylases (McKay et al., 2008) were detected in FC and samples that received intravitreal saline injections (Fig 1d). To determine if we were truly detecting biotinylated protein transport, instead of diffusion or transport of free biotin, we injected saline or NHS-biotin intravitreally, and collected both retinal and LGN fractions. Analysis of the biotin in these samples revealed substantial protein-bound biotin in the retina with NHS-biotin compared to background biotin detected in saline. In the LGN, only protein-bound biotin was detected, indicating that protein labeling was confined to the retina and no free biotin diffused down the visual pathway (Fig 1d).

Although our questions were focused on anterograde protein transport in the visual system, we confirmed our protein-labelling technique was adaptable to different experimental

designs by coating the surface of the SC with NHS-biotin (Fig 1e) and visualizing retrograde protein transport through the optic tract and ON by histology and western blot (Fig 1f).

Figure 1.1. *In vivo* intravitreal NHS-biotin injection labels retinal proteins transported into the visual pathway

a. Diagram of the rat visual system schematizing the retinal injection of NHS-biotin and retinal ganglion cell projection sites from which transported biotinylated proteins were analyzed. Biotiylated proteins are only visualized in eyes injected with NHS-biotin. **b.** Workflow for *in vivo* protein labeling strategy and analysis of biotinylated proteins. NHS-biotin binds irreversibly to amino groups of lysine residues and N-terminals of proteins. Biotinylated proteins are either analyzed in histological sections or purified from brain regions and used for biochemical analysis or tandem MS (MS/MS). Biotin-labeled peptides are identified directly by MS/MS. **c.** Western blot detection of biotinylated proteins from retina, ON, LGN, SC and the non-visual area, FC, following *in vivo* intravitreal injection of NHS-biotin or saline. Endogenously biotinylated carboxylases at ~60kDa and 120 kDa are the only labeled proteins in FC. **d**. Comparison of biotin incorporated into proteins from retina (left) and LGN (right) and free biotin from LGN (right) after intravitreal NHS-biotin or saline injections. Significantly more biotin was bound to protein in NHS-biotin samples compared to background values in saline. In LGN samples, significantly more biotin was bound to protein in animals with intravitreal NHS-biotin injections compared to saline. Comparable low levels of free biotin were detected in LGN from NHS-biotin and saline injected animals, indicating that most biotin in LGN samples was bound to protein. Retina N=3, *** $p<0.001$, Two-tailed Student T-test. LGN N=4, *** $p<0.001$, Two-tailed Holm-Sidak corrected T-test. Mean +/- S.E.M. **e.** Retrograde biotin labelling with gelfoam placed directly on the SC surface. Histological sections and western blot of SC, OT, or ON taken 10 days after labeling show retrograde transport of biotinylated proteins.

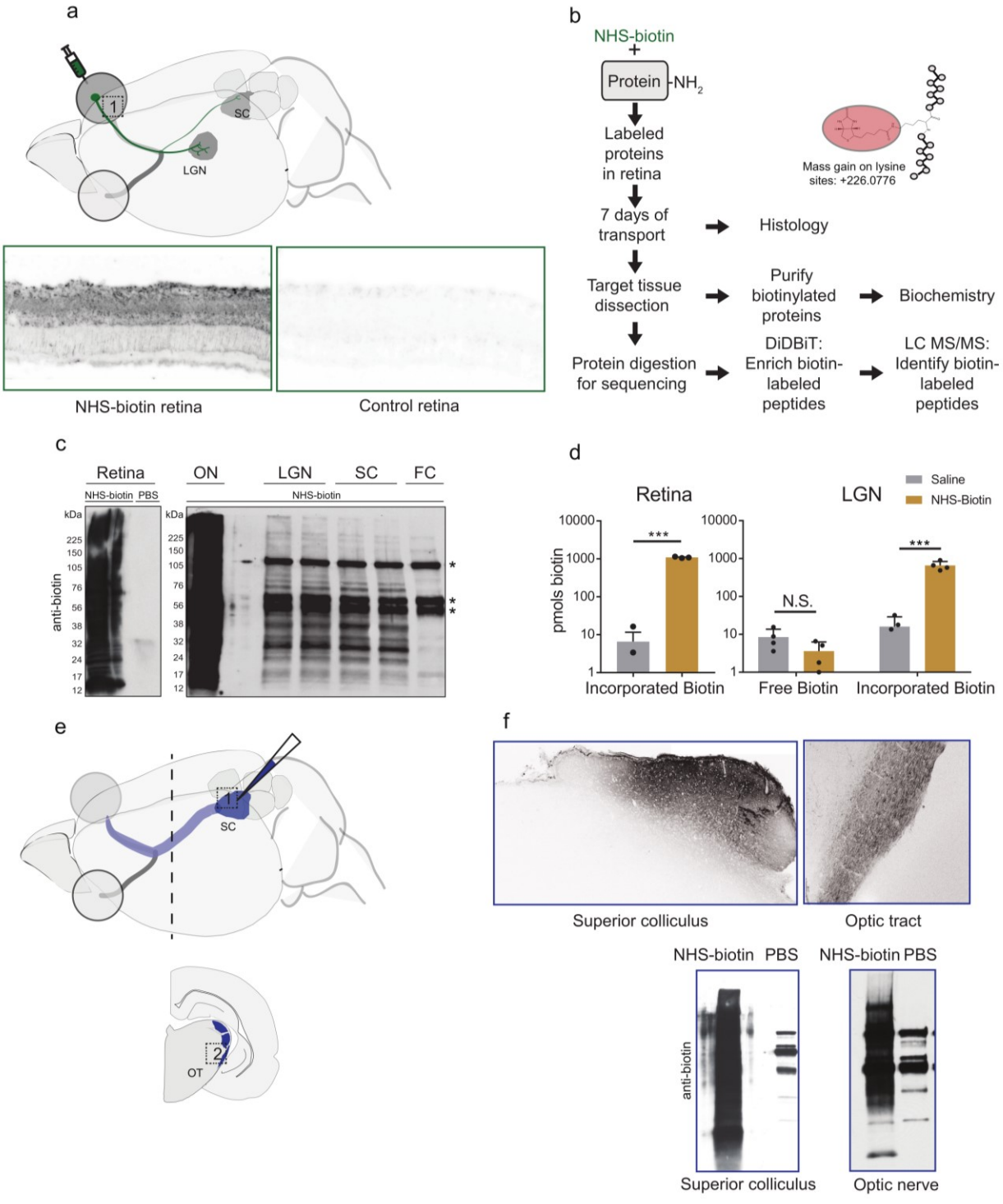
a
1
SC
LGN
NHS-biotin retina
Control retina
b
NHS-biotin
+
Protein
NH2
Labeled proteins in retina
7 days of transport
Histology
Target tissue dissection
Purify biotinylated proteins
Biochemistry
Protein digestion for sequencing
DiDBiT: Enrich biotin-labeled peptides
LC MS/MS: Identify biotin-labeled peptides
Mass gain on lysine sites: +226.0776
c
Retina
ON
LGN
SC
FC
NHS-biotin
PBS
kDa
anti-biotin
d
Retina
LGN
Saline
NHS-Biotin
pmols biotin
***
N.S.
Incorporated Biotin
Free Biotin
e
1
SC
2
OT
f
Superior colliculus
Optic tract
NHS-biotin
PBS
anti-biotin
Optic nerve

To visualize biotinylated proteins in RGC projections, we immunolabeled sagittal brain sections through the optic tract and LGN of animals that received intravitreal NHS-biotin injections with anti-biotin antibodies. Biotin-immunolabel was restricted to the optic tract and LGN (Fig 2a, b, c). No immunolabeling was seen in corresponding sections from animals that received intravitreal injections of free biotin (Fig 2c) or biocytin (biotinyl-lysine) (data not shown). Similarly, biotinylated proteins were immunolabeled in the ON of animals following intravitreal injection of NHS-biotin, but not saline (Fig 2d). We determined the ultrastructural distribution of NHS-biotin labeled proteins using immunoelectron microscopy with streptavidin coupled to HRP (Fig 2d) or 1.4 nm Streptavidin-nanoGold particles. These data indicate that biotinylated proteins in the ON were confined to RGC axons and no biotinylated proteins were detected in the surrounding myelinated sheath (Fig 2e). We observed gold particles in close apposition to axonal microtubules (Fig 2e), demonstrating the advantage of immunolabeling with 1.4 nm nanoGold particles in revealing the distribution of biotinylated proteins in the context of subcellular ultrastructure (Fig 2f). Fluorescent streptavidin labeling in sections through the LGN revealed labeled retinogeniculate axons with intensely labeled boutons (Fig 2f), indicating presynaptic accumulation of biotinylated proteins, as well as an indication of healthy RGCs after NHS-biotin injections. Immunoelectron microscopy with HRP (Fig 2h) or nanoGold (Fig 2i) identified biotinylated proteins within presynaptic terminals in LGN. These data indicate that *in vivo* protein labeling with NHS-biotin allows detection of transported proteins by biochemical analysis (Fig 1) and visualization at the light and ultrastructural levels in histological sections from the intact visual system (Fig 2). The restriction of labeling to RGC compartments gives us confidence to proceed with biochemical and proteomic analysis to discover the identity and subcellular distribution of neuronal proteins in the visual system.

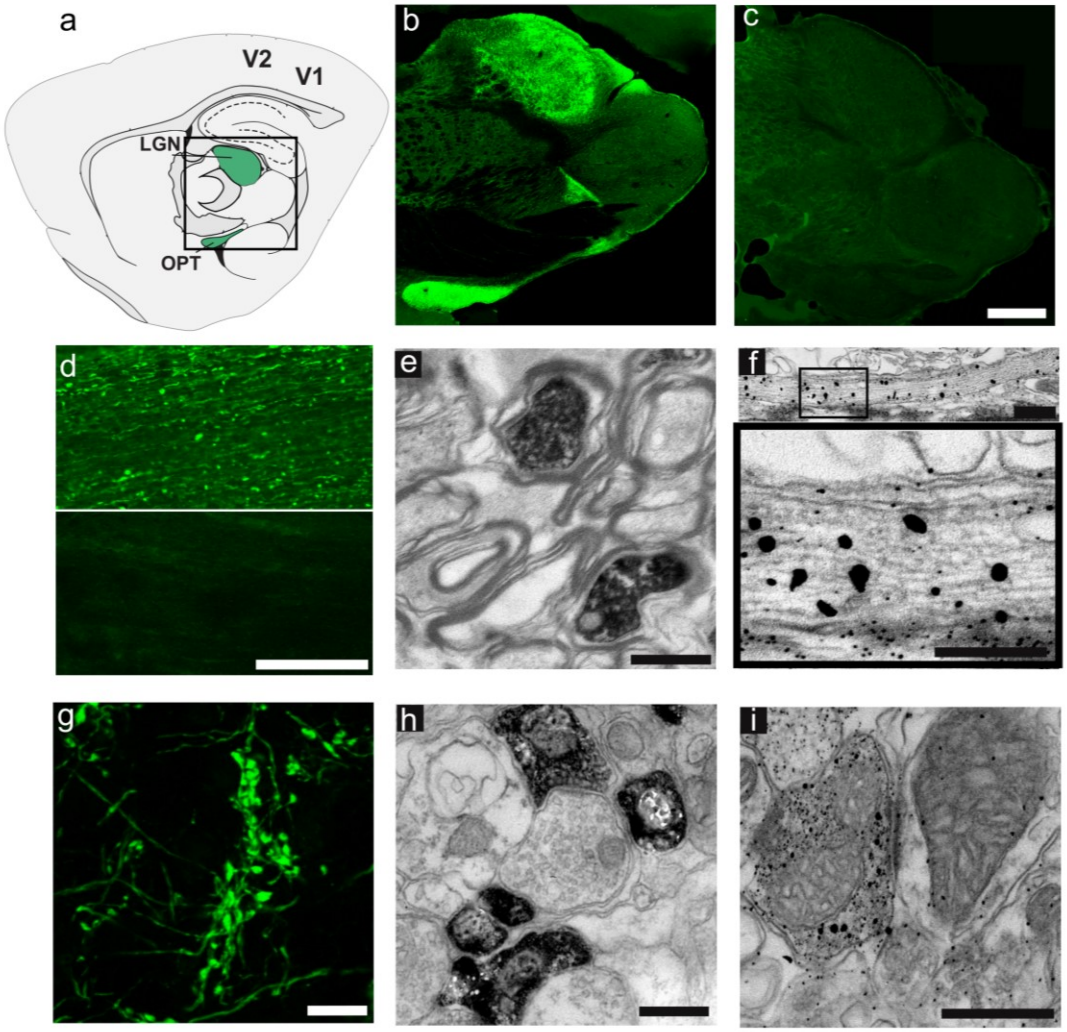

Figure 1.2. Light and electron microscope detection of transported biotinylated proteins in the visual pathway. **a.** Diagram of a sagittal section through the rat brain adapted from the Paxinos atlas showing the optic tract and LGN (green) in the central boxed region**. b, c**. Distribution of biotinylated proteins in the optic tract and LGN, detected with fluorescent streptavidin in sagittal brain sections from animals after intravitreal injection of NHS-biotin (**b**) or biotin **(c)**. Scale bar in c = 1mm, applies to b and c. **d**. Immunolabeled biotinylated proteins in the ON after intravitreal injection of NHS-biotin (top) or saline (bottom). Scale bar = 200 μm **e.** Transmission immuno-electron micrograph of a cross section through the optic tract labeled with avidin-HRP and DAB/nickel. Biotinylated proteins are contained within the axoplasm of RGC axons. Scale bar = 1 μm. **f.** Immuno-electron micrograph of a transverse section through the optic nerve labeled with streptavidin-gold plus gold enhancement showing association of biotinylated proteins with microtubules in RGC axons at low (top) and higher (bottom) magnification. **g-i**. Intravitreal NHS-biotin injections label the RGC projections in LGN. Scale bar = 500 nm **g**. Confocal single optical section of fluorescent streptavidin immunolabeled retinogeniculate axons showing intensely labeled boutons. Scale bar = 10 μm. **h, i.** Transmission immuno-electron micrographs showing the distribution of axonally transported biotinylated proteins labeled with avidin-HRP plus DAB (**h**) or streptavidin-nanoGold (**i**) in presynaptic profiles in the LGN. Scale bars = 1 μm.

Proteomic identification of the RGC transportome

Although previous proteomic analyses of retinal cells have helped determine the complement of proteins present in the retina, it is not yet known how these proteins distribute throughout the visual system. To study the population of retinal ganglion cell proteins that is transported into the ON to RGC targets, the 'RGC transportome', we analyzed biotinylated proteins isolated from retina, ON, LGN, and SC using tandem mass spectrometry (MS/MS) combined with DiDBiT, a strategy to enrich biotinylated peptides that facilitates direct MS/MS identification of biotinylated proteins (Schiapparelli et al., 2014). Eyes of adult rats were injected with NHS-biotin, as described above, and tissue from 3 groups of 10-12 animals were pooled and processed for DiDBiT and MS/MS. We detected 1765 biotinylated proteins in the retina, and 997 biotinylated proteins in the RGC transportome, pooled from ON, LGN and SC samples (Fig 3a-b and Supplementary Table 1). By considering only directly detected biotinylated peptides, with an exact mass shift of +226.0776 on lysines, we increased our confidence that the identified proteins were NHS-biotin labeled, axonally-transported proteins and not contaminants from surrounding tissue. Only 6 biotinylated proteins, corresponding to endogenously biotinylated pyruvate carboxylase, were detected in samples processed in parallel from saline injected controls. Of the 997 proteins in the RGC transportome, 272 were only detected in RGC projections (Fig 3b and Supplementary Table 1). Our ability to detect these proteins in the RGC transportome was likely due to their selective enrichment in the transportome and the decreased complexity of the transportome samples, in which only RGC axonal proteins are biotinylated compared to the mixture of biotinylated proteins from diverse cell types in the retinal sample. By isolating the axonal compartment of neurons from their somata *in vivo*, we can now ask how RGC protein distribution differs from canonical localization patterns and explore potential functions of neuronal proteins with proteomic methods.

Figure 1.3. Mass spectrometric identification of the RGC transportome. a. Diagram of the retinal projection to LGN and SC. The RGC transportome includes the biotinylated proteins transported from retina to ON, SC and LGN. **b.** Venn diagram of the population of biotinylated proteins in the retina compared to the RGC transportome. **c.** Venn diagram of the populations of biotinylated nuclear proteins found in the retina and in the RGC transportome. Nuclear proteins in RGC transportome are involved in signaling between nucleus and cytoplasm, transcriptional regulation, and RNA transport. Nuclear proteins in the retina but not in the RGC transportome are DNA interacting proteins and RNA splicing and maturation factors. **d.** Volcano plot comparing biotinylated proteins in retina and the ON transportome. Proteins marked in red are significantly different between the 2 datasets, N=3, $p<0.05$, t-test with Benjamini-Hochberg (BH) correction. Datapoints plotted on the left or right Y axes represent proteins that are only detected in one type of dataset. **e**. Ingenuity analysis of the categories of most significantly enriched protein in the RGC transportome. Proteomic data used to generate these figure panels are in Supplementary Tables 1-4. Right-tailed Fisher's Exact Test.

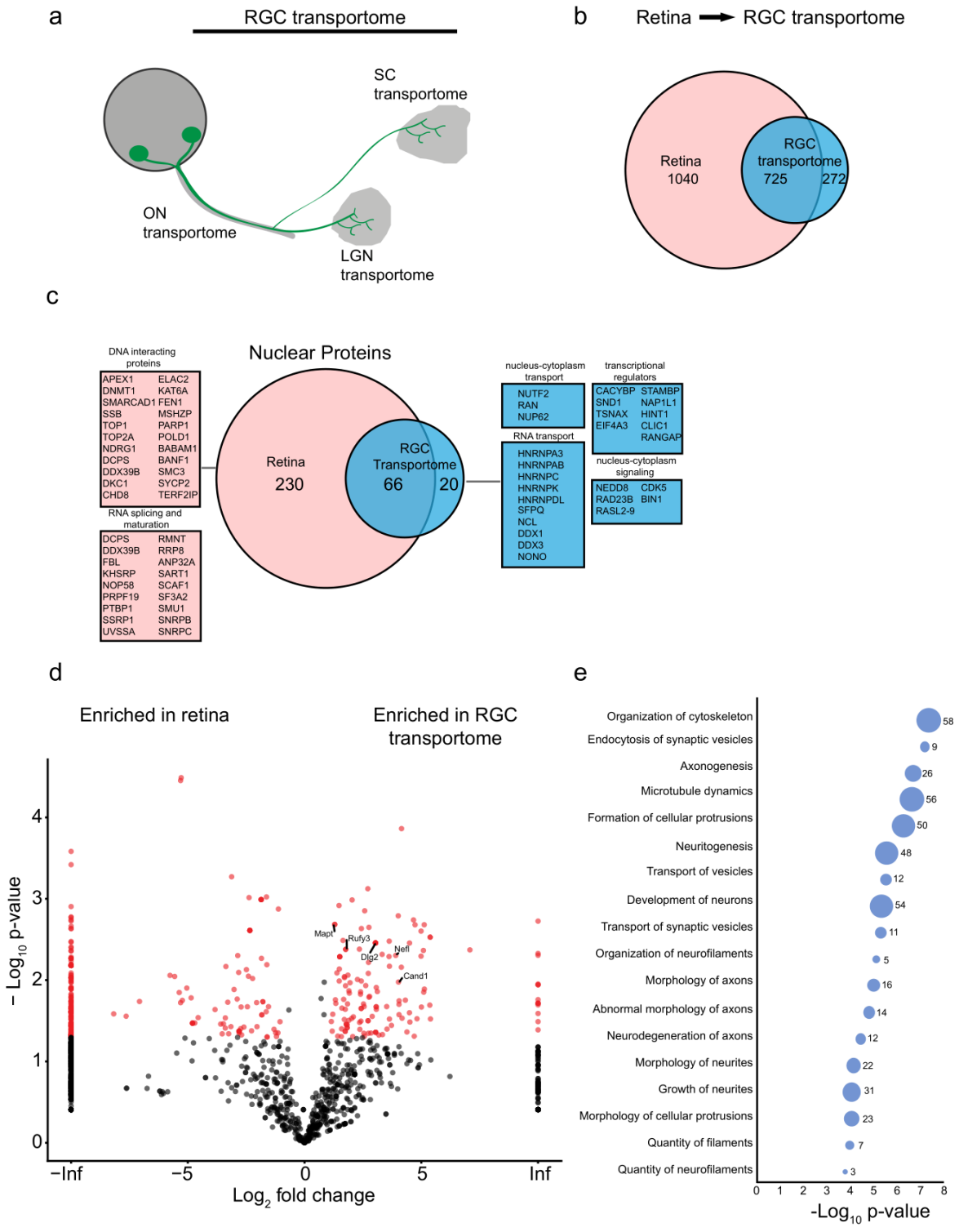
a
RGC transportome
SC transportome
ON transportome
LGN transportome
b
Retina → RGC transportome
Retina 1040
RGC transportome 725 272
c
Nuclear Proteins
DNA interacting proteins
APEX1 ELAC2
DNMT1 KAT6A
SMARCAD1 FEN1
SSB MSHZP
TOP1 PARP1
TOP2A POLD1
NDRG1 BABAM1
DCPS BANF1
DDX39B SMC3
DKC1 SYCP2
CHD8 TERF2IP
RNA splicing and maturation
DCPS RMNT
DDX39B RRP8
FBL ANP32A
KHSRP SART1
NOP58 SCAF1
PRPF19 SF3A2
PTBP1 SMU1
SSRP1 SNRPB
UVSSA SNRPC
Retina 230
RGC Transportome 66 20
nucleus-cytoplasm transport
NUTF2
RAN
NUP62
RNA transport
HNRNPA3
HNRNPAB
HNRNPC
HNRNPK
HNRNPDL
SFPQ
NCL
DDX1
DDX3
NONO
transcriptional regulators
CACYBP STAMBP
SND1 NAP1L1
TSNAX HINT1
EIF4A3 CLIC1
RANGAP
nucleus-cytoplasm signaling
NEDD8 CDK5
RAD23B BIN1
RASL2-9
d
Enriched in retina
Enriched in RGC transportome
Mapt
Rufy3
Dlg2
Nefl
Cand1
− Log10 p-value
Log2 fold change
−Inf
−5
0
5
Inf
e
Organization of cytoskeleton 58
Endocytosis of synaptic vesicles 9
Axonogenesis 26
Microtubule dynamics 56
Formation of cellular protrusions 50
Neuritogenesis 48
Transport of vesicles 12
Development of neurons 54
Transport of synaptic vesicles 11
Organization of neurofilaments 5
Morphology of axons 16
Abnormal morphology of axons 14
Neurodegeneration of axons 12
Morphology of neurites 22
Growth of neurites 31
Morphology of cellular protrusions 23
Quantity of filaments 7
Quantity of neurofilaments 3
-Log10 p-value

Nuclear proteins in the RGC transportome

The RGC transportome is enriched in proteins known to be present in axons and presynaptic terminals, including neurofilament proteins, tau, kinesins and proteins that function in vesicular transport and cycling. Recent studies have highlighted the importance of communication between the nucleus and distal processes in neurons, the most polarized cells in the body, however protein components underlying this communication are not fully known (Shigeoka et al., 2016). Surprisingly, the RGC transportome is also enriched in proteins not previously annotated to axons, including several nuclear proteins. A Venn diagram of the distribution of nuclear proteins among the biotinylated proteins in retina and the RGC transportome shows that 296 nuclear proteins were detected in retina and 86 were detected in the transportome (Fig 3c and Supplementary Table 2). Gene ontology analysis showed that nuclear proteins recovered from retina were enriched in chromatin- and chromosome-interacting proteins, whereas nuclear proteins in the transportome showed enrichment of perinuclear, cytoplasmic-nucleus and ER-nucleus interacting proteins, categories of proteins that shuttle in and out of the nucleus (Supplementary Fig 1 and Supplementary Table 3). It is possible that axonally-targeted nuclear proteins acquired distinct functions in neurons based on their distribution into cellular compartments that don't exist in other cell types. Examples of proteins annotated to the nucleus that were enriched in the RGC transportome include members of the HNRNP family. HNRNPs are a large family of proteins with known functions in splicing, mRNA stabilization and protein synthesis (Geuens et al., 2016). HNRNP K is required for axon development and regeneration (Liu et al., 2008; Liu et al., 2012), suggesting that other HNRNPs, thus far not studied in neurons, might function in axons and synapses. In addition, we identified Nucleolin and MTOR that cooperatively regulate RNA localization and translation in axons (Terenzio et al., 2018), DDX1 is involved in RNA granule transport (Kanai et al., 2004); and the small GTPase, RAN, known for its role in nucleocytoplasmic transport in non-neuronal

cells, coordinates retrograde axonal-nuclear signaling in response to axon injury (Yudin et al., 2008). We also identified transcriptional regulators, including calcyclin-binding protein CACYBP, that translocates from cytosol to nucleus in a calcium dependent manner and is involved in ERK1/2-mediated transcriptional regulation (Filipek et al., 2002; Kilanczyk et al., 2015), the transcriptional regulator SND1 (Cappellari et al., 2014), and TSNAX, which interacts with the axonal protein GAP43 and regulates transcription involved in axonal regeneration (Schroer et al., 2007). These findings provide evidence of a novel localization pattern of nuclear proteins in retinal projections which may foster discovery of previously unrecognized functions for these proteins in axons and axon terminals.

Dissection of the RGC transportome into cellular compartments: the ON transportome

The RGC transportome was pooled from ON, LGN and SC MS/MS samples. The LGN and SC samples are the biotinylated proteins in retinal terminals in each target. Here, we consider the constituent cellular compartments separately: the ON transportome, the presynaptic transportome, combined from the SC and LGN samples, and finally the separate LGN transportome and the SC transportome, providing increasing resolution of proteins in different cellular compartments of RGC projections.

The ON transportome is the population of biotinylated proteins labeled in the retina by intravitreal NHS-biotin injection and detected in optic nerve samples. We identified 844 proteins in the ON transportome by MS/MS, providing the first inventory of axonally-transported proteins from intact CNS tissue. ImmunoEM images (Fig 2) indicate that the biotinylated proteins are confined to axons. We first compared the ON transportome with biotinylated retinal proteins. The volcano plot in Figure 3d shows the $\log_2$ fold change in enrichment of normalized spectral counts for each protein in the retina and the ON transportome against the $-\log_{10}$ p-value, a measure of statistical significance. Proteins that are enriched in the transportome include MAPT (tau) as well as proteins not previously described in retinal projections: RUFY3, PSMA5, DLG2,

PARK7, ARHGDIA, and CAND1. Ingenuity Pathway Analysis of the proteins enriched in the ON transportome indicated that the top 5 most significantly enriched categories are related to diverse axonal functions: organization of cytoskeleton, endocytosis of synaptic vesicles, axonogenesis, microtubule dynamics, and formation of cellular protrusions (Fig 3e and Supplementary Table 4). Even in the adult animal, the majority of the top 20 enriched categories in the ON transportome pertain to growth, development, and morphological dynamics, consistent with the capacity for structural changes in axons in the mature visual system (Hensch and Quinlan, 2018; Stryker and Lowel, 2018).

Previous methods of isolating axonal tissue for proteomics involve either full isolation of myelin-coated nerves, or axoplasm extraction from dissected nerves (Jiménez et al., 2005; Michaelevski et al., 2010). Similarly in the optic nerve, whole tissue dissection includes the optic nerve sheath with diverse non-neuronal cell types intermingled with RGC axons. To determine the specificity of the biotinylated proteins identified in the ON transportome to just RGC axons, we compared the ON transportome to the proteome of the total dissected ON. The total dissected ON proteome consisted of 2197 proteins, of which 725 were present in the ON transportome and 154 proteins were detected in the ON transportome but not in the total ON proteome (Fig 4b and Supplementary Table 5). This increased detection of biotinylated proteins in the ON transportome, despite the significantly greater input used for the total ON proteome sample (see Methods) likely arises because biotin enrichment enhances the MS detection limit of proteins that might be diluted in the more complex total ON sample (Schiapparelli et al., 2014).

Analyzing this further, we compared replicates of the ON transportome and dissected ON proteome for the presence of markers of oligodendrocytes (MOG, MOBP, CSPG4), astrocytes (GFAP, GLAST1, GLT-1, ALDH1L1), immune cells (CD81, CD44, CD38), fibroblasts (LAMB2, CD151) and neurons (CAMKII, NEFL, NCAM). While neuronal markers and

ubiquitously expressed proteins (i.e. GADPH) were detected in both samples, astrocyte, oligodendrocyte, immune cell and fibroblast components were not detected in the ON transportome (Fig 4c,d and Supplementary Table 5). Interestingly, we detected Apolipoprotein E (APOE) in the ON transportome, as well as neuronal receptors for Apolipoproteins, LRPAP1 and VLDLR. Although APOE is of glial origin, it is released and taken up by neurons as a mechanism of lipid distribution in the brain (Vance and Hayashi, 2010). Some of the most abundant proteins in the ON transportome include Alpha Synuclein (SCNA), and the metabolic proteins GADPH, Enolase, and Aldolase (Fig 4d, Supplementary Tables 3 and 4), which provide ATP to fuel axon transport (Zala et al., 2013). We also detect and validate the presence of biotinylated MAPT, RAS, MTOR, PSMD2, GAPDH, ALIX, and CAMKII in the ON after intravitreal NHS-biotin, but not saline, injection (Fig 4e). Together, these results demonstrate the specificity of *in vivo* biotinylation to identify the axonal proteome of a specific cell type, RGCs, from intact complex tissue without requiring isolation of cells of interest.

Figure 1.4. Characterization of the optic nerve transportome. **a**. Diagram of the retinal projection to LGN and SC, highlighting the tissue source of the ON transportome. **b**. Venn diagram comparing the MS/MS datasets of the total dissected ON ("Total ON") from animals without NHS-biotin label and the ON transportome from animals with intravitreal NHS-biotin label. The Total ON proteome includes proteins from all cell types in the ON (fibroblasts, oligodendrocytes, endothelium, immune cells, and astrocytes). **c.** Table of the spectral counts for proteins from different cell types in the Total ON proteome and ON transportome. The ON transportome does not contain any proteins that serve as unique identifiers of non-neuronal cell types seen in the Total ON proteome. **d**. Volcano plot comparing the Total ON and ON transportome shows significant enrichment of some neuronal proteins in the ON transportome and a large population of proteins in the Total ON that are not in the ON transportome. N=3, $p<0.05$, t-test with BH correction. **e**. Western blot validation of proteins in the ON transportome. Western blots of input protein (Left) and neutravidin purified proteins (Right) comparing immunolabel in ON from animals with intravitreal injection of NHS-biotin and control. TAU, RAS, MTOR, PSMD2, GAPDH, ALIX, and CaMKII are enriched in IPs from animals that received NHS-biotin and not in control animals. Experiment were done in triplicate.

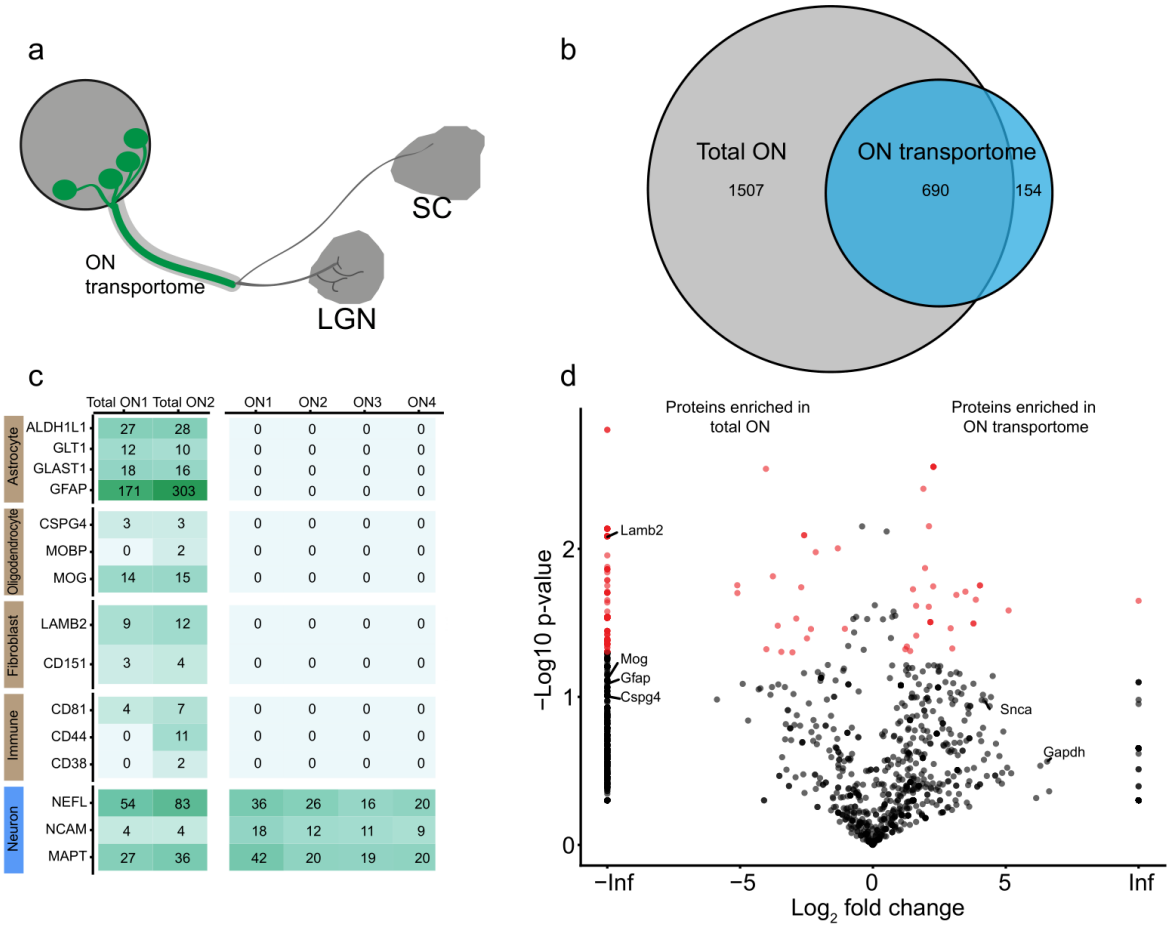
a
SC
ON
transportome
LGN
b
Total ON
1507
ON transportome
690
154
c
Total ON1 Total ON2 ON1 ON2 ON3 ON4
Astrocyte
ALDH1L1 27 28 0 0 0 0
GLT1 12 10 0 0 0 0
GLAST1 18 16 0 0 0 0
GFAP 171 303 0 0 0 0
Oligodendrocyte
CSPG4 3 3 0 0 0 0
MOBP 0 2 0 0 0 0
MOG 14 15 0 0 0 0
Fibroblast
LAMB2 9 12 0 0 0 0
CD151 3 4 0 0 0 0
Immune
CD81 4 7 0 0 0 0
CD44 0 11 0 0 0 0
CD38 0 2 0 0 0 0
Neuron
NEFL 54 83 36 26 16 20
NCAM 4 4 18 12 11 9
MAPT 27 36 42 20 19 20
d
Proteins enriched in total ON
Proteins enriched in ON transportome
Lamb2
Mog
Gfap
Cspg4
Snca
Gapdh
−Log10 p-value
Log2 fold change
−Inf
−5
0
5
Inf
e
Input
Biotin purified
NHS-biotin Control
kDa
TAU
RAS
MTOR
PSMD2
GAPDH
ALIX
CaMKII

.

Distribution of proteins into subcellular compartments: Analysis of the presynaptic transportome

Neurons are highly polarized cells with diverse subcellular compartments, such as pre- and postsynaptic elements and the axon initial segment, which are thought to be composed of uniquely localized proteins. Understanding neuronal function and the contributions of subcellular specializations to neuronal and circuit function requires an accurate assessment of protein components and their distribution in neurons. Therefore, we next asked if subsets of proteins in the RGC transportome were specifically enriched in presynaptic terminals. To identify these molecular components, we compared proteins recovered from retinal targets SC and LGN, the presynaptic transportome, to those recovered from the ON transportome. Comparing this dataset of 576 proteins in the presynaptic transportome to the dataset of 844 proteins in the ON transportome, we found that half (421) are detected only in ON transportome and half (423) overlap between the ON and presynaptic transportome datasets. 153 proteins in the presynaptic transportome were not detected in the ON transportome, likely due to the relative enrichment of these latter proteins in the presynaptic compartment (Fig 5a and Supplementary Table 6). Proteins detected in the presynaptic transportome include components of the core synaptic vesicle fusion machinery, and known synaptic proteins, such as VAMP proteins, Synaptophysin, RAB3 isoforms, Synapsin 1, Syntaxin 1b (Fig 5a, and Supplementary Table 6). We compared the ON and the SC transportome in a volcano plot, as described previously (Fig 5b). In addition to proteins detected uniquely in the ON or SC transportomes, proteins enriched in the SC transportome include mitochondrial proteins, the guanine nucleotide-binding protein, GNAO1, whereas those significantly enriched in the ON transportome include NEDD8, Actin, and microtubule associated proteins (Supplementary Table 7).

We compared results from our strategy of protein labeling and proteomic analysis of transported biotinylated proteins recovered from presynaptic compartments in intact brain

circuits with the current public knowledgebase of presynaptic proteins, compiled from published studies and proteomic resources of synaptosomes, presynaptic proteins, presynaptic active zone and synaptic vesicles from heterogeneous samples (Bayes et al., 2011; Pirooznia et al., 2012). We determined the fraction of biotinylated proteins in the retinal, ON and presynaptic proteomes that were also present in the public database of presynaptic proteins and calculated their enrichment in the ON and presynaptic transportomes compared to the retina (Fig 5c). About 15% of biotinylated retinal proteins were annotated as presynaptic proteins, increasing almost 2.5-fold in the presynaptic transportome compared to the biotinylated retinal proteome. As secondary validation, we detected biotinylated MTOR, MUNC18, and ALIX in the SC only after NHS-biotin injections. Additionally, we found co-localization of biotin and both Synaptotagmin-1 and ALIX in the LGN by immunofluorescence, showing their presence in RGC boutons. These data indicate that presynaptic proteins are biotinylated in the retina and become progressively more enriched in the ON and presynaptic transportomes, suggesting specific transport to and retention in presynaptic compartments.

We next compared the dataset of our 576 proteins in the presynaptic transportome with the 462 proteins in the public presynaptic databases to better understand how our *in vivo* findings match prior efforts to dissect the presynaptic complex. We find that 192 proteins overlap between our presynaptic transportome and the public presynaptic database, while 384 proteins in the presynaptic transportome were not previously annotated as presynaptic proteins (Fig 5d and Supplementary Table 8). Many of the proteins present in both datasets have been described as playing diverse roles in the presynaptic compartment, such as vesicular transport and sorting, synaptic vesicle exocytosis and endocytosis, and adhesion to postsynaptic compartments. The proteins detected in the presynaptic transportome, but not present in the presynaptic databases, constitute a new population of proteins that we have localized to presynaptic compartments in the retinogeniculate and retinocollicular projections. Exploring this

dataset will provide new insights into proteins targeted to axons and/or presynaptic compartments in the visual pathway. The biological functions of many of these proteins have been described, largely based on data from non-neuronal cells, as playing roles in vesicle sorting, recycling, transport, and secretion; local protein translation; transcriptional regulation; protein transport; membrane adhesion, and RNA transport, all of which may occur in presynaptic compartments. In addition, 270 proteins annotated to the public presynaptic database were not detected in the biotinylated presynaptic transportome of glutamatergic RGCs. These include proteins from non-glutamatergic presynaptic compartments, such as GAD1 and GAD2 (from GABAergic presynaptic neurons), which can be detected in total LGN proteomics where isolation of a subtype of excitatory terminals is difficult (Supplementary Table 8). This indicates that our methodology allows the characterization of specific types of presynaptic compartments, which cannot be otherwise achieved by subcellular fractionation of intact brain tissue.

Finally, we compared our datasets with a PSD-enriched proteomic dataset, consisting of 983 proteins (Bayes et al., 2011; Pirooznia et al., 2012). About 25% of the biotinylated retinal proteins are annotated as postsynaptic proteins, and this representation was enriched ~1.5-fold in the presynaptic transportome (Supplementary Fig 2 and Supplementary Table 8). Some classical excitatory and inhibitory postsynaptic proteins such as glutamatergic/GABAergic receptor subunits and postsynaptic scaffolding proteins including GRIP2, Homer, and Gephryn were only detected in the biotinylated retinal samples but not in the RGC transportome. These data are consistent with the hypothesis that proteins transported from the retina into axons would segregate pre- from postsynaptic proteins. Some of the proteins in the RGC transportome that overlap with the PSD dataset are also annotated as presynaptic proteins, such as SYT1, STX1B, STX1BP, NSF, SNAP25 (Supplementary Table 8). These proteins support vesicle fusion in both pre- and postsynaptic compartments (Shimojo et al., 2015; Steinberg et al., 2004),

suggesting that the RGC transportome dataset may identify proteins that have more diverse functions in neurons than previously thought. For instance, PSD93 (DLG2), which is part of the postsynaptic scaffold, was present in the ON transportome, consistent with data showing that PSD93 also scaffolds KV1 channels at axon initial segments (Ogawa and Rasband, 2008), which could be captured in the ON transportome. Given the paucity of data about protein localization in the visual system, let alone neuronal compartments in general, these data dissect the various compartments of the RGC transportome using a suite of novel methods for unbiased protein labeling and MS/MS analysis for discovery and initial characterization of proteins from a uniform neuron cell type in the intact brain.

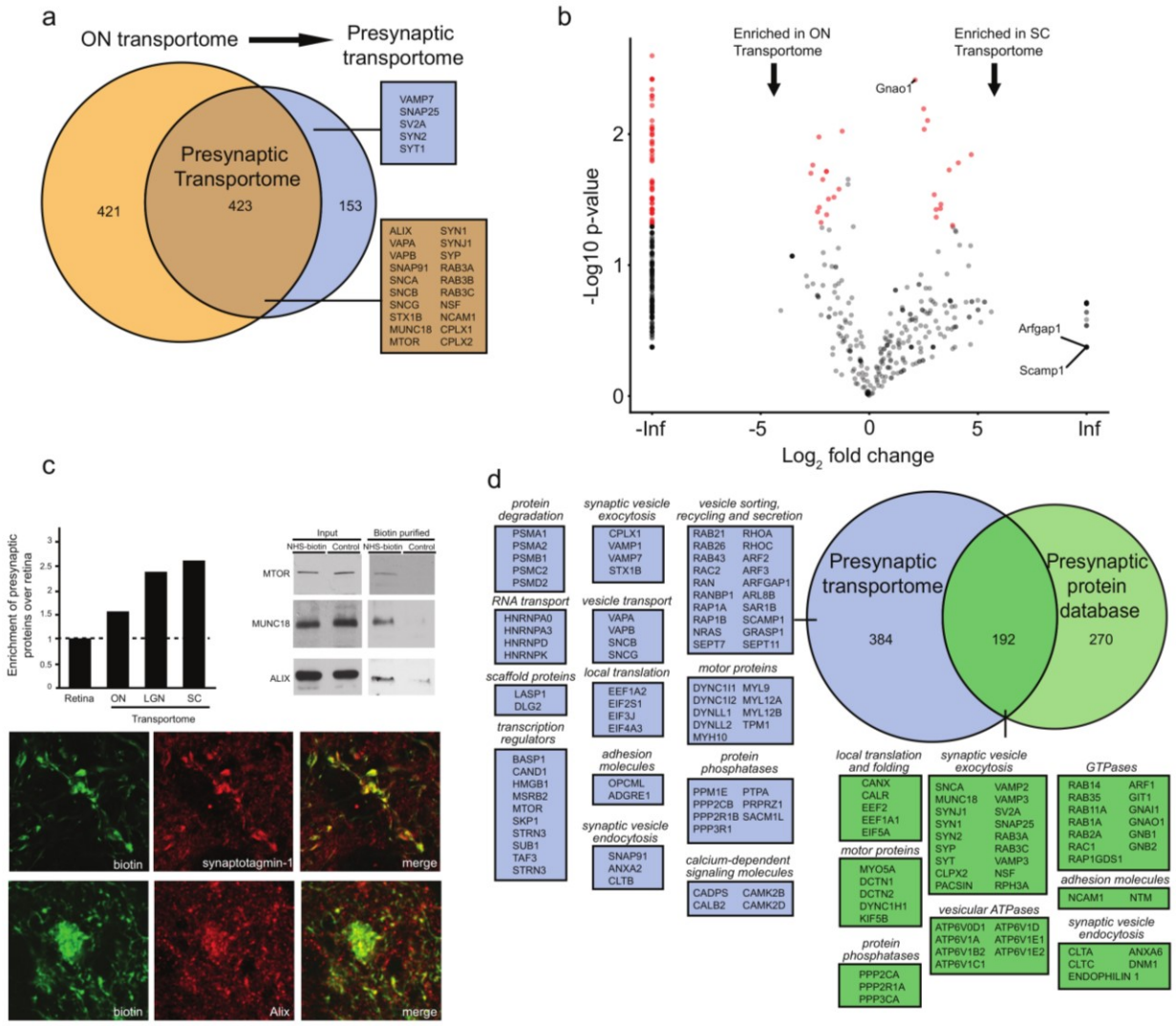

Figure 1.5. Analysis of the presynaptic transportome. a. Venn diagram comparing the ON transportome and presynaptic transportome. The presynaptic transportome contains many classical presynaptic proteins involved in the presynaptic machinery for neurotransmitter release. **b**. Volcano plot comparing protein abundance in the ON transportome and the SC transportome. Significant protein enrichment is highlighted in red. Datapoints plotted on the left or right Y axes represent proteins that are only detected in one type of dataset. N=3, $p<0.05$, t-test with BH correction. **c**. Enrichment of proteins in the annotated presynaptic protein databases in the presynaptic transportome compared to the ON transportome and retina. Western blot validation of biotinylated proteins at presynaptic sites in dissected SC tissue, with neutravidin enrichment of MTOR, MUNC18 and ALIX in NHS-biotin treated animals vs control. SC tissue from 3 animals was pooled per sample. Experiments were done in triplicate. Confocal images of coronal sections of LGN from animals with intravitreal administration of NHS-biotin show labeled biotinylated proteins (green) in RGC presynaptic boutons, with either endogenous Synaptotagmin 1 or ALIX (red). Images show colocalization of endogenous proteins with biotin label in presynaptic boutons. Scale bar= 50 μm. **d**. Venn diagram comparing the presynaptic transportome with public databases of presynaptic proteins. The proteins detected only in the presynaptic transportome include those that function in vesicle trafficking, as well as those involved in proteostasis.

Analysis of transportomes to different retinal targets

The retina projects to over 30 distinct targets in the CNS, each thought to have distinct functions (Dhande et al., 2015; Martersteck et al., 2017). The extent to which diverse functions in different retinal targets are subserved by distinct proteins remains unknown. To address this question, we first can compare proteins targeted to different retinal projections. Immunolabeling transported biotinylated RGC proteins in LGN and SC indicates that retinogeniculate inputs are more densely clustered than retinocollicular inputs (Fig 6a), consistent with previous reports (Hooks and Chen, 2006). While the mechanisms behind these different synaptic structures is not completely understood, we hypothesized that differential trafficking of proteins from the cell body to specific presynaptic terminals could contribute to maintaining that specific synapse. When we compared the LGN and SC transportomes, we identified 216 proteins that were transported to both LGN and SC, 238 proteins that were preferentially transported to LGN, and 122 proteins that are preferentially transported to SC (Fig 6a and Supplementary Table 9). Although more than 75% and 86% of proteins in LGN and SC transportomes, respectively, were also detected in ON transportome, some proteins were identified in the SC and LGN transportomes alone, likely because of their enrichment in the target areas as mentioned above (Fig 5a). The unique members of the retinogeniculate and retinocollicular transportomes may be involved in distinct presynaptic functions in these two retinal targets. For instance, the ARF and RHO GTPase families, which regulate membrane and vesicle fusion at presynaptic sites (Binotti et al., 2016) are selectively enriched in the SC and LGN transportomes, respectively (Figure 6b, Supplementary Table 9). These data suggest that presynaptic release and plasticity at SC and LGN retinal projections could be regulated differently, consistent with the distinct functions of LGN and SC in visual information processing (Hong et al., 2014; Kay and Triplett, 2017; Moore et al., 2005; Stein and Rowland, 2011; Stein et al., 2014; Suresh et al., 2016). Indeed, validation of differential protein transport by western blotting confirmed enrichment of transported

Complexin 1/2 in the LGN compared to the SC, and enrichment of transported MTOR in the SC compared to LGN (Figure 6c,d). These results show that target-specific transportomes from a common source may provide information about the diversity of presynaptic inputs and facilitate hypothesis generation regarding circuit function.

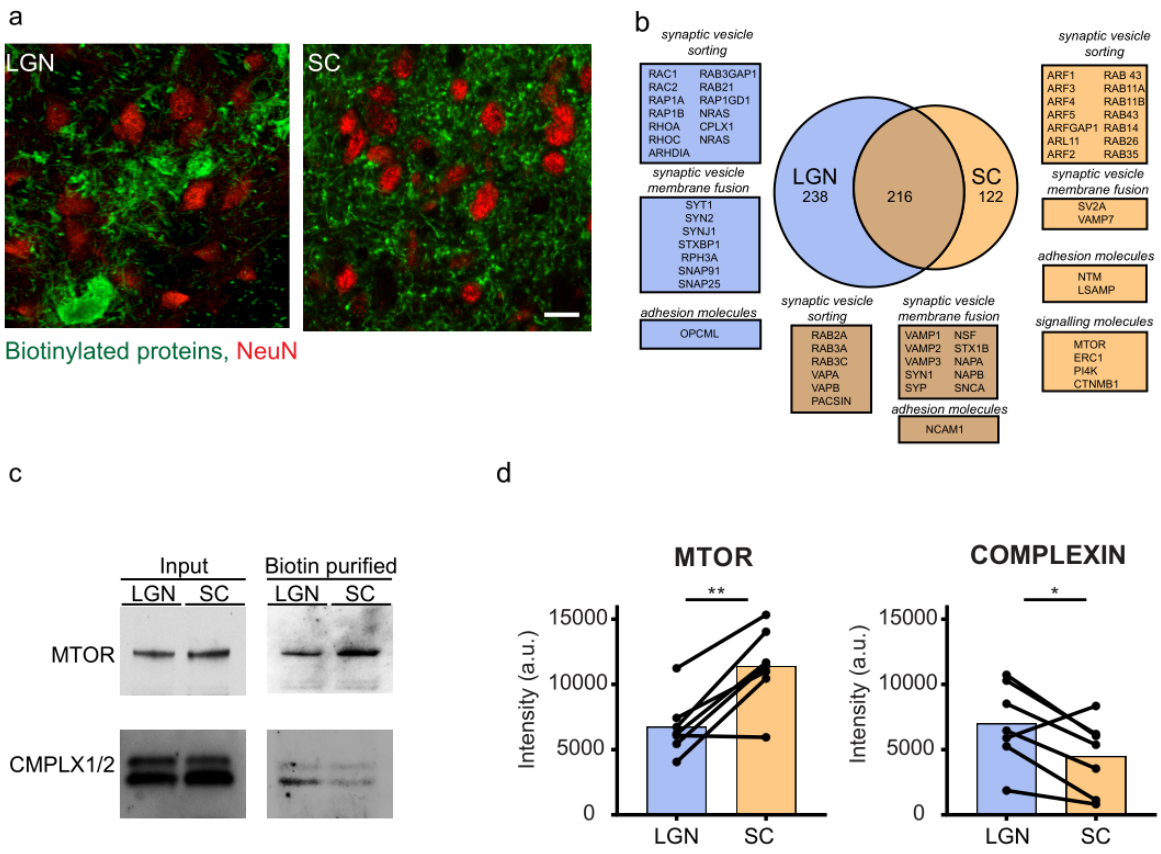

Figure 1.6. Comparison of LGN and SC transportomes a. Confocal single optical sections through the LGN (left) and SC (right) showing the distribution of biotinylated proteins (green) in characteristic clustered presynaptic profiles in LGN and more evenly distributed presynaptic profiles at superficial layers of SC. Local neuronal somata in the LGN and SC were labeled with NeuN antibodies (red). **b.** Venn diagram of the LGN and SC transportomes shows that proteins unique to each transportome include different families of GTPases. c-d. Western blot validation of biotinylated proteins at either SC or LGN. Neutravidin enrichment of both samples showed an enrichment of MTOR in the SC, and CMPLX1/2 in the LGN. Quantification of samples done using normalized optic density of each blot. MTOR N=7, ** p=0.005, COMPLEXIN N=7, * p=0.03, Two-tailed Student T-test.

Discussion

Here we show that combining an *in vivo*, spatially-targeted protein labeling strategy with histological, biochemical and proteomic analysis of labeled proteins provides the opportunity to visualize and identify endogenous transported proteins throughout the visual system. This is the first cell-type-specific proteomic study of axonal projections in the intact brain, using RGC projections in the visual system to study differential transportomes between targets.

Previous studies in multiple species labeled retinal proteins with radioactive amino acids to trace axonal transport (Grafstein and Forman, 1980). However, these methods did not allow purification of labeled proteins and limited identification of radiolabeled proteins to a candidate-based approach, and may have also been confounded by recycling of radioactive amino acids into new proteins locally or even in adjacent (e.g. post-synaptic) cells (Grafstein and Forman, 1980). Since in our experiments biotinylated proteins cannot be recycled (Gallivan et al., 1997; Watanabe et al., 2007), confidence is increased that the biotinylated proteins are only drawn from those transported from the retina to the presynaptic retinogeniculate and retinocollicular compartments. Other targeted protein labeling strategies, such as proximity-based biotin-tagging, have been invaluable for studying subcellular and molecular phenomena, such as proteomic characterization of organelles or synaptic cleft proteins in reduced experimental systems (Loh et al., 2016; Rhee et al., 2013), however, these have not yielded the breadth of the protein transportome as in this new approach. Proteins in synaptic compartments in the brain have been analyzed by brain homogenization and subcellular fractionation of synaptosomes, yet contamination of the isolated synaptic compartments with other cellular structures, such as astrocyte end feet (Pielot et al., 2012), or lack of efficient protein extraction from the isolated subcellular compartments limit our understanding of the molecular organization of these specialized neuronal structures. On the other hand, our system has little to no contamination from extra-cellular sources confirmed by the exclusion of non-neuronal cell

markers in the ON transportome that were enriched in total ON tissue (Fig 3, 4), by the enrichment of neuronal and synaptic proteins in the transportome (Fig 5) and by the exclusion of inhibitory synaptic proteins (such as GAD1 and GAD2, markers of GABAergic synapses) in the presynaptic transportomes (Fig 5, Supplementary Tables 8). In this manner, we solved a common problem of contaminant proteins in the analysis of compartment-targeted proteomics, which bedevils studies of biotinylated proteins (Alvarez-Castelao et al., 2017) and subcellular fractionation strategies (Pielot et al., 2012).

Strategies similar to ours have demonstrated spatial, temporal and genetic control over analysis of newly synthesized proteins (Alvarez-Castelao et al., 2017; Cagnetta et al., 2018; Liu et al., 2018; Schanzenbacher et al., 2016; Shigeoka et al., 2018), although the modification used here with NHS-biotin greatly increases protein labeling and detection by removing the dependence on new protein synthesis, and thus allow much greater protein recovery and thereby the unbiased study of protein transport. Indeed the breadth of protein ontologies detected yielded interesting and in some cases surprising identification. For example, we detected nuclear proteins in the RGC transportome that are known to shuttle between the nucleus and cytoplasm in non-neuronal cells (Kanai et al., 2004; Liu et al., 2012; Terenzio et al., 2018; Yudin et al., 2008). Such findings including validation of identity and function that could be carried forward into future work, support the premise that such *in vivo* protein labeling and analysis will be valuable for unbiased discovery of proteins involved in diverse neuronal functions.

The visual system, and the nervous system in general, relies heavily on compartmentalized signaling and long-distance communication to link together complex circuits for information transmission. Given the different roles that the LGN and SC play in visual processing, investigating differentially transported proteins could provide insight into distinct functions of these brain areas. The retinogeniculate synapse transforms RGC action potentials

into LGN neuronal firing patterns, yet the post-synaptic spike trains do not faithfully resemble the pre-synaptic signals, both *in vivo* and in slice electrophysiology (Blitz and Regehr, 2003; Usrey et al., 1999). Although AMPA and NMDA receptor dynamics affect how the post-synaptic cell represents RGC action potentials (Blitz and Regehr, 2003), less is known about how presynaptic modulation affects signal transduction. Through target-specific RGC transportomics, we found a significantly higher transport of Complexin 1/2 to the retinogeniculate synapse than the retinocollicular synapse. In cultured cortical neurons, knockdown of Complexin 1/2 decreased fast synchronous synaptic vesicle fusion and increased spontaneous fusion (Maximov et al., 2009). If we extend this prediction to the intact visual system, we hypothesize the enrichment or lack of Complexin 1/2 contributes towards differential Ca^{2+}-dependent vesicular release, influencing the divergent postsynaptic responses in LGN and SC. Further exploration of the differential transport of other synaptic vesicle regulators, as discovered through transport proteomics presented here, will help define the molecular foundation of differential synaptic transmission.

Dissecting target-specific protein transport of RGCs also informs strategies for regenerating axons after injury. After optic nerve crush, RGCs fail to regenerate their axons and die, eventually leading to blindness. However, RGCs can regenerate their axons after MTOR pathway activation and visual stimulation, reaching multiple brain targets including SC, LGN, and others. Nonetheless, functional behavioral recovery was only seen in the retinocollicular and oculomotor brainstem, and not in the retinogeniculate pathway (Lim et al., 2016). While true that the looming avoidance task which depends on the retinocollicular circuit does not require visual cortex (Dhande et al., 2015; Lim et al., 2016), while the visual cliff test of retinogeniculate function does (Leamey et al., 2007), our transportome finding of MTOR detection and enrichment in the SC over the LGN terminals leads to a hypothesis of biased recovery of RGC pathways towards those that transport MTOR over others. Significant advances in our

understanding of the consequences of impaired protein transport between different neuronal compartments in neurological diseases, including axon transport deficits in neurogenerative diseases (Devine et al., 2016), highlight the requirement of proper intracellular distribution of proteins for brain function. In fact, we now further hypothesize that functional recovery of additional visual pathways will require re-establishment of key protein transport to each specific RGC terminal.

While we establish marked differences in protein transport from the retina to two target regions in the brain, it is not known if these differences are due to transport regulation at branch points of individual RGCs, or differences in projection patterns of RGC subtypes. Transportomics of RGC subtypes by genetic labeling (Dhande et al., 2015; Huberman et al., 2008) and differences in presynaptic protein complements of dual-projecting RGCs will advance our understanding of mechanisms underlying RGC target specification, signal transduction, and maintenance. Deeper understanding of the pathways regulating differential transport may lead to novel understanding of wiring in the visual system as well as target-specific transport regulation. In fact, in addition to providing new information on the identity of proteins transported from RGC cell bodies into different cellular compartments, these data spark hypothesis-generating insights into the protein components underlying structure and function of neuronal circuits.

Materials and Methods

In vivo biotinylation of retinal proteins

Male Sprague Dawley rats (30-45 day old) were used for all experiments. Five milligrams of NHS-biotin (EZ-Link® from Pierce) were dissolved in 300 μl of sterile DMSO immediately before eye injection. NHS-biotin covalently attaches biotin to lysines and N-terminals of proteins. In the event of degradation of biotinylated proteins, the biotin cannot bind to other proteins because the succinimide group is quenched after reacting with amino groups,

and because the free biotin-labeled amino acids such as biotinyl-lysine cannot be used for synthesis of new proteins by endogenous protein synthesis machinery (Gallivan et al., 1997; Watanabe et al., 2007). Intravitreal injections of 5 μl, were given to one or both eyes, depending of the experiment, using a microinjector pressure system (Picosprizer II) with a pulled glass micropipette. The procedure was repeated once a day over 7 days under deep anesthesia with 0.5 mg/kg Medetomidine and 75mg/kg ketamine *ip*. The eyes were treated with topical antibiotics and analgesics and examined daily. Control animals were injected following the same protocol with biotin (from Pierce) dissolved in sterile DMSO or with PBS. 15-20 days after the first injection, rats were divided into different 2 groups: 1. Rats were euthanized with CO_2, and decapitated for brain removal. The tissue was frozen immediately in isopentane in dry ice and stored at -80°C for biochemistry studies. 2. Animals were perfused with PBS and then with 4 % PFA in 0.1 M phosphate buffer. Tissue was cut into 50 μm sagittal or coronal sections using a vibratome (Leica) and stored in PBS at 4°C for immunofluorescence studies. For electron microscopy, animals were perfused with cold artificial cerebrospinal fluid (ACSF) and then cold 4 % PFA plus 0.1 % glutaraldehyde in 0.1 M phosphate buffer and sectioned with a vibratome as above.

Biotin Measurements

Unincorporated free biotin and biotin incorporated to proteins were measured using a Fluorescence Biotin Quantitation Kit (Thermo) and a fluorescence plate reader (Synergy Mx Microplate Reader, Biotek) by measuring fluorescent excitation/emission at 495/520 according to manufacturer's instructions. Dissected samples from retina and LGN from 6 animals were weighed and pooled. Protein extracts were generated by homogenizing and sonicating 122 mg of wet tissue from LGN or retina in 1ml of 1 mM EDTA, 50 mM Tris, pH7.5 (TE) buffer and centrifuged at 10,000 g for 15 min at 4° C to remove nuclei and cell debris. The lysates were mixed with 4 ml of cold acetone, incubated at -20° C overnight and centrifuged for 1 h at 4500 g

in a swinging bucket rotor to precipitate proteins. Supernatants were collected and evaporated to a volume of ~20 μl in a SpeedVac concentrator (Thermo Scientific) and protein pellets were solubilized in RIPA buffer. As a standard, we used a series of biocytin dilutions (from 0.5 to 10 pmol/μl) according to the manufacturer's instructions.

Immunohistochemistry in rat brain sections

Sagittal or coronal 50 μm sections containing optic tract, LGN or SC were quenched with 1% Sodium borohydrate for 5 minutes and blocked for 1 h with 3 % normal donkey serum and 0.3 % Tween 20 in PBS (PBST). Sections were incubated overnight at 4°C with the following primary antibodies:1:500 Goat anti-biotin (Pierce), 1:200 mouse anti-MAP2 (Chemicon), 1:200 mouse anti-NeuN (Millipore), 1:500 rabbit anti-Alix, 1:500 mouse anti-Synaptotagmin (Millipore). After three washes in PBST, sections were incubated in secondary antibodies (1:200 dilution of anti-goat alexa 488 or anti-mouse alexa 564 (Invitrogen)) for 1 hour at room temperature in blocking buffer. Sections were mounted in Vectashield mounting medium (Vector Labs) and images were collected using a Spinning disc confocal (Ultraview VOX, Perkin Elmer) or a laser scanning confocal (Olympus FV500) microscope.

Electron Microscopy

Detection of biotinylated proteins in the retinogeniculate pathway: Sagittal or coronal 50 μm vibratome sections through LGN were incubated with 100mM glycine in PBS for 2 h and endogenous peroxidase activity was blocked with 0.5% of H_2O_2 and 1% normal goat serum (NGS) in PBS for ½ hour. Sections were blocked with 10% NGS in PBS for 1 h and incubated overnight with ABC reagent (1 drop of A and 1 drop of B in 5 ml PBS with 1% NGS, Vector Lab). Signal was amplified using tyramide amplification system (TSA kit (Perkin Elmer)) and detected by diaminobemzidine reagent (DAB, SigmaFast™) with nickel enhancement. In some sections, biotinylated proteins were labeled by overnight incubation with 1:100 streptavidin-nanoFluorogold 1.4 nm particle size (Nanoprobes) in 1% NGS and 0.001 % Triton x (Roche),

postfixed for 20 min in Karnovsky fixative, containing 4% paraformaldehyde, 5% glutaraldehyde in PBS, and enhanced for visualization with Goldenhance kit (Nanoprobes) as described (Schikorski, 2010). Sections that contained labeled retinogeniculate axons with DAB or gold particles were then postfixed with 1% OsO_4 in PBS for 1 h, dehydrated in ethanol series in water (50%, 70% with 4% uranyl acetate, 90%, 100%), washed 3 times with pure acetone and flat embedded in epoxy resin (Embed-812, Electron Microscopy Sciences) between two sheets of Aclar plastic (Electron Microscopy Sciences) and polymerized in a vacuum oven overnight at 60 ℃.

Western blots

To purify biotinylated proteins for western blot validation, 0.8-2 mg of proteins from ON, LGN, SC or retinal homogenates in a total volume of 1 ml were incubated with 30 μl neutravidin beads (Thermo) at 4°C overnight. The beads were then washed 6 times with 1 ml of RIPA buffer. The bound biotinylated proteins where eluted from the beads with 50 μl Laemmli sample buffer containing 2.5% of 2-mercaptoethanol. Eluates containing purified biotinylated protein were loaded onto 4-20% SDS/PAGE gradient gel (TGX, Bio-Rad). Proteins were separated by electrophoresis, transferred to nitrocellulose membranes (Bio-Rad) and incubated for 1 h in blocking buffer containing 0.05% Tween 20, 20 mM Tris.HCl, 133 mM NaCl, pH7.4 (TBST) and 5% non-fat milk. The membranes were then incubated in blocking buffer for 24 h with the following antibodies: 1:1000 goat anti-biotin antibody (Thermo); 1:1000 mouse anti-Tau 1 (Millipore); 1:1000 rabbit anti-Alix (Millipore); 1:1000 mouse anti-mTOR (Cell Signaling), 1:500 rabbit anti-Ras (Abcam); 1:1000 rabbit anti-Munc18 (Sigma). Membranes were washed 3 times for 10 min in TBST and incubated in blocking buffer at room temperature for 1 h with a 1:1600 anti-mouse, anti-rabbit or anti-goat secondary antibodies conjugated with HRP (Bio-Rad). Bands were detected by chemiluminescence using ECL western blotting substrate® or

SuperSignal West femto® (Pierce) and KodaK Biomax XAR films. Quantification of optical densities of the bands was made using ImageJ software.

Sample processing for direct identification of biotin labeled proteins using DiDBiT

For mass spectroscopy, tissue samples from 10 to12 brains were pooled for total protein extraction. Retinas, ON, SC, LGN and FC were dissected from fresh brain and homogenized in cold lysis buffer containing 150 mM NaCl, 50 mM TrisHCl pH7.4, 1% NP40, 0.5% sodium deoxycholate, 0.1% SDS and protease inhibitor Cocktail (Complete® from Roche). The protein homogenates were briefly sonicated, rotated for 1 h at 4°C and centrifuged for 15 min at 10,000 g at 4°C. Supernatants were collected and protein concentration was measured by DC Protein Assay kit® (Bio-Rad).

For direct identification of biotinylated proteins, we followed the DiDBiT protocol (Schiapparelli et al., 2014). Tissue samples were collected from 10 to 12 animals administrated intravitreal NHS-biotin or saline, pooled and homogenized in RIPA buffer as described above. Protein was quantified and precipitated by adding 3 volumes of methanol, 1 volume of chloroform and 3 volumes of water, vortexed and centrifuged at 15,000 g for 2 min at room temperature. The aqueous and organic phases were removed carefully from the tube without disturbing the protein disc at the interface. Protein pellets were washed once in methanol, air dried for 10 min and resuspended the in 200 µl of a buffer containing 4 M urea, 50 mM NH_4HCO_3 and 0.1% ProteaseMax surfactant (Promega) with a brief sonication pulse using a Sonic Dismembrator Model 100 (Fisher Scientific). The protein suspension was reduced by adding of 5 mM Tris(2-carboxyethyl)phosphine (Sigma). The solution was incubated at 55°C with vigorous orbital shaking using a Thermomixer (Eppendorf). Protein alkylation was done by adding 10 mM iodoacetamide (Sigma) and incubating with vigorous shaking in the dark for 20 min. To digest the proteins, we added in the following order: 150 µl of 50 mM NH_4HCO_3, 2.5 µl of 1% ProteaseMAX dissolved in 50 mM NH_4HCO_3 and 1:100 (enzyme/protein, w/w)

sequencing grade trypsin (Promega) to a final reaction volume of 500 µl. The digestion reactions were incubated for 3 h at 37ºC with vigorous orbital shaking. The digestion were stopped by adding 0.1% trifluoroacetic acid, (TFA) (Sigma) and centrifuged at 20,000 g for 20 min at room temperature to remove undigested insoluble material and supernatant containing the peptide mixture was collected and desalted using Sep-Pak tC18 solid-phased extraction cartridges (Waters). Prior to loading the mixture of peptides, the cartridges were washed sequentially with 3 ml of acetonitrile, 3 ml of 0.5% acetic acid ,50% acetonitrile in water, and with 3 ml of 0.1% TFA in water. After loading the peptide mixtures, the cartridges were washed with 3 ml of 0.1% TFA and then with 0.250 ml of 0.5 % acetic acid in water. The peptides were eluted into a clean tube with 1 ml of 0.5% acetic acid, 80% acetonitrile in water and dried with an Speed Vac (Thermo). Ten milligrams of dried peptide pellet were solubilized in 1 ml of PBS and incubated with a 200 µl slurry of NeutrAvidin beads (Pierce) for 1 h at room temperature. The beads were precipitated by centrifugation at 1000 g for 5 min and flow through was collected for MS analysis of unbound peptides. Beads were washed 3 times by adding 1 ml of PBS, 3 times with 1 ml of 5% acetonitrile in PBS and with a last wash in ultrapure water. Excess liquid was completely removed from the beads using a micropipette and biotinylated peptides were eluted by adding 0.3 ml of solution containing 0.2% TFA, 0.1% formic acid, 80% acetonitrile in water. The beads were centrifuged at 1000 g and the first elution of biotinylated peptides was transferred to an eppendorf tube. A second elution of 0.3 ml was boiled for 5 min for maximum release of peptides from the beads. A total of 10 elutions were collected and dried separately in a Speed Vac. The enriched biotinylated peptides were resuspended in 0.2 ml PBS and the pH was corrected by adding 20 µl of 1.5 M TrisHCl buffer (pH7.4). A 10 µl aliquot of the elution was taken to measure biotinylated peptide content using fluorescence biotin quantitation kit as mentioned above.

Mass spectrometry

Soluble peptides were pressure-loaded onto a 250-µm i.d capillary with a kasil frit containing 2 cm of 10 µm Jupiter C18-A material (Phenomenex) followed by 2 cm 5 µm Partisphere strong cation exchanger (Whatman). This column was washed with Buffer A after loading. A 100 µm i.d capillary with a 5 µm pulled tip packed with 15 cm 4 µm Jupiter C_{18} material (Phenomenex) was attached to the loading column with a union and the entire split-column (loading column–union–analytical column) was placed in line with an Agilent 1100 quaternary HPLC (Palo Alto). For transportome analysis, the sample was analyzed using a modified 4-step separation described previously (Washburn et al., 2001). The buffer solutions used were 5% acetonitrile/0.1% formic acid (Buffer A), 80% acetonitrile/0.1% formic acid (Buffer B), and 500 mM ammonium acetate/5% acetonitrile/0.1% formic acid (Buffer C). Step 1 consisted of a 35 min gradient from 0-55% Buffer B, a 5 min gradient from 55-70% Buffer B, 10 min 100% Buffer B and 27 min 100% Buffer A . Steps 2-3 had the following profile: 5 min of x % Buffer C with (100-x)% buffer A, a 10 min Buffer A, a 5 min gradient from 0-15% Buffer B, a 70 min gradient from 15-55% Buffer B, a 5 min gradient from 55-100% Buffer B, a 5 min 100% Buffer B, and 20 min 100% Buffer A. The Buffer C percentages (X) were 10 and 40 for the steps 2-3, respectively. In the last step, the gradient contained: 5 min of 90% Buffer C with 10% buffer B, a 10 min Buffer A, a 5 min gradient from 0-15% Buffer B, a 70 min gradient from 15-55% Buffer B, a 5 min gradient from 55-100% Buffer B, a 5 min 100% Buffer B, and 20 min 100% Buffer A. For whole proteome analysis, the sample was analyzed using a 11-step separation exactly described as above except the buffer C percentages (X) were 10, 15, 20, 30, 40, 50, 60 and 80% for the steps 2-9, respectively. In the last two steps(I.e. 10 and 11), the gradient contained: 1 min 100% Buffer A, 5 min of 100 % Buffer C, a 5 min Buffer A, a 5 min gradient from 0-15% Buffer B, 70 min gradient from 15-55% Buffer B, 5 min gradient from 0-10% Buffer B, 75 min gradient from 10-45% Buffer B, 10 min 100% Buffer B, and 10 min 100% Buffer A. As peptides eluted from the microcapillary column, they were electrosprayed directly into a Velos

mass spectrometer (ThermoFisher) with the application of a distal 2.4 kV spray voltage. A cycle of one full-scan FT mass spectrum (300-2,000 m/z) at 60,000 resolution followed by 20 data-dependent IT MS/MS spectra at a 35% normalized collision energy was repeated continuously throughout each step of the multidimensional separation. Application of mass spectrometer scan functions and HPLC solvent gradients were controlled by the Xcalibur data system.

MS Data analysis

MS2 (tandem mass spectra) was extracted from the XCalibur data system format (.RAW) into MS1 and MS2 formats using in house software (RAW_Xtractor)(McDonald et al., 2004). Tandem mass spectra remaining after filtering were searched with Prolucid (Xu et al., 2006) against the UniProt_rat_03-25-2014 concatenated to a decoy database in which the sequence for each entry in the original database was reversed(Peng et al., 2003). All searches were parallelized and performed on a Beowulf computer cluster consisting of 100 1.2 GHz Athlon CPUs (Sadygov et al., 2002). No enzyme specificity was considered for any search. The following modifications were searched for analysis for transportome analyses: a static modification of 57.02146 on cysteine for all analyses, a differential modification of 226.0776 on lysine for modified peptides. For whole proteome analyses, a static modification of 57.02146 on cysteine was searched. Prolucid results were assembled and filtered using the DTASelect (version 2.0) program (Cociorva et al., 2007; Tabb et al., 2002). DTASelect 2.0 uses a linear discriminant analysis to dynamically set XCorr and DeltaCN thresholds for the entire dataset to achieve a user-specified false discovery rate (FDR). In DTASelect, the modified peptides were required to be partially tryptic, less than 10ppm deviation from peptide match, and a FDR at the protein level of 0.01. The FDRs are estimated by the program from the number and quality of spectral matches to the decoy database. For all datasets, the protein FDR was < 1% and the peptide FDR was < 1%.

The Datasets from “ON transportome”, “SC Transportome” and “LGN Transportome” and “Retina biotinylated proteins” are composed of the total detected biotinylated proteins in 6, 4, 3, 4 individual MS runs, respectively. Each sample was prepared by pooling tissue from 10-12 animals. The datasets from “Total ON” are the total detected proteins from two individual MS runs. The starting material of each run was whole ON tissue homogenate in RIPA buffer from 2 animals.

The STAT ID function (t-test with Benjamini-Hochberg (BH) correction) from Integrated Proteomics Applications, Inc. San Diego, CA. (http://www.integratedproteomics.com) for quantitative proteomic comparisons between: “ON transportome” and “Retina biotinylated proteins”, “ON transportome” and “Total ON” and “SC transportome” and “ON transportome” from figures 3, 4 and 5, respectively.

Chapter 1, in part, has been submitted for publication of the material as it currently appears in: Schiapparelli LM*, Shah SH*, McClatchy D, Ma Y, Sharma P, Yates III JR, Goldberg JL, Cline HT. “Retinal ganglion cell transportome identifies proteins transported to axons and presynaptic compartments in the visual system *in vivo*”. The dissertation author was a primary investigator and author of this paper.

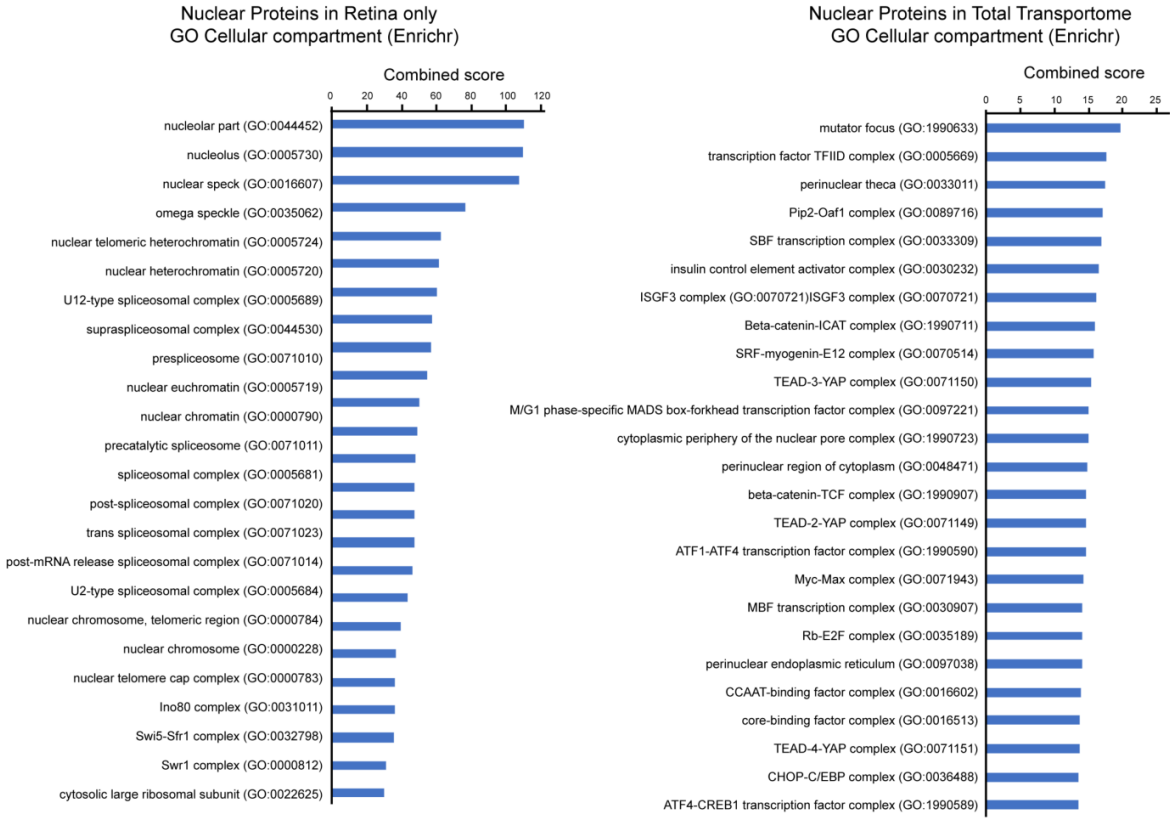

Supplemental Figure 1.1. Ontology of nuclear proteins in different cellular compartments. GO Analysis by the Enrichr platform (http://amp.pharm.mssm.edu/Enrichr/), GO Jensen Compartments. Ontological categorization of nuclear proteins in retinal samples highlight nucleolar and chromatin-interacting functions. In the transportome samples, nuclear proteins include perinuclear and nuclear shuttling functions. Combined score is computed by taking the log of the p-value from the fisher exact test and multiplying that by z-score of the deviation from the expected rank.

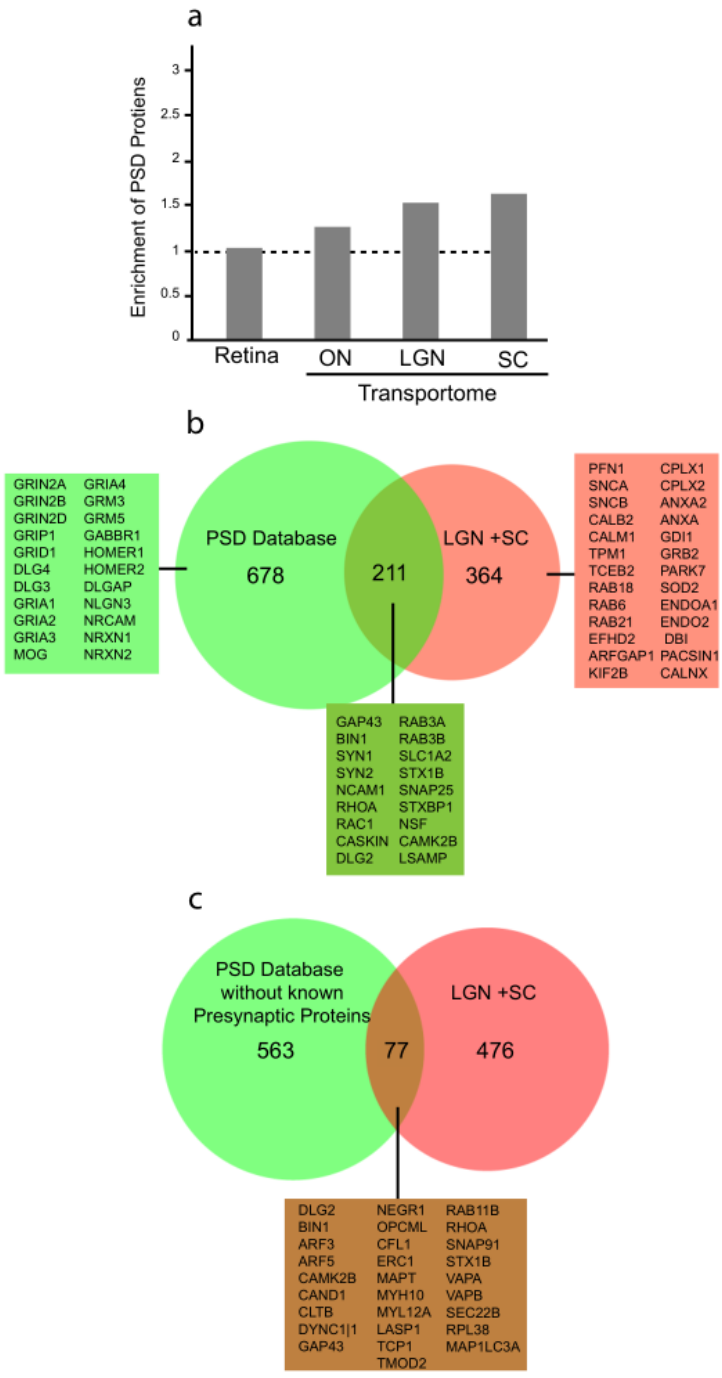

Supplemental Figure 1.2. Comparison of RGC transportome proteins with known postsynaptic proteins. a. We compare each transportome fraction to a known postsynaptic protein database. There is enrichment of annotated PSD proteins through the visual system. **b.** We find an absence of most known PSD in our pre-synaptic dataset, with an overlap of 211 proteins (several listed here). As many proteins are found in both pre-and post-synaptic compartments, we removed those proteins from the PSD list that were also found in the pre-synaptic database. **c.** Only 12% of PSD-only annotated proteins are found in our dataset.

References

Alvarez-Castelao, B., Schanzenbacher, C.T., Hanus, C., Glock, C., Tom Dieck, S., Dorrbaum, A.R., Bartnik, I., Nassim-Assir, B., Ciirdaeva, E., Mueller, A., Dieterich, D.C., Tirrell, D.A., Langer, J.D., and Schuman, E.M. (2017). Cell-type-specific metabolic labeling of nascent proteomes in vivo. Nature biotechnology 35, 1196-1201.

Bayes, A., van de Lagemaat, L.N., Collins, M.O., Croning, M.D., Whittle, I.R., Choudhary, J.S., and Grant, S.G. (2011). Characterization of the proteome, diseases and evolution of the human postsynaptic density. Nature neuroscience 14, 19-21.

Binotti, B., Jahn, R., and Chua, J.J. (2016). Functions of Rab Proteins at Presynaptic Sites. Cells 5.

Blitz, D.M., and Regehr, W.G. (2003). Retinogeniculate Synaptic Properties Controlling Spike Number and Timing in Relay Neurons. Journal of neurophysiology 90, 2438-2450.

Cagnetta, R., Frese, C.K., Shigeoka, T., Krijgsveld, J., and Holt, C.E. (2018). Rapid Cue-Specific Remodeling of the Nascent Axonal Proteome. Neuron 99, 29-46 e24.

Cappellari, M., Bielli, P., Paronetto, M.P., Ciccosanti, F., Fimia, G.M., Saarikettu, J., Silvennoinen, O., and Sette, C. (2014). The transcriptional co-activator SND1 is a novel regulator of alternative splicing in prostate cancer cells. Oncogene 33, 3794-3802.

Cociorva, D., D, L.T., and Yates, J.R. (2007). Validation of tandem mass spectrometry database search results using DTASelect. Curr Protoc Bioinformatics Chapter 13, Unit 13 14.

Devine, M.J., Norkett, R., and Kittler, J.T. (2016). DISC1 is a coordinator of intracellular trafficking to shape neuronal development and connectivity. The Journal of physiology 594, 5459-5469.

Dhande, O.S., Stafford, B.K., Lim, J.A., and Huberman, A.D. (2015). Contributions of Retinal Ganglion Cells to Subcortical Visual Processing and Behaviors. Annual review of vision science 1, 291-328.

Filipek, A., Jastrzebska, B., Nowotny, M., Kwiatkowska, K., Hetman, M., Surmacz, L., Wyroba, E., and Kuznicki, J. (2002). Ca2+-dependent translocation of the calcyclin-binding protein in neurons and neuroblastoma NB-2a cells. J Biol Chem 277, 21103-21109.

Gallivan, J.P., Lester, H.A., and Dougherty, D.A. (1997). Site-specific incorporation of biotinylated amino acids to identify surface-exposed residues in integral membrane proteins. Chem Biol 4, 739-749.

Geuens, T., Bouhy, D., and Timmerman, V. (2016). The hnRNP family: insights into their role in health and disease. Human genetics 135, 851-867.

Grafstein, B., and Forman, D.S. (1980). Intracellular transport in neurons. Physiol Rev 60, 1167-1283.

Hensch, T.K., and Quinlan, E.M. (2018). Critical periods in amblyopia. Visual neuroscience 35, E014.

Hong, Y.K., Park, S., Litvina, E.Y., Morales, J., Sanes, J.R., and Chen, C. (2014). Refinement of the retinogeniculate synapse by bouton clustering. Neuron 84, 332-339.

Hooks, B.M., and Chen, C. (2006). Distinct roles for spontaneous and visual activity in remodeling of the retinogeniculate synapse. Neuron 52, 281-291.

Huberman, A.D., Manu, M., Koch, S.M., Susman, M.W., Lutz, A.B., Ullian, E.M., Baccus, S.A., and Barres, B.A. (2008). Architecture and activity-mediated refinement of axonal projections from a mosaic of genetically identified retinal ganglion cells. Neuron 59, 425-438.

Jiménez, C.R., Stam, F.J., Li, K.W., Gouwenberg, Y., Hornshaw, M.P., De Winter, F., Verhaagen, J., and Smit, A.B. (2005). Proteomics of the Injured Rat Sciatic Nerve Reveals Protein Expression Dynamics During Regeneration. Molecular & Cellular Proteomics 4, 120-132.

Kanai, Y., Dohmae, N., and Hirokawa, N. (2004). Kinesin transports RNA: isolation and characterization of an RNA-transporting granule. Neuron 43, 513-525.

Kay, R.B., and Triplett, J.W. (2017). Visual Neurons in the Superior Colliculus Innervated by Islet2(+) or Islet2(-) Retinal Ganglion Cells Display Distinct Tuning Properties. Frontiers in neural circuits 11, 73.

Kilanczyk, E., Filipek, A., and Hetman, M. (2015). Calcyclin-binding protein/Siah-1-interacting protein as a regulator of transcriptional responses in brain cells. J Neurosci Res 93, 75-81.

Leamey, C.A., Merlin, S., Lattouf, P., Sawatari, A., Zhou, X., Demel, N., Glendining, K.A., Oohashi, T., Sur, M., and Fässler, R. (2007). Ten_m3 Regulates Eye-Specific Patterning in the Mammalian Visual Pathway and Is Required for Binocular Vision. PLOS Biology 5, e241.

Lim, J.H., Stafford, B.K., Nguyen, P.L., Lien, B.V., Wang, C., Zukor, K., He, Z., and Huberman, A.D. (2016). Neural activity promotes long-distance, target-specific regeneration of adult retinal axons. Nature neuroscience 19, 1073-1084.

Liu, H.H., McClatchy, D.B., Schiapparelli, L., Shen, W., Yates, J.R., 3rd, and Cline, H.T. (2018). Role of the visual experience-dependent nascent proteome in neuronal plasticity. eLife 7.

Liu, Y., Gervasi, C., and Szaro, B.G. (2008). A crucial role for hnRNP K in axon development in Xenopus laevis. Development 135, 3125-3135.

Liu, Y., Yu, H., Deaton, S.K., and Szaro, B.G. (2012). Heterogeneous nuclear ribonucleoprotein K, an RNA-binding protein, is required for optic axon regeneration in Xenopus laevis. J Neurosci 32, 3563-3574.

Loh, K.H., Stawski, P.S., Draycott, A.S., Udeshi, N.D., Lehrman, E.K., Wilton, D.K., Svinkina, T., Deerinck, T.J., Ellisman, M.H., Stevens, B., Carr, S.A., and Ting, A.Y. (2016). Proteomic Analysis of Unbounded Cellular Compartments: Synaptic Clefts. Cell 166, 1295-1307 e1221.

Martersteck, E.M., Hirokawa, K.E., Evarts, M., Bernard, A., Duan, X., Li, Y., Ng, L., Oh, S.W., Ouellette, B., Royall, J.J., Stoecklin, M., Wang, Q., Zeng, H., Sanes, J.R., and Harris, J.A. (2017). Diverse Central Projection Patterns of Retinal Ganglion Cells. Cell Rep 18, 2058-2072.

Maximov, A., Tang, J., Yang, X., Pang, Z.P., and Südhof, T.C. (2009). Complexin Controls the Force Transfer from SNARE Complexes to Membranes in Fusion. Science 323, 516-521.

McDonald, W.H., Tabb, D.L., Sadygov, R.G., MacCoss, M.J., Venable, J., Graumann, J., Johnson, J.R., Cociorva, D., and Yates, J.R., 3rd (2004). MS1, MS2, and SQT-three unified, compact, and easily parsed file formats for the storage of shotgun proteomic spectra and identifications. Rapid communications in mass spectrometry : RCM 18, 2162-2168.

McKay, B.E., Molineux, M.L., and Turner, R.W. (2008). Endogenous biotin in rat brain: implications for false-positive results with avidin-biotin and streptavidin-biotin techniques. Methods Mol Biol 418, 111-128.

Michaelevski, I., Medzihradszky, K.F., Lynn, A., Burlingame, A.L., and Fainzilber, M. (2010). Axonal Transport Proteomics Reveals Mobilization of Translation Machinery to the Lesion Site in Injured Sciatic Nerve. Molecular & Cellular Proteomics 9, 976-987.

Moore, B.D.t., Alitto, H.J., and Usrey, W.M. (2005). Orientation tuning, but not direction selectivity, is invariant to temporal frequency in primary visual cortex. Journal of neurophysiology 94, 1336-1345.

Ogawa, Y., and Rasband, M.N. (2008). The functional organization and assembly of the axon initial segment. Curr Opin Neurobiol 18, 307-313.

Peng, J., Elias, J.E., Thoreen, C.C., Licklider, L.J., and Gygi, S.P. (2003). Evaluation of multidimensional chromatography coupled with tandem mass spectrometry (LC/LC-MS/MS) for large-scale protein analysis: the yeast proteome. Journal of proteome research 2, 43-50.

Pielot, R., Smalla, K.H., Muller, A., Landgraf, P., Lehmann, A.C., Eisenschmidt, E., Haus, U.U., Weismantel, R., Gundelfinger, E.D., and Dieterich, D.C. (2012). SynProt: A Database for Proteins of Detergent-Resistant Synaptic Protein Preparations. Front Synaptic Neurosci 4, 1.

Pirooznia, M., Wang, T., Avramopoulos, D., Valle, D., Thomas, G., Huganir, R.L., Goes, F.S., Potash, J.B., and Zandi, P.P. (2012). SynaptomeDB: an ontology-based knowledgebase for synaptic genes. Bioinformatics 28, 897-899.

Rhee, H.W., Zou, P., Udeshi, N.D., Martell, J.D., Mootha, V.K., Carr, S.A., and Ting, A.Y. (2013). Proteomic mapping of mitochondria in living cells via spatially restricted enzymatic tagging. Science 339, 1328-1331.

Sadygov, R.G., Eng, J., Durr, E., Saraf, A., McDonald, H., MacCoss, M.J., and Yates, J.R., 3rd (2002). Code developments to improve the efficiency of automated MS/MS spectra interpretation. Journal of proteome research 1, 211-215.

Schanzenbacher, C.T., Sambandan, S., Langer, J.D., and Schuman, E.M. (2016). Nascent Proteome Remodeling following Homeostatic Scaling at Hippocampal Synapses. Neuron 92, 358-371.

Schiapparelli, L.M., McClatchy, D.B., Liu, H.H., Sharma, P., Yates, J.R., 3rd, and Cline, H.T. (2014). Direct detection of biotinylated proteins by mass spectrometry. Journal of proteome research 13, 3966-3978.

Schikorski, T. (2010). Pre-embedding immunogold localization of antigens in mammalian brain slices. Methods Mol Biol 657, 133-144.

Schroer, U., Volk, G.F., Liedtke, T., and Thanos, S. (2007). Translin-associated factor-X (Trax) is a molecular switch of growth-associated protein (GAP)-43 that controls axonal regeneration. Eur J Neurosci 26, 2169-2178.

Shigeoka, T., Jung, H., Jung, J., Turner-Bridger, B., Ohk, J., Lin, J.Q., Amieux, P.S., and Holt, C.E. (2016). Dynamic Axonal Translation in Developing and Mature Visual Circuits. Cell 166, 181-192.

Shigeoka, T., Jung, J., Holt, C.E., and Jung, H. (2018). Axon-TRAP-RiboTag: Affinity Purification of Translated mRNAs from Neuronal Axons in Mouse In Vivo. Methods Mol Biol 1649, 85-94.

Shimojo, M., Courchet, J., Pieraut, S., Torabi-Rander, N., Sando, R., 3rd, Polleux, F., and Maximov, A. (2015). SNAREs Controlling Vesicular Release of BDNF and Development of Callosal Axons. Cell Rep 11, 1054-1066.

Stein, B.E., and Rowland, B.A. (2011). Organization and plasticity in multisensory integration: early and late experience affects its governing principles. Progress in brain research 191, 145-163.

Stein, B.E., Stanford, T.R., and Rowland, B.A. (2014). Development of multisensory integration from the perspective of the individual neuron. Nature reviews Neuroscience 15, 520-535.

Steinberg, J.P., Huganir, R.L., and Linden, D.J. (2004). N-ethylmaleimide-sensitive factor is required for the synaptic incorporation and removal of AMPA receptors during cerebellar long-term depression. Proc Natl Acad Sci U S A 101, 18212-18216.

Stryker, M.P., and Lowel, S. (2018). Amblyopia: New molecular/pharmacological and environmental approaches. Visual neuroscience 35, E018.

Suresh, V., Ciftcioglu, U.M., Wang, X., Lala, B.M., Ding, K.R., Smith, W.A., Sommer, F.T., and Hirsch, J.A. (2016). Synaptic Contributions to Receptive Field Structure and Response Properties in the Rodent Lateral Geniculate Nucleus of the Thalamus. J Neurosci 36, 10949-10963.

Tabb, D.L., McDonald, W.H., and Yates, J.R., 3rd (2002). DTASelect and Contrast: tools for assembling and comparing protein identifications from shotgun proteomics. Journal of proteome research 1, 21-26.

Terenzio, M., Koley, S., Samra, N., Rishal, I., Zhao, Q., Sahoo, P.K., Urisman, A., Marvaldi, L., Oses-Prieto, J.A., Forester, C., Gomes, C., Kalinski, A.L., Di Pizio, A., Doron-Mandel, E., Perry, R.B., Koppel, I., Twiss, J.L., Burlingame, A.L., and Fainzilber, M. (2018). Locally translated mTOR controls axonal local translation in nerve injury. Science 359, 1416-1421.

Usrey, W.M., Reppas, J.B., and Reid, R.C. (1999). Specificity and Strength of Retinogeniculate Connections. Journal of neurophysiology 82, 3527-3540.

Vance, J.E., and Hayashi, H. (2010). Formation and function of apolipoprotein E-containing lipoproteins in the nervous system. Biochim Biophys Acta 1801, 806-818.

Washburn, M.P., Wolters, D., and Yates, J.R., 3rd (2001). Large-scale analysis of the yeast proteome by multidimensional protein identification technology. Nature biotechnology 19, 242-247.

Watanabe, T., Muranaka, N., Iijima, I., and Hohsaka, T. (2007). Position-specific incorporation of biotinylated non-natural amino acids into a protein in a cell-free translation system. Biochem Biophys Res Commun 361, 794-799.

Xu, T., Venable, J.D., Park, S.K., Cociorva, D., Lu, B., Liao, L., Wohlschlegel, J., Hewel, J., and Yates, J.R. (2006). ProLuCID, a fast and sensitive tandem mass spectra-based protein identification program. Molecular & Cellular Proteomics 5, S174-S174.

Yudin, D., Hanz, S., Yoo, S., Iavnilovitch, E., Willis, D., Gradus, T., Vuppalanchi, D., Segal-Ruder, Y., Ben-Yaakov, K., Hieda, M., Yoneda, Y., Twiss, J.L., and Fainzilber, M. (2008). Localized regulation of axonal RanGTPase controls retrograde injury signaling in peripheral nerve. Neuron 59, 241-252.

Zala, D., Hinckelmann, M.V., Yu, H., Lyra da Cunha, M.M., Liot, G., Cordelieres, F.P., Marco, S., and Saudou, F. (2013). Vesicular glycolysis provides on-board energy for fast axonal transport. Cell 152, 479-491.

CHAPTER 2: Quantitative transportomics identifies Kif5a as a major regulator of neurodegeneration

Abstract

Neurons in the adult central nervous system (CNS) degenerate and die after injury. Early molecular trafficking failure is a key component observed in many neurodegenerative disorders, but axoplasmic protein transport changes in disease models have not yet been quantified. Using *in vivo* proteomics, we quantified early changes to the retinal ganglion cell (RGC) transportome after optic nerve injury. Interestingly, the anterograde motor Kif5a was among the proteins most affected by relative axon transport failure, and transportome proteomics of Kif5a knockout mice allowed identification of proteins whose axon localization was dependent on Kif5a. We further found that loss of Kif5a, without additional injury, resulted in progressive RGC degeneration without optic nerve injury in a dose-dependent manner, and that conversely overexpressing Kif5a before injury accelerated RGC death. Together, these data identify Kif5a transport failure as a novel contributor to RGC neurodegeneration.

Introduction

Adult, mammalian central nervous system (CNS) neurons often undergo cell death and axon degeneration after injury and in disease. Neurodegenerative diseases like glaucoma result in progressive, irreversible retinal ganglion cell (RGC) loss. Mechanisms underlying this degeneration include intracellular events such as acute calcium influx into the axon (Knoferle et al., 2010), loss of constitutive axon survival factors like Nmnat2 (Gilley et al., 2015), inhibition of trophic survival and growth pathways as with suppressors of cytokine signaling (e.g. SOCS3) and ciliary neurotrophic factor signaling or DUSP14 and mitogen-activated protein kinases (Cai et al., 1999; Galvao et al., 2018; Leaver et al., 2006; Park et al., 2010; Smith et al., 2009; Zhou et al., 2005), and neuron-extrinsic degenerative signaling such as from aspects of reactive astrocytosis (Liddelow et al., 2017). Major strides in detailing neurodegeneration in neurons

including RGCs have been made in recent years, including transcriptomic (Yasuda et al., 2016), proteomic (Belin et al., 2015), and metabolomic (Sato et al., 2018) cellular changes.

Axon transport failure has been pathophysiologically linked to RGC death in glaucoma, as well as to other neurodegenerative diseases such as amyotrophic lateral sclerosis (ALS) and Alzheimer's Disease (Nicolas et al., 2018; Pasinelli and Brown, 2006; Zhang et al., 2004). While changes described in transcriptional and gene-regulatory networks in neurons can be a proxy for a neuron's or an axon's molecular complement, it does not capture changes in expression or localization of proteins. Proteomics experiments in RGCs have identified axon injury-induced pathways (Belin et al., 2015), but it is not known how molecular trafficking to the damaged optic nerve is changed. Unbiased temporal and spatial quantification of protein transport *in vivo* has presented technical challenges, including the overall low proportion of transported proteins, and the need to purify target axon proteins from surrounding mixed cellular populations.

We have previously developed a mass spectrometry-compatible technique for characterizing the axon transportome in the visual system (Schiapparelli et. al., *submitted*). Here, we adapt this technique to quantify for the first time changes in the transportome after axon injury. We identify transport failure of a kinesin-1 motor protein, Kif5a, a protein also implicated in genetics of neurodegeneration outside the visual system (Nicolas et al., 2018; Tessa et al., 2008). We use transportome proteomics to identify proteins whose transport is dependent on Kif5a, and finally we validate the importance of Kif5a for adult RGC survival *in vivo*. Together these novel methods identify a contributor to RGC death after injury and offer new insights into kinesin motor cargo specificity.

Results

Pulsed NHS-biotin can label proteins for differential Immunofluorescence and proteomics

To label anterogradely transported proteins in the optic nerve, intravitreal injections of *N*-hydroxysuccinimidobiotin (NHS-biotin) were delivered to the rat eye, as described previously

(Schiapparelli et al., 2014, Schiapparelli et al., *submitted*). Briefly, NHS-biotin covalently binds to primary amines on proteins, including lysines and N-terminal amino acids, adding a biotin group with a defined molecular weight (Figure 1a). Previous work with *in vivo* biotinylation used daily injections of NHS-biotin over 1 week to label transported proteins for steady-state quantification (Schiapparelli et. al., *submitted*). We tested two other labelling reagents, NHS-azide and biotin-beta-alanine. NHS-azide covalently binds to primary amines similar to NHS-biotin, but allows the chemical addition of alkyne-containing compounds after tissue collection by azide-alkyne cycloaddition, a process termed click chemistry (Best, 2009; Kolb et al., 2001). This allows post-isolation mass tagging and in theory quantitative comparisons between samples (Figure S1a). When injected into the eye and recovered from optic nerve samples, we observed sufficient biochemical labeling of proteins in control and injured conditions for detection by western blot when pooling multiple samples, but only visualized NHS-azide-labeled proteins by fluorescent noncanonical amino acid tagging (FUNCAT) in the retina, not the optic nerve, and therefore did not attempt mass spectrometry for the axon transportome. We next tested biotin-beta-alanine, which has similar chemical properties to NHS-biotin but a different mass shift, which should then allow quantitative comparison to NHS-biotin-labeled samples. Biotin-beta-alanine efficiently labeled proteins in HEK cells *in vitro* and in the optic nerve after intravitreal injection *in vivo*, but minimally labeled peptides by mass spectrometry analysis (Figure S1b). Thus while NHS-azide and biotin-beta-alanine each demonstrated advantages for either histology or biochemistry, we continued these experiments using NHS-biotin as it remained superior for mass spectrometry.

We first determined the early time window of NHS-biotin-labeled protein transport after optic nerve crush (ONC) by histochemistry. After ONC in rats, 65% of RGCs die within 1 week, while less than 1% die after 1 day (Sánchez-Migallón et al., 2016). To assay protein transport changes in response to axon injury before cell death with improved temporal resolution, we adapted our NHS-biotin protocol to a 24-hour window**.** Two intravitreal injections were given, the first alongside a crush or sham surgery and a second 21 hours later, 3 hours before tissue

collection, to label both fast and slow transported proteins (Figure 1b). Biotinylated transported proteins were visualized with tyramide signal amplification in the control optic nerve and pre-crush region of the injured optic nerve. Notably, there is no biotin signal past the crush site, confirming the disruption of protein transport and lack of biotin leakage (Figure 1c). Thus this protocol generated axon-specific protein labeling in both the control and injury conditions.

We next asked whether mass-spectrometry could reliably detect proteins in these samples. We used tandem mass spectrometry (MS/MS) combined with Direct Detection of Biotin-containing Tags (DiDBiT), an enrichment strategy to selectively isolate biotinylated peptides. Directly measuring biotinylated peptides with MS/MS facilitates direct quantification of biotinylated proteins with improved specificity (Schiapparelli et al., 2014). To minimize biological and surgical variability, and increase protein yield, we combined 8 optic nerves of either control or injury conditions for each MS sample. During dissection, we included optic nerve fragments from the end of the orbit to the chiasm from both injured and sham tissues to ensure comparable tissue processing. Each of the 6 samples, 3 each of control or ONC, was run independently through tandem mass spectrometry. We detected 206-300 transported proteins with a range of detection of expression of 300-fold Normalized Spectral Abundance Factor (NSAF) values. To determine if quantitative proteomics were reproducible in each of these conditions, we used pairwise correlation of NSAF values of both control and crush samples which showed high correlation between replicates (R=0.805 and R= 0.914, respectively) (Figure 1d). Reducing the labelling window to 24 hours and comparing changes in NSAF values, two modifications to the DiDBiT-axon transportome methodology, allow relative quantification between two conditions, a tight temporal window before widespread apoptosis, and high correlation between replicates.

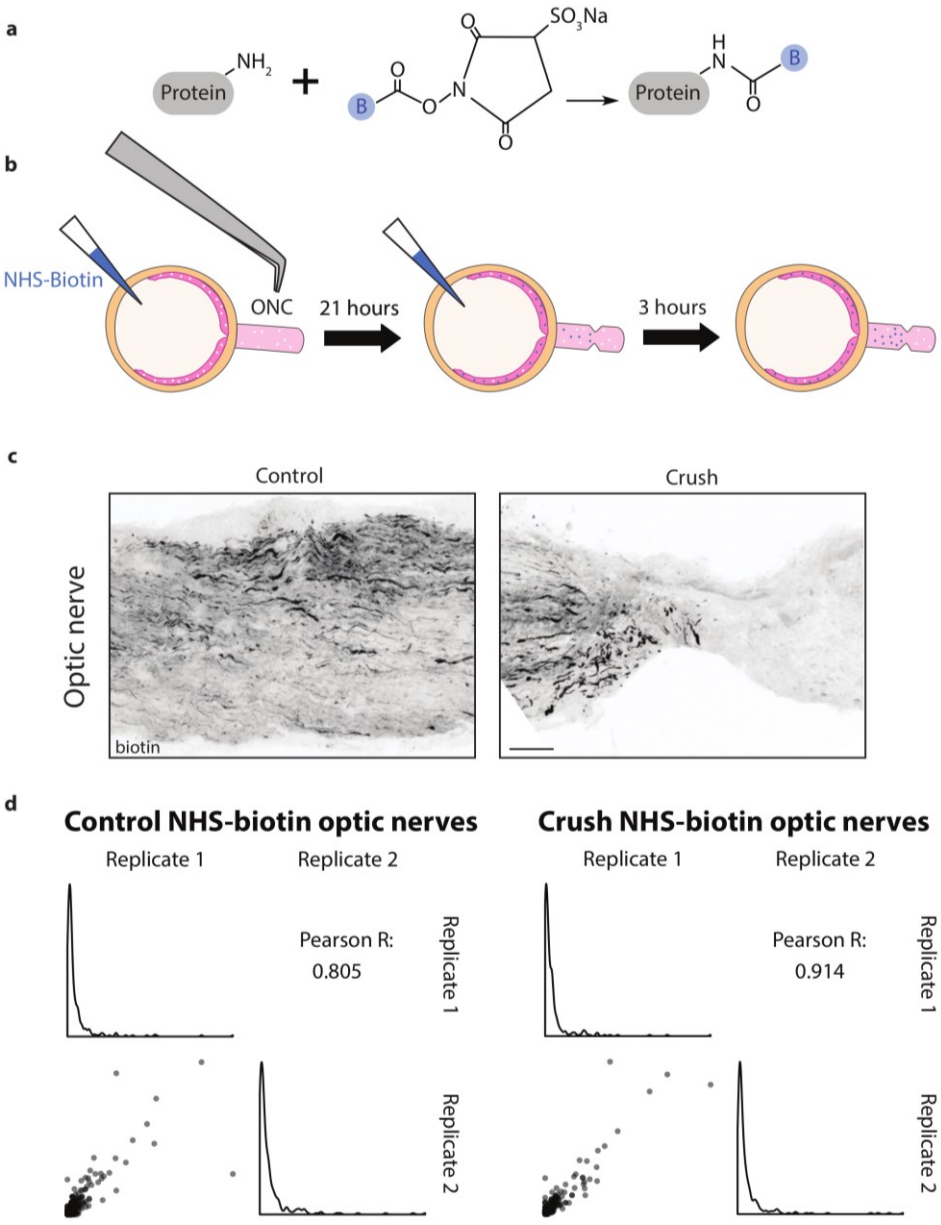

Figure 2.1. Pulsed NHS-biotin can label proteins for differential immunofluorescence and proteomics. a. NHS-Biotin reacts with primary amines on proteins, chiefly lysine side chain and N-terminal amines. NHS is a leaving group in this reaction. The biotin addition adds a small, defined mass shift to tagged molecules. **b.** 5µl of NHS-biotin was injected immediately prior to optic nerve crush (ONC) or sham surgery and again 21 hours later. 3 hours after, the eyes and optic nerves were collected and frozen after the rat was euthanized. At 24 hours, western blot demonstrates proteins labeled in the retina ganglion cell (RGC) somas have had enough time to transport to the axonal compartment. **c.** Biotinylated proteins in the optic nerve were visualized by avidin-biotin complex reaction followed by tyramide signal amplification conjugated to Alex Fluor 488. There were no biotinylated proteins found past the crush site. Scale bar=100 µm **d.** Pearson's R correlation of two proteomic replicates of NHS-biotin-injected control or ONC optic nerve samples. Top left and bottom right corners show the distribution of replicate 1 and replicate 2, respectively.

Quantitative transportomics identifies specific proteins whose transport differs after injury

We next asked whether protein transport to the optic nerve changed after injury. First, we measured the total protein abundance in control and injured retinas and optic nerve by electrophoresis, blotting and Ponceau S membrane staining. Total protein content was equivalent in optic nerve crush and control retinas and optic nerves (Figure 2a). We compared the biotinylated portion of total protein in either crush or control conditions and found a significant decrease in transported protein after injury (Figure 2b), consistent with previous studies of total transport after injury (McKerracher et al., 1990a, 1990b; Quigley et al., 1979).

To validate transport changes at the protein level, we specifically probed for Sncb, Gap43, and Arf3, neuronal proteins known to transport down the optic nerve (Figure 2c). Four rat optic nerves were labeled and homogenized using the same protocol as above for proteomics, and then biotin-tagged proteins were immunoprecipitated with neutravidin-bound agarose beads. We compared retinal and optic nerve total proteins (input), as well as the biotinylated fraction pulled down by IP, with and without injury. In the retina, there was little to no change in total protein levels (input, figure 2c) or in the biotinylated fraction (IP, figure 2c) in any of the three proteins, suggesting the abundance of these proteins is equivalent with and without injury in the retinal cell bodies. In contrast, in the optic nerve axon transportome, decreased protein transport was apparent after isolating the biotinylated, acutely transported component for SNCB and ARF3 but not GAP43 (IP, figure 2c) even though the total protein in the optic nerve tissues was not changed for any of the three. Thus deficits in transport of specific proteins are detected very early in the first 24 hours after optic nerve injury before changes in total protein are seen. These data exemplify the need for axon-specific, temporally-restricted protein labeling to accurately assess early axon transportome changes in the degenerative process.

We then examined the transportome changes after optic nerve crush using mass spectrometry. We normalized relative abundance of detected proteins within each condition to

determine whether specific proteins are transported down the axon in greater or lesser amount than the average (decreased) level. Individual protein transport was quantified using NSAF in injured or control conditions across 3 replicates containing 8 optic nerves each. The resulting volcano plot displays the relative log-normalized fold change of anterogradely-transported proteins from RGC cell bodies to their axons in the optic nerve (Figure 2d). Because mass spec undersamples the total proteome and thus we did not want to set filtering too stringently, we analyzed proteins that had a $\log_2$ fold change of greater than 1.5 of relative abundance in the transportome, or a p-value <0.05, or both. This identified 16 proteins that fell into 3 ontologies of identified function: cytoskeletal, protein synthesis, and protein transport. For cytoskeletal proteins, there was a relative increase in Tmsb4x, which sequesters actin (Hertzog et al., 2004; Li et al., 1996), and Tcp1, a chaperonin which helps fold actin and tubulin (Liang and MacRae, 1997; Yaffe et al., 1992), plus a relative decrease in 3 isoforms of alpha-tubulin, Tuba1a, Tuba1b, and Tuba3a. Together these might be expected to associate with decreased axon growth or stabilization. On the other hand, there was a relative increase in detection of cytoskeletal proteins Nefl and Ina, both subunits of neurofilaments. Neurofilament proteins can physiologically regulate axon diameter, but abnormally aggregate in axons in several neurodegenerative diseases like ALS (Xiao et al., 2006) and Alzheimer's disease (Liu et al., 2011; Perry et al., 1985). Within protein synthesis, there was a relative increase in the transport of Impact, which maintains protein translation during stress (Roffe et al., 2013). Finally, with protein transport itself, there was a significant relative decrease in the transport of Kif5a, a neuronal kinesin heavy chain motor protein. Thus analyzing the dynamic transportome after axon injury reveals several protein synthesis and transport homeostatic mechanisms changing acutely after axon injury.

Kif5a, the protein with highest both significance and magnitude of change criteria, is a motor protein in the 45-member kinesin superfamily (Hirokawa et al., 2009). When all motor proteins in our transportome data were examined (Figure S2a), two findings stood out. First,

another kinesin heavy chain, Kif5b, did not change in relative transport after injury, suggesting specificity in kinesin isoform transport failure. Second, transport of Klc1, a partner light chain to the heavy chain Kif5a, also was not reduced to the same extent as Kif5a. As kinesin and dyneins work in tandem to regulate cargo transport (Hendricks et al., 2010; Soppina et al., 2009; Verhey and Hammond, 2009), we hypothesized there may be a similar change to dynein subunits. We did not discover any significant change in transport of both dynein subunits identified in our transportome, although more work may be needed to explore this question.

We validated our mass spectrometry findings by biotin immunoprecipitation and quantitative western blot (Figure 2e). We normalized biotin-tagged kif5a to each sample's total biotin-tagged protein (similar to that shown in Figure 2b), and compared injury versus control, which resulted in a similar (about 2.5-fold) significant decrease in kif5a transport relative to the decrease in total axon transport after injury (Figure 2f). Importantly, we saw an equal amount of Kif5a in the retina with and without injury, suggesting that the cause of decreased detected transport is not due to changes in Kif5a abundance, but in fact a specific anterograde transport deficit. Thus western blotting against whole kif5a protein validates the data derived from the peptide-based mass spectrometry.

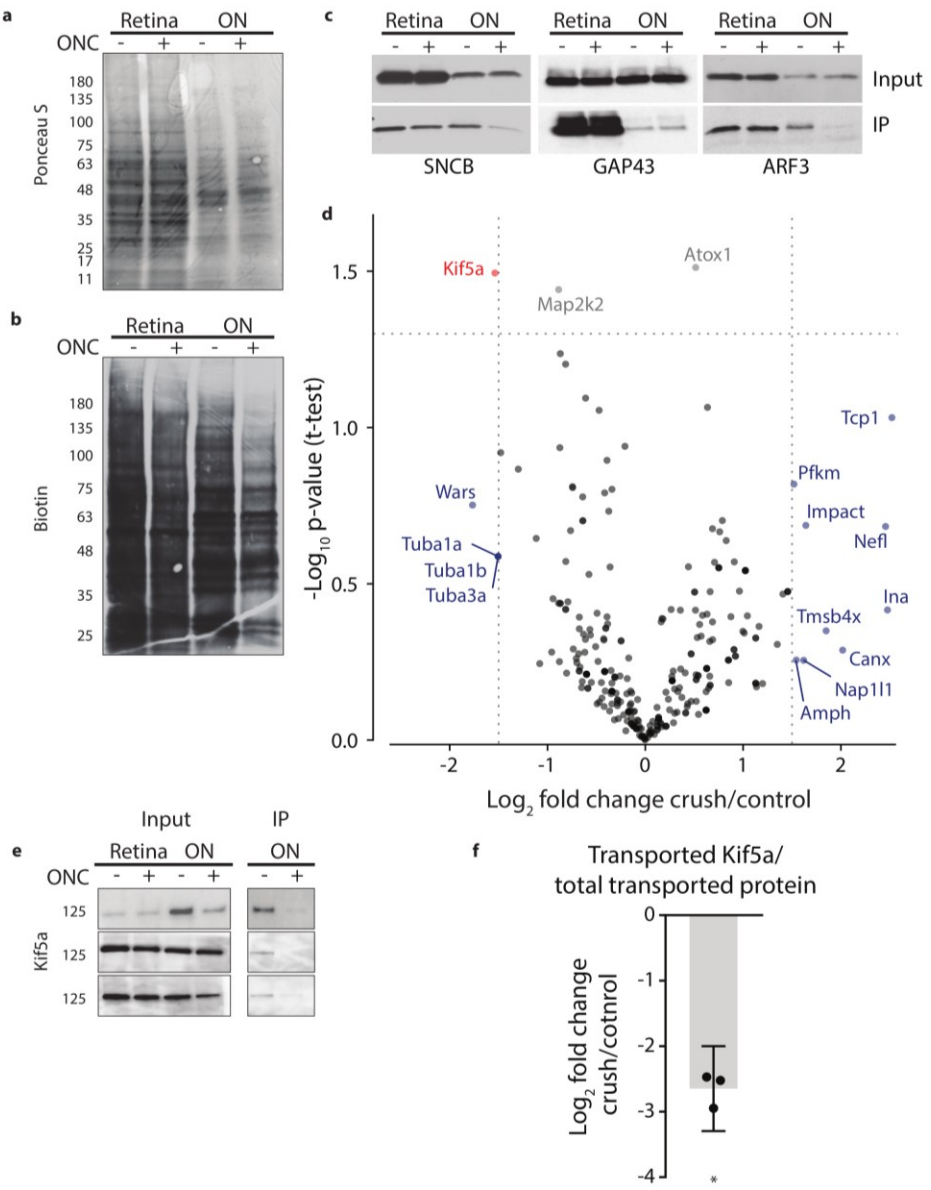

Figure 2.2. Quantitative transportomics identifies specific proteins whose transport differs after injury. a. Ponceau S stain of normalized protein from biotinylated retinas and optic nerves, with and without ONC, showing equivalent total protein. **b.** Western blot of the same samples run in parallel, probing for biotin. There is a noticeable decrease in biotinylated protein in both ONC samples, more apparent in the optic nerve sample. **c.** IP of biotinylated protein from retinal and optic nerve samples, probed with antibodies against SNCB, GAP43, or ARF3. **d.** Volcano plot comparing biotinylated proteins from control versus ONC optic nerve samples. NSAF values for each sample type were averaged across 3 replicates and plotted as $\log_2$ fold change versus $-\log_{10}$ p-value. Proteins with an absolute fold change greater than 1.5, p-value less than 0.05, or both, are colored blue, grey, and red respectively. **e.** Three replicates of biotin IP probed with an antibody against Kif5a. The IP was stripped and re-probed with an antibody against biotin for a measurement of total biotinylated protein pulled down (not shown). **f.** Quantification of the change in transported Kif5a compared to the change in total transported protein after ONC. One-sample, two-tailed t-test, p=0.003, n=3. The bar height represents the mean, and the error bar represents the 95% confidence interval.

Transportomics of Kif5a Knockout (KO)

Given our finding of an association of early Kif5a transport decrease with optic nerve injury, we sought to understand the importance of Kif5a, and its associated cargoes, in RGC function. Discovering specific kinesin-dependent cargoes e.g. by mass spectrometry has not been undertaken, but we hypothesized that characterizing the optic nerve transportome with and without Kif5a should yield Kif5a-dependent cargo localization. For this approach, we used homozygous conditional floxed Kif5a adult mice (Figure 3a) as Kif5a knockout mice have seizures and die soon after birth (Nakajima et al., 2012; Xia et al., 2003). We delivered either cre-recombinase or GFP intravitreally to specifically knock out Kif5a in adult RGCs. One-month after injection, there is almost a complete loss of Kif5a in the retina, and a complete loss in the optic nerve fraction (Figure 3b). We confirmed this loss by immunofluorescence for Kif5a at 1 month and 4 months after cre-mediated knockout (Figure 3c). Kinesin-1 motors are composed of 2 heavy chain and 2 light chain proteins, where the heavy chains are any of Kif5a, Kif5b, and Kif5c. Of these, Kif5a and Kif5c are neuron-specific, and present in RGCs (Butowt and Von Bartheld, 2007; Rahman et al., 1999). As kif5c may increase in expression to compensate for kif5a loss, we also probed the western blots for kif5c, and found no difference in protein expression after kif5a knockout (Figure 3b).

We next explored the kif5a-dependent transportome. In uninjured mice 3 weeks after viral cre injection, we injected NHS-biotin intravitreally three times, 24 hours apart, to determine transport deficits. The resulting volcano plot of transportome changes identified several proteins decreased in transport after loss of Kif5a (Figure 3d). Bin1, for example, was identified as a Alzheimer's disease locus through GWAS studies (Seshadri et al., 2010), and localizes to the axon initial segment and nodes of Ranvier (Butler et al., 1997) acting downstream of c-myc, an injury-response transcription factor in RGCs (Belin et al., 2015). Sh3gl2, also known as endophilin A1, is enriched in synaptic terminals and interacts with synaptic proteins such as synaptojanin and regulates clathrin-mediated synaptic endocytosis (Milosevic et al., 2011). We

asked whether the Kif5a-dependent proteins interact with each other using STRING (Szklarczyk et al., 2017) (see Methods), and found that many form protein-protein interaction networks (Figure 3e). The protein transport changes seen in ONC versus Kif5a knockout were largely non-overlapping (R= -0.2, Figure S3a), suggesting that ONC response is much broader than the transportome changes attributable just to kif5a loss.

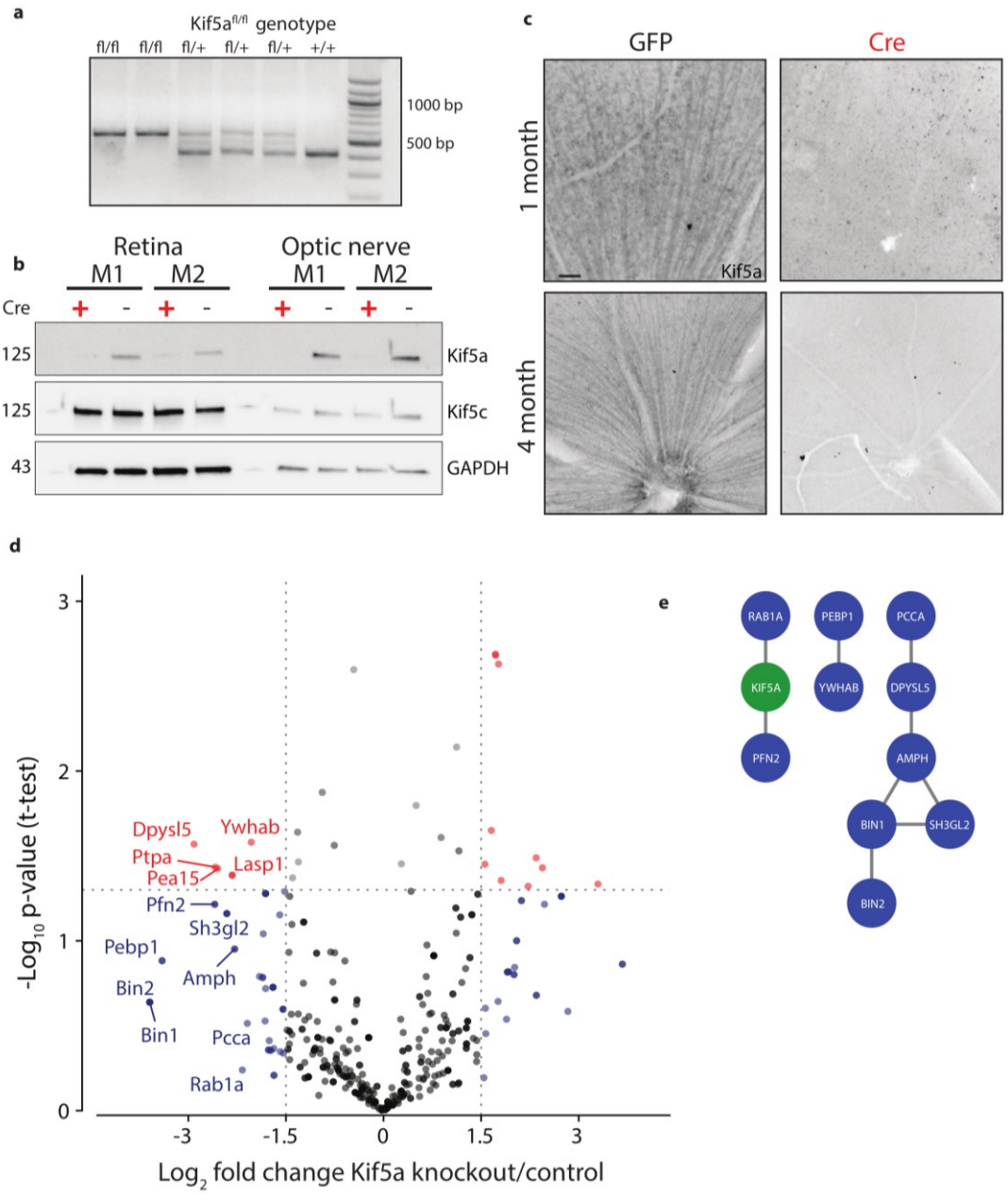

Figure 2.3. Transportomics of Kif5a knockout (KO). a. PCR amplification of the Kif5a locus in transgenic conditional KO mice confirms the presence of a loxP base pair shift in hetero-and homozygous floxed animals. **b.** Western blot validation of Kif5a knockout one month after intravitreal cre-recombinase injection in whole retina and optic nerve lysates. Kif5c, a related kinesin, was unaffected by the loss of Kif5a. Cre-positive lanes are designated with a red '+', cre-negative lanes are designated with a black '-'. **c.** Wholemount retinas immunostained for Kif5a are positive in RGC axons projecting towards the optic nerve head. Kif5a-positive fibers are decreased at 1 month, and even more so at 4 months after cre injection. Scale bar=100 µm. **d.** Volcano plot comparing biotinylated proteins in the optic nerve 3 weeks after intravitreal AAV-GFP compared to AAV-Cre-GFP. Proteins with a $\log_2$ fold change decrease of greater than 2 after knockout are shown in blue, and those which additionally had a p-value less than 0.5 are shown in red. **e.** STRINGdb interaction diagram for all labeled proteins plus Kif5a create three networks incorporating 11/14 proteins.

Kif5a KO leads to progressive, dose-dependent RGC degeneration

As Kif5a KO lead to disruption of protein transport, we asked whether the loss of Kif5a affected RGC survival in the absence of optic nerve injury. Using either Kif5a or Kif5b floxed adult mice and intravitreal AAV-cre delivery, we quantified RGC survival using Brn3a, a nuclear RGC-specific marker, in retinal wholemounts (Figure 4a). There was no change in RGC density 1 month after Kif5b homozygous KO (S4a-b), but there was a significant, 44% decrease in RGCs 1 month after Kif5a homozygous KO (Figure 4b). We assayed gene dose-dependency using a heterozygous $Kif5a^{fl/+}$ mouse line with AAV-cre and found a significant decrease of 22%, about half of the cell death seen in the homozygous Kif5a KO. To determine if only 44% of RGCs are susceptible to cell death or if kif5a loss results in progressive degeneration, we aged a cohort of mice to 4 months after KO and observed an almost complete loss of RGCs (Figure 4a-b). To confirm this effect was not a downregulation of Brn3a, we also measured pattern electroretinograms (pERG) for function of RGCs. There was an almost complete loss of visual response 6 months after knockout, quantified by P50 to N95 amplitude (Figure 4c). Thus the loss of a specific motor protein Kif5a induces a progressive, dose-dependent neurodegeneration of RGCs.

Given the importance of proper Kif5a transport to RGC survival we also hypothesized that exogenous delivery of of Kif5a would rescue RGC survival after injury. We validated that our AAV-Kif5a vector was transported down the optic nerve and bound TUBB3 (Figure 5a-b) with no effect on RGC survival without optic nerve injury (Figure 5c). Contrary to our hypothesis, there was a 33% decrease in RGC survival after ONC with Kif5a overexpression compared to control (Figure 5d-e). Thus, maintaining physiological levels of Kif5a transport is crucial for RGC survival.

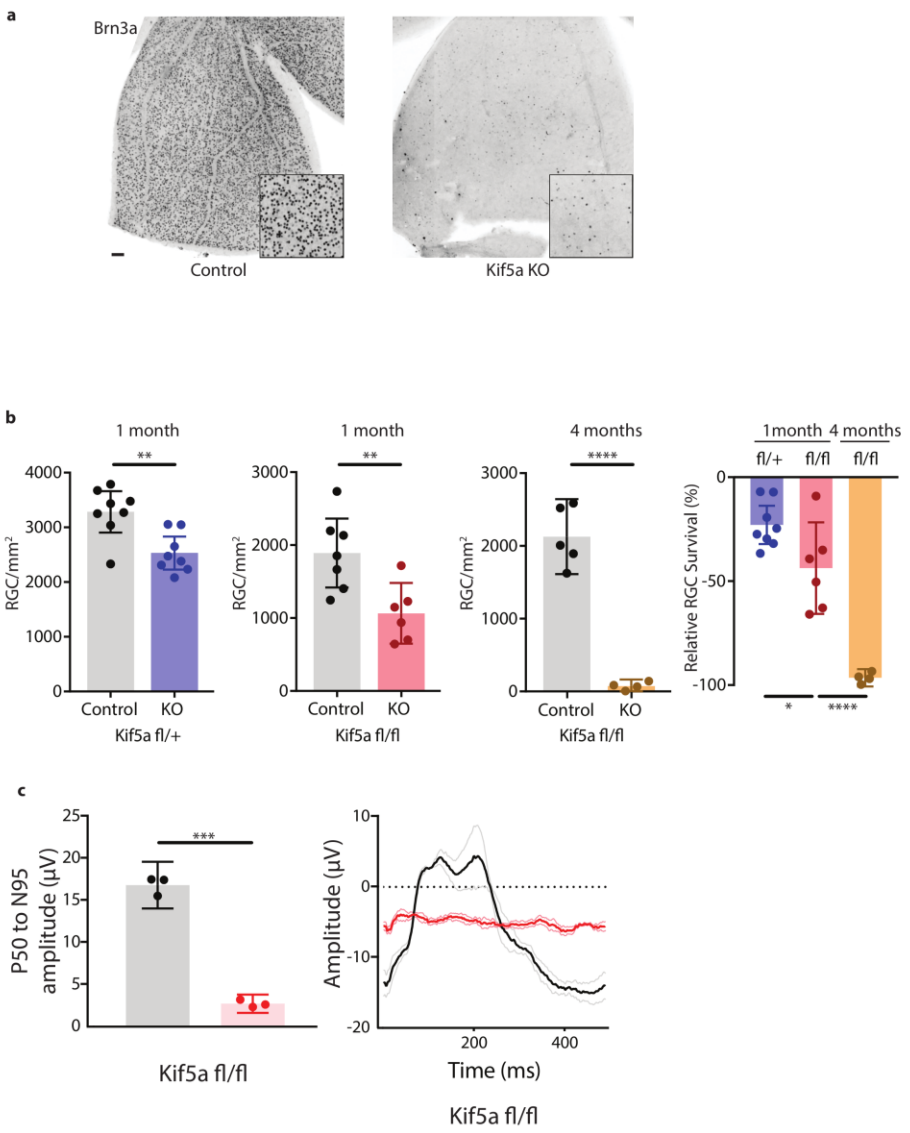

Figure 2.4. Kif5a KO leads to progressive, dose-dependent RGC degeneration. a. Representative example of whole mount Kif5a$^{fl/fl}$ retinas stained with RGC-specific marker Brn3a, 4 months after either AAV-GFP or AAV-Cre-GFP. Scale bar=100 μm. **b.** Quantification of Brn3a+ cell density across entire wholemount retinal surface. Each point represents one retina. The graphs, in order, show pairwise comparisons between heterozygous Kif5a KO at 1 month after viral injection (control n=8, KO n=8), homozygous Kif5a KO at 1 month after viral injection (control n=7, KO n=6), homozygous Kif5a KO at 4 months after viral injection (control n=5, KO n=4), and a comparison of the three previous experiments normalized to their control population. B_1-B_3 are two-sample, two-tailed t-tests, p= 0.003, p=0.008, and p<0.0001, respectively. B_4 is an ordinary one-way ANOVA with post-hoc Sidak correction. Between the blue and red columns, p=0.034. Between red and gold columns, p<0.0001. The bar heights represent the mean, and the error bars represents the 95% confidence interval. **c.** Pattern electroretinogram quantification on mice 6 months after Kif5a KO or control. On the left, the amplitude difference between the P50 peak and the N95 trough were quantified and compared with a two-sample, two-sided t-test (n=3), p<0.0001. The bar heights represent the mean, and the error bars represents the 95% confidence interval. On the right, the average traces of each condition are bold, with lighter shades +/- SEM.

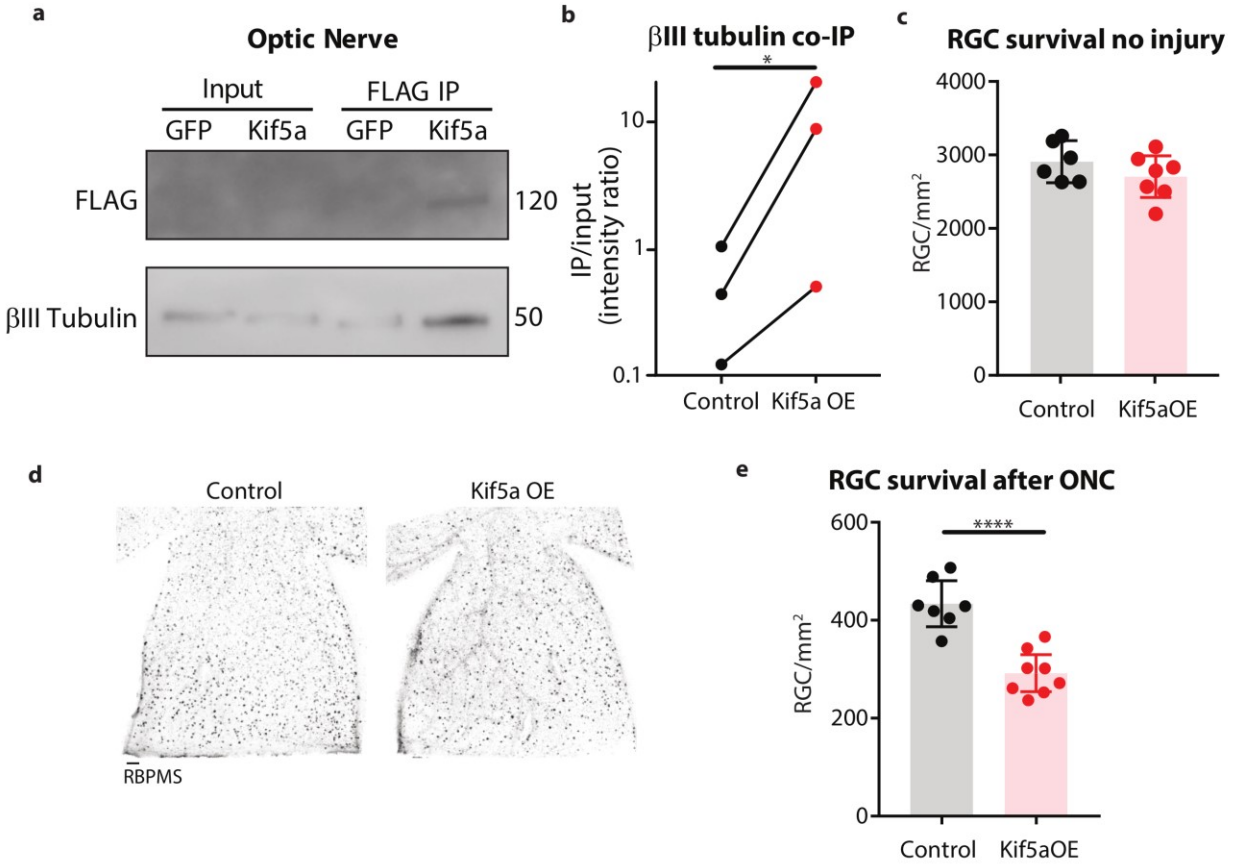

Figure 2.5. Kif5a overexpression accelerates RGC death after ONC. a. Co-immunoprecipitation (co-IP) of FLAG-tagged Kif5a in the optic nerve, 1 month after AAV-GFP or AAV-Kif5a-FLAG intravitreal injection. An antibody against FLAG showed a positive band at the expected molecular weight after IP. Beta-III tubullin, a known binding partner of Kif5a, was also increased after FLAG IP in the Kif5a condition compared to GFP. **b.** Quantification of co-IPs with a two-sample, two-tailed, ratio-paired t-test, p=0.043, n=3. **c.** Quantification of Brn3a+ wholemount retinas (control n=6, OE n=7) 1 month after viral injection. Two-sample, two-tailed t-test, p=0.24. **d.** Representative wholemount retinas stained with RGC-specific marker RBPMS. Either AAV-GFP or AAV-Kif5a-FLAG was injected 2 weeks prior to ONC, and retinas were collected two weeks after ONC. Scale bar=100 μm. **e.** Quantification of RBPMS+ cell density (control n=7, OE=8), two-sample, two-tailed t test, p<0.0001. The bar heights represent the mean, and the error bars represents the 95% confidence interval.

Discussion

In diseases such as ALS and glaucoma, axon transport failure has been a long-standing hypothesis for the pathophysiology of cell death. We hypothesized that quantifying transport deficits and particularly discovering the changes in the complement of transported proteins should increase our understanding of the degenerative process. For the first time, we present quantification of axon transportome changes after injury, separating their identification from the surrounding glial and other cells. Using a novel proteomic approach for quantifying this transport, we identify Kif5a transport failure to RGC axons 24 hours after optic nerve injury. Previous approaches to characterizing axon-specific protein responses to injury depended on physically extracting cytoplasm from axons in whole nerve preparations (Michaelevski et al., 2010), a technically challenging approach with inconsistent results noted by those authors. We previously used a biotin labeling, mass spectrometry-based transportome technique to study steady-state protein transport in the visual system (Schiapparelli et. al., *submitted*). Here, adapting this technique to NHS-biotin injections within a 24-hour window allowed the capture of dynamic, defined transport changes immediately following axon injury. This improved temporal resolution quantitatively detected loss of specific proteins' transport before total protein changes are apparent, as seen through western blotting and immunoprecipitation against biotinylated proteins. In fact, many of the axonal changes that occur after injury may begin earlier than previously thought, with rapid changes to the axon transportome. Additional examination of the time course of axon transport changes in the period after injury or in other models of neurodegenerative diseases are now possible and can be pursued.

Disruptions to the kinesin motor protein family can manifest in a variety of neurological diseases. Charcot-Marie-Tooth disease type 2A can be caused by mutations in Kif1b (Zhao et al., 2001), congenital fibrosis of the extraocular muscles can be caused by mutations in Kif21a, and a loss-of-function mutation in Kif5a motor domain can result in Hereditary Spastic Paraplegia (Blair et al., 2006; Morfini et al., 2009; Reid et al., 2002; Tessa et al., 2008; Xia et al.,

2003). Different loss-of-function mutations in Kif5a, all affecting the cargo binding domain, are causative in some cases of ALS (Brenner et al., 2018; Nicolas et al., 2018).

The finding of Kif5a transport failure after injury is especially interesting given the relative lack of change in other motor proteins, such as Kif5b. Increasing evidence has shown that kinesin subtypes and adaptor proteins have at least partial cargo specificity (Chevalier-Larsen and Holzbaur, 2006), yet the extent of shared and specific cargo within a subtype has not been fully understood. Through immunoprecipitation and immunoisolation assays, several synaptic proteins such as SNAP25, synaptotagmin and syntaxin 1a have been identified as cargoes of the Kif5 family (Toda et al., 2008), but only a few proteins have been shown to be specific to Kif5a, such as GABARAP (Nakajima et al., 2012), or Kif5b, such as Myo5a (Huang et al., 1999). Quantitative changes in cargo transport after the loss of a specific motor protein may give insight into the role of that motor. Consistent with the specificity of decreased transport we detected after optic nerve injury, Kif5a loss, and not Kif5b loss, results in the progressive, dose-dependent degeneration of adult RGCs.

Although here we describe initial data on the axon transportome cargoes dependent on Kif5a for their RGC axon localization, we do not yet understand which cargoes of Kif5a contribute to these diseases, especially *in vivo*. By quantifying the transportomic changes in an adult acute knockout model, we highlighted just those proteins whose transport was not adequately compensated by other mechanisms or motors. Indeed, many of these proteins have known interactions with each other, and several have previously been reported as associated with degenerative diseases in other systems. Another possibility is that these proteins, instead of being direct cargoes of Kif5a, are downregulated or mis-localized after Kif5a loss. Increased protein degradation can also contribute to decreased detected biotinylated protein, as detection of transported proteins is the net of protein transport and protein degradation. Finally, these data are limited to transport of proteins. The loss of Kif5a-dependent RNA and organelle transport

may also contribute to neurodegeneration. Characterizing these cargoes and searching for their potential roles in neuronal survival will be important in future work.

Interestingly, rescue of Kif5a transport deficit is not as straightforward as simply overexpressing it before axon injury. Kif5a abundance in the retina was unchanged while transport was decreased after injury, suggesting that loss of transport is specific to axon entry rather than any lack of Kif5a itself. Regulation of kinesin transport is known to depend on phosphorylation states (Morfini et al., 2001), calcium-dependent inhibition by mitochondrial cargo (Wang and Schwarz, 2009), conformational state changes by kinesin light chains, and autoinhibition of the motor domain by inactive kinesin heavy chains (Cai et al., 2007). Removing autoinhibitory domains or truncation of the motor beyond the first coiled-coil domain creates constitutively active kinesins, potentially circumventing any inherent axonal inhibition (Hammond et al., 2010; Homma et al., 2003; Yang et al., 2016). Overexpressed full-length Kif5a was transported to the axon and functioned as expected at least in its binding to tubulin, but accelerated RGC death after injury. Increasing expression of Kif5a in the cell body without improving axonal transport may exacerbate cell death, and future experiments exploring whether constitutively transporting Kif5a mutants rescue cell death could address this model of cell body toxicity versus axon rescue and provide potential therapeutic avenues to counter the neurodegenerative process.

Materials and Methods

Animal surgeries

Detailed protocols are available upon request. Animal experiments were conducted in accordance with the guidelines of the Institutional Animal Care and Use Committee (IACUC) and the Institutional Biosafety Committee of University of California, San Diego, Scripps Research, and Stanford University, and complied with the ARVO Statement for the Use of Animals in Ophthalmic and Vision Research.

Animal lines

C57BL/6 mice or Sprague Dawley rats were used for all wildtype experiments. Kif5a$^{fl/fl}$ and Kif5b$^{fl/fl}$ from a C57Bl/6 background were a gift from David Williams (Xia et al., 2003).

Intravitreal Injection

Sprague Dawley rats or mice (30-45 day old) were used for all experiments. A microinjector pressure system (Picosprizer II) with a pulled glass micropipette in a micromanipulator was used to inject reagents intravitreally. For viral injections, mice were injected intravitreally with 1.5 µl volume of AAV2-GFP, AAV2-cre-GFP, or AAV7m8-3xFLAG/Kif5a (titers ranged from 0.5 to 1 × 10^{13} genome copies/ml). For *in vivo* biotinylation experiments, 5 milligrams of NHS-biotin (EZ-Link® from Pierce) were dissolved in 300 µl of sterile DMSO immediately prior to use, as described previously (Schiapparelli, *submitted*). Briefly, intravitreal injections (5 µl for rats, 1.5 µl for mice), were given to both eyes. The injections were given twice over 24 hours under deep anesthesia with either 0.5 mg/kg Medetomidine and 75mg/kg ketamine *ip* or 2% isofluorane under nose cone. The eyes were treated with topical antibiotics and analgesics.

Optic nerve crush

Under deep anesthesia, the optic nerve was exposed and crushed using fine forceps (Dumont #5) at 1.5 mm behind the optic nerve head for 5 seconds. Care was taken to avoid damaging the blood supply to the retina. Sham surgeries exposed the optic nerve, but no crush was given. All optic nerve crush procedures were performed by a surgeon blinded to the viral treatment. Postoperatively, animals were allowed to recover on a heating pad and were given subcutaneous injections of buprenorphine hydrochloride, 0.1 mg/kg, twice a day for 3 consecutive days to minimize discomfort.

Pattern electroretinogram

Anesthetized mice were placed on a feedback- controlled heating pad (TCAT-2LV, Physitemp Instruments Inc., Clifton, New Jersey) to maintain body temperate at 37°C.

Simultaneous binocular PERG recording was completed with the Miami PERG system (Intelligent Hearing Systems, Miami, FL) according to published protocol (Chou et al., 2018). Eye drops were added as needed to prevent corneal drying (Systane Ultra Lubricant Eye Drops, Alcon Laboratories, Ft. Worth, Texas). The reference electrode was placed subcutaneously on the back of the head between the two ears and the ground electrode was placed at the root of the tail. The signal electrode was placed subcutaneously on the snout for the simultaneous acquisition of left and right eye responses. Two 14 cm x 14 cm LED-based screens were placed 10cm in front of each eye. The pattern remained at a contrast of 85% and a luminance of 800 cd/m2, and consisted of four cycles of black-gray elements, with a spatial frequency of 0.052 c/d. Upon stimulation, the PERG signals were recorded by asynchronous binocular acquisition. Two consecutive recordings of 200 traces were averaged to achieve one readout. The first positive peak in the waveform was designated as P50 and the second negative peak as N95. The investigators who measured the amplitudes were blinded to the treatment of the samples.

Immunohistochemistry

At different time points after surgeries, animals were deeply anesthetized and transcardially perfused with 4% PFA in PBS. Optic nerves and retinas were dissected and fixed in 4% PFA for 1 hour and subsequently washed in PBS. Optic nerves were sequentially incubated in 15% and 30% sucrose at 4°C overnight before mounting in optimal cutting temperature mounting medium for sectioning. Retinas were kept in PBS at 4°C until ready for antibody staining. Retinas were incubated with anti-Brn3a (1:100; Millipore, MAB1585) and anti-RBPMS (1:300; PhosphoSolutions, 1830-RBPMS), and anti-Kif5a (1:300, Abcam ab5628). Secondary antibodies were Alexa Fluor 488-, 594-, or 647-conjugated, highly cross-adsorbed antibodies (1:500; Invitrogen). Wholemount retinal images were acquired using a laser scanning confocal microscope (Carl Zeiss 880 or Olympus FV500) and quantified by a researcher blinded to the experimental condition. Biotinylated optic nerves sections were incubated with 100mM glycine in PBS for 2 h and endogenous peroxidase activity was blocked with 0.5% of H_2O_2 and

1% normal goat serum (NGS) in PBS for ½ hour. Sections were blocked with 10% NGS in PBS for 1 h and incubated overnight with ABC reagent (1 drop of A and 1 drop of B in 5 ml PBS with 1% NGS, Vector Lab). Signal was amplified using tyramide amplification system (TSA kit (PerkinElmer)) conjugated to Alexa Fluor 488.

RGC quantification

The RBPMS quantification were performed in a masked fashion as previously described (Wang et al., 2015). Briefly, the retinas were divided into 4 quadrants, and one digital micrograph was taken from a fixed distance from the periphery of each of the 4 fields. Whole retina Brn3a was quantified using a semi-automated protocol in Velocity (PerkinElmer) and ImageJ in a masked fashion. Tiled images of entire retinal wholemounts were imported into ImageJ for quantification of total area. During this step, care was taken to remove sections of retina damaged during tissue processing. These modified images were then moved to Velocity, where 'Find object' using thresholds for minimum object size, intensity, and touching neighbors. Once the protocol was set for one randomly selected retina, it was applied to all retinas in the experiment.

Fluorescent noncanonical amino acid tagging (FUNCAT)

NHS-Azide-injected samples were processed for click chemistry according to the following protocol, modified from previous studies (Dieterich et al., 2010; Hinz et al., 2012). Sections or wholemounts were transferred to Eppendorf tubes or six-well plates with reaction mixture composed of 100 μm Tris [(1-benzyl-1H-1,2,3-triazol-4-yl)methyl]amine (TBTA, Sigma) dissolved in 4:1 tBuOH/DMSO (Sigma), 100 μm CuSO4 (Sigma), 1.25 μm Alexa Fluor 488 alkyne (Invitrogen), and 250 μm Tris(2-carboxyethyl)phosphine (TCEP, Sigma). The reaction proceeded overnight at room temperature.

Biotin click reaction

Optic nerves or retinas were lysed in 0.5% SDS in PBS plus a cocktail of endogenous protease inhibitors (Complete Protease Inhibitor Cocktail Tablets, Roche) by homogenizing and

sonicating with 10 pulses using a tip sonicator (Sonic Dismembrator model 100, Fisher Scientific). Samples were boiled for 10 min and cooled to room temperature. Any remaining insoluble material was resuspended with additional sonication pulses. Protein concentration in the suspension was measured, and aliquots of 1.5 mg of protein suspension were transferred to eppendorf tubes. NHS-azide that was incorporated into proteins was labeled with PEG4 carboxamide-Propargyl Biotin (biotin-alkyne) (Invitrogen) by click chemistry reaction performed in the total protein suspension as described previously (Hulce et al., 2013; Speers and Cravatt, 2009). Centrifugation steps that can result in loss of NHS azide-labeled material were avoided. For each reaction, an aliquot of 1.5 mg of protein suspension was used, adding PBS to reach 346 µL before adding the click reaction reagents. We added the following reagents in sequence, vigorously vortexing after each addition: 30 µL of 1.7 mM tris[(1-benzyl-1*H*-1,2,3-triazol-4-yl)methyl]amine (TBTA) (Sigma) dissolved in 4:1 *tert*-butanol/DMSO (Sigma), 8 µL of 50 mM $CuSO_4$ dissolved in ultrapure water (Sigma), 8 µL of 5 mM of PEG4 carboxamide-Propargyl Biotin (biotin-alkyne) (Invitrogen) dissolved in DMSO, and 8 µL of 50 mM TCEP (Sigma) dissolved in water. The click reactions were incubated at room temperature for 1–2 h or overnight with gentle rotation at 4 °C. After the completion of each click reaction, samples were aliquoted by transferring 200 µL of each click reaction suspension to 2 mL eppendorf tubes.

Fresh tissue collection

Rats or mice were euthanized with CO_2 and decapitated for brain removal. The tissue was frozen immediately in isopentane in dry ice and stored at -80°C for biochemistry studies. Co-immunoprecipitation studies continued directly without freezing.

Immunoprecipitation and western blot

For western blot, after defrosting frozen tissue the retinas or optic nerves were dissected and homogenized by sonication in 50-100ul RIPA Lysis Buffer with protease and phosphatase inhibitor cocktail (Holt, 78440). Samples were centrifuged at 10,000 x g for 10 minutes at 4°C,

and the supernatants collected. Total protein concentration was determined using a BCA assay (Pierce BCA Protein Assay Kit 23225).

To purify biotinylated proteins for western blot validation, 0.8-2 mg of proteins from ON or retinal homogenates in a total volume of 1 ml were incubated with 30 μl neutravidin beads (Thermo) at 4°C overnight. The beads were then washed 6 times with 1 ml of RIPA buffer. The bound biotinylated proteins where eluted from the beads with 50 μl Laemmli sample buffer containing 2.5% of 2-mercaptoethanol.

For co-immunoprecipitation, retinas and optic nerves were mechanically homogenized in buffer (20 mmol/L HEPES, pH 7.4, 150 mmol/L NaCl, 5 mmol/L EDTA, 0.5% Triton, 50 mmol/L NaF, 1 mmol/L sodium orthovanadate, 1 mmol/L DTT, and protease inhibitors). After centrifugation at 10,000 x g for 10 minutes at 4°C, the clarified extracts were used for immunoprecipitation using appropriate antibodies (2μg rabbit anti-FLAG, CST, 14793S) and 20 μL protein G sepharose (Millipore, Fastflow) for 3 hours to at 4°C. The beads were washed 3-5 times with lysis buffer, and the immunoprecipitated proteins were eluted with 2x Laemmli buffer for western blotting.

For all electrophoresis, 10-30ug of protein was loaded on a 4-20% Tris-Glycine Gel (Thermo Fisher Scientific XP04202) and transferred to an activated 0.2 um PVDF membrane for immunoblotting. The membranes were saturated with Ponceau S stain for 5 minutes and imaged, before washing with ddH20. The membranes were saturated with TBS 1x, 0.05% Tween-20, and 5% nonfat dry milk for 1 hour at room temperature, then incubated overnight at 4°C with rabbit anti-Kif5a (1:1000, Abcam,ab5628), rabbit anti-Kif5c (1:1000, Abcam,ab192883), goat anti-biotin (1:1000, Thermo, 31852), rabbit anti-FLAG (1:2000, CST, 14793S), rabbit anti-β-III tubulin (1:2000, 5568S, CST), rabbit anti-GAPDH (1:2000, CST, 2118), mouse anti-SNCB (1:1000, SAB1406458, Sigma) rabbit anti-GAP43 (1:1000, ab16053, Abcam), rabbit anti-ARF3 (1:1000, ab97490, Abcam). All membranes were washed with TBS-Tween between incubations.

The membranes were then saturated with peroxidase-conjugated goat anti-mouse, anti-rabbit, or anti-goat (1:2000, Abcam, ab6789, ab6721, and ab97110) secondary antibodies for 3 hours at room temperature and revealed with SuperSignal West Femto Chemiluminescent Substrate using ImageQuant LAS4000. Stripping to ensure equal loading was done with ReBlot Plus Strong Antibody Stripping Solution (EMD Millipore 2504). All quantifications were done with ImageJ densitometry analysis.

***In vitro* cell culture**

HEK 293T cells were grown to 100% confluence in 75 or 150 cm^2 flasks, dissociated, and resuspended with TrypLE, transferred to 15 mL falcon tubes, centrifuged for 5 min at 1000 rpm at room temperature, and washed three times in Dulbecco's modified PBS (DPBS, Gibco). Cells were incubated in suspension with 1 mg/mL of biotin-beta-alanine in 10 mL of DPBS at 4 °C with gentle rotation. Cells were washed three times in DPBS, pelleted by centrifugation, and frozen on dry ice. The biotinylated cell pellets were homogenized in RIPA buffer containing 1% NP40, 0.5% sodium deoxycholate, 0.1% SDS, 150 mM NaCl, 1 mM EDTA, and 25 mM TrisHCl, pH 7.4. Lysates were rotated at 4 °C for 30 min and centrifuged at 10 000*g* for 10 min at 4 °C to remove DNA and cell debris. After measuring the protein concentration using the DC Protein Assay Kit II (Bio-Rad), the lysates were aliquoted by transferring 1–2 mg of protein to 2 mL eppendorf tubes.

Biotin measurements

Unincorporated free biotin and biotin incorporated to proteins were measured using a Fluorescence Biotin Quantitation Kit (Thermo) and a fluorescence plate reader (Synergy Mx Microplate Reader, Biotek) by measuring fluorescent excitation/emission at 495/520 according to manufacturer's instructions. Dissected samples from retinas and optic nerves from 6 animals were weighed and pooled. Protein extracts were generated by homogenizing and sonicating 122 mg of wet tissue from retina or optic nerve in 1ml of 1 mM EDTA, 50 mM Tris, pH7.5 (TE) buffer and centrifuged at 10,000 g for 15 min at 4° C to remove nuclei and cell debris. The

lysates were mixed with 4 ml of cold acetone, incubated at -20° C overnight and centrifuged for 1 h at 4500 g in a swinging bucket rotor to precipitate proteins. Supernatants were collected and evaporated to a volume of ~20 μl in a SpeedVac concentrator (Thermo Scientific) and protein pellets were solubilized in RIPA buffer. As a standard, we used a series of biocytin dilutions (from 0.5 to 10 pmol/μl) according to the manufacturer's instructions. After intravitreal injection of NHS-biotin, we found 18-20 mouse optic nerves to have equivalent biotinylated protein as 8 rat optic nerves.

Mass spectrometry

Soluble peptides were pressure-loaded onto a 250-μm i.d capillary with a kasil frit containing 2 cm of 10 μm Jupiter C18-A material (Phenomenex) followed by 2 cm, 5 μm Partisphere strong cation exchanger (Whatman). This column was washed with Buffer A after loading. A 100 μm i.d capillary with a 5 μm pulled tip packed with 15 cm, 4 μm Jupiter C_{18} material (Phenomenex) was attached to the loading column with a union and the entire split-column (loading column–union–analytical column) was placed in line with an Agilent 1100 quaternary HPLC (Palo Alto). For transportome analysis, the sample was analyzed using a modified 4-step separation described previously (Washburn et al., 2001). The buffer solutions used were 5% acetonitrile/0.1% formic acid (Buffer A), 80% acetonitrile/0.1% formic acid (Buffer B), and 500 mM ammonium acetate/5% acetonitrile/0.1% formic acid (Buffer C). Step 1 consisted of a 35 min gradient from 0-55% Buffer B, a 5 min gradient from 55-70% Buffer B, 10 min 100% Buffer B and 27 min 100% Buffer A. Steps 2-3 had the following profile: 5 min of x % Buffer C with (100-x)% buffer A, a 10 min Buffer A, a 5 min gradient from 0-15% Buffer B, a 70 min gradient from 15-55% Buffer B, a 5 min gradient from 55-100% Buffer B, a 5 min 100% Buffer B, and 20 min 100% Buffer A. The Buffer C percentages (X) were 10 and 40 for the steps 2-3, respectively. In the last step, the gradient contained: 5 min of 90% Buffer C with 10% buffer B, a 10 min Buffer A, a 5 min gradient from 0-15% Buffer B, a 70 min gradient from 15-55%

Buffer B, a 5 min gradient from 55-100% Buffer B, a 5 min 100% Buffer B, and 20 min 100% Buffer A. For whole proteome analysis, the sample was analyzed using a 11-step separation exactly described as above except the buffer C percentages (X) were 10, 15, 20, 30, 40, 50, 60 and 80% for the steps 2-9, respectively. In the last two steps (I.e. 10 and 11), the gradient contained: 1 min 100% Buffer A, 5 min of 100 % Buffer C, a 5 min Buffer A, a 5 min gradient from 0-15% Buffer B, 70 min gradient from 15-55% Buffer B, 5 min gradient from 0-10% Buffer B, 75 min gradient from 10-45% Buffer B, 10 min 100% Buffer B, and 10 min 100% Buffer A. As peptides eluted from the microcapillary column, they were electrosprayed directly into a Velos mass spectrometer (ThermoFisher) with the application of a distal 2.4 kV spray voltage. A cycle of one full-scan FT mass spectrum (300-2,000 m/z) at 60,000 resolution followed by 20 data-dependent IT MS/MS spectra at a 35% normalized collision energy was repeated continuously throughout each step of the multidimensional separation. Application of mass spectrometer scan functions and HPLC solvent gradients were controlled by the Xcalibur data system.

MS data analysis

MS2 (tandem mass spectra) was extracted from the XCalibur data system format (.RAW) into MS1 and MS2 formats using in house software (RAW_Xtractor) (McDonald et al., 2004). Tandem mass spectra remaining after filtering were searched with Prolucid (Xu et al., 2015) against the UniProt_rat_03-25-2014 or UniProt_mouse_20170219_04-17-2017 concatenated to a decoy database in which the sequence for each entry in the original database was reversed (Peng et al., 2003). All searches were parallelized and performed on a Beowulf computer cluster consisting of 100 1.2 GHz Athlon CPUs (Sadygov et al., 2002). No enzyme specificity was considered for any search. The following modifications were searched for analysis for transportome analyses: a static modification of 57.02146 on cysteine for all analyses, a differential modification of 226.0776 on lysine for modified peptides. Prolucid results were assembled and filtered using the DTASelect (version 2.0) program (Cociorva et al., 2006; Tabb et al., 2002). DTASelect 2.0 uses a linear discriminant analysis to dynamically set XCorr

and DeltaCN thresholds for the entire dataset to achieve a user-specified false discovery rate (FDR). In DTASelect, the modified peptides were required to be partially tryptic, less than 10ppm deviation from peptide match, and an FDR at the protein level of 0.01. The FDRs are estimated by the program from the number and quality of spectral matches to the decoy database. For all datasets, the protein FDR was < 1% and the peptide FDR was < 1%. The Datasets from “Control Rat Transportome”, “ONC Rat Transportome”, Control Mouse Transportome” and “Kif5a KO Mouse Transportome” are composed of the total detected biotinylated proteins in 3, 3, 2, and 3 individual MS runs, respectively. Each sample was prepared by pooling tissue from 8-10 rats or 18-20 mice. Normalized Spectral Abundance Factor was exported per UniProt accession ID for further quantitative analysis.

Protein-protein interaction analysis

All proteins labeled in Figure 3e plus Kif5a were input into STRINGdb (http://string-db.org) (Szklarczyk et al., 2017). Interactions sources included: textmining, experiments, databases, co-expression, neighborhood, gene fusion, and co-occurrence, with a medium 0.400 required interaction score. These data were exported into Cytoscape 3.7 for graphical organization.

Statistical analysis

Data were analyzed using R version 3.5.0 (The R Foundation for Statistical Computing) or Graphpad Prism 7 (Graphpad, San Diego, CA, USA). For correlation between proteomic samples, significance testing used Pearson’s correlation coefficient in package ‘GGally’. Quantitative proteomic comparisons of individual proteins were made using the ‘t-test’ function of the ‘limma’ package in R. For statistical comparison of Kif5a transport after ONC by western blot, a one-sample, two-sided t-test was used. For comparison of Beta III Tubulin co-IP, ratio-paired two-sided t-test was used as replicates were exposed and imaged independently. For all other comparisons between two samples, two-sided unpaired t-tests were used. For group comparisons, ordinary one-way ANOVA with post-hoc Sidak correction was used.

Chapter 2, in part, is currently being prepared for submission for publication of the material. Shah SH*, Schiapparelli LM*, Ma Y, Atkins M, Xia X, Saturday S, Sun C, Knasel C, Yates III JR, Cline HT, Goldberg JL. “Quantitative transportomics identifies Kif5a as a major regulator of neurodegeneration”. The dissertation author was a primary investigator and author of this paper.

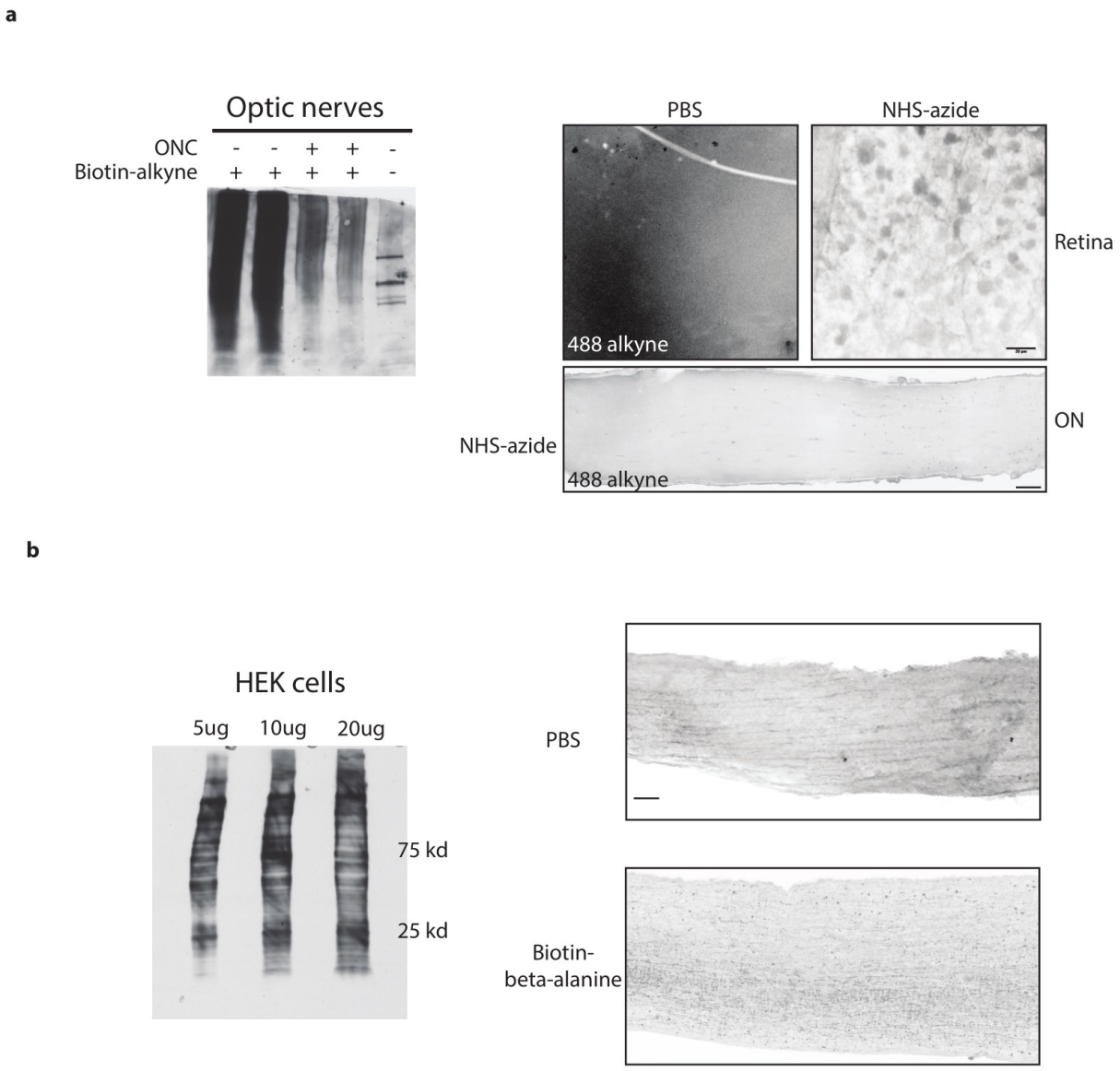

Supplemental Figure 2.1. Alternative strategies for transported protein labeling a. ONs injected with NHS-azide underwent either ONC or sham surgeries. After tissue collection, protein isolation, and biotin conjugation through alkyne-azide cycloaddition, samples were probed for biotin through western blot. Parallel mice were immunolabeled with FUNCAT for histology. Cell bodies are visible in the retina after NHS-azide injection, yet signal was low in RGC axons in the ON. b. Different amounts of protein isolated from HEK cells treated with biotin-beta-alanine were probed for biotin by western blot. After *in vivo* injection, immunofluorescence for biotin showed positive signal in RGC axons in the ON after biotin-beta-alanine, but only background signal in the control ON.

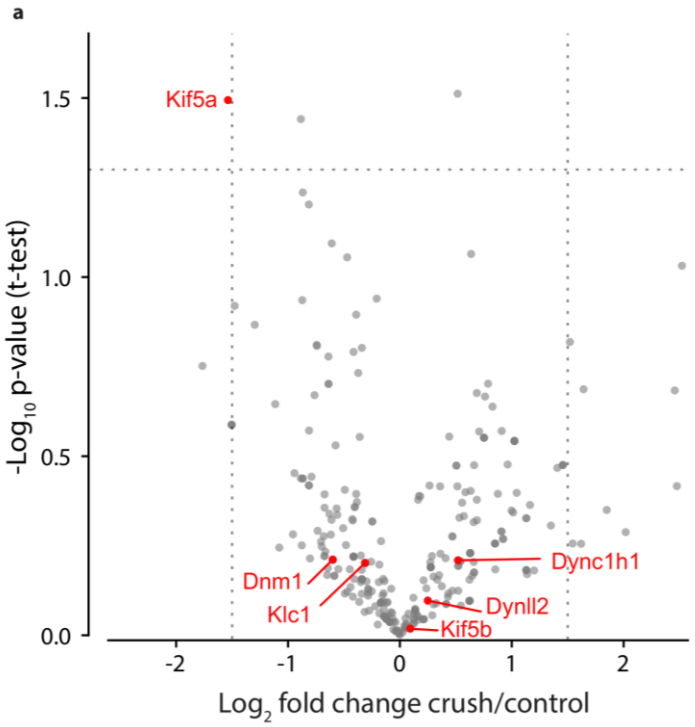

Supplemental Figure 2.2. Transport changes in motor proteins after injury A. Motor proteins present in the ON transportome after injury, labeled in red. No motor protein other than Kif5a showed significant changes in transport, with related isoform Kif5b showing almost no change in transport before and after injury.

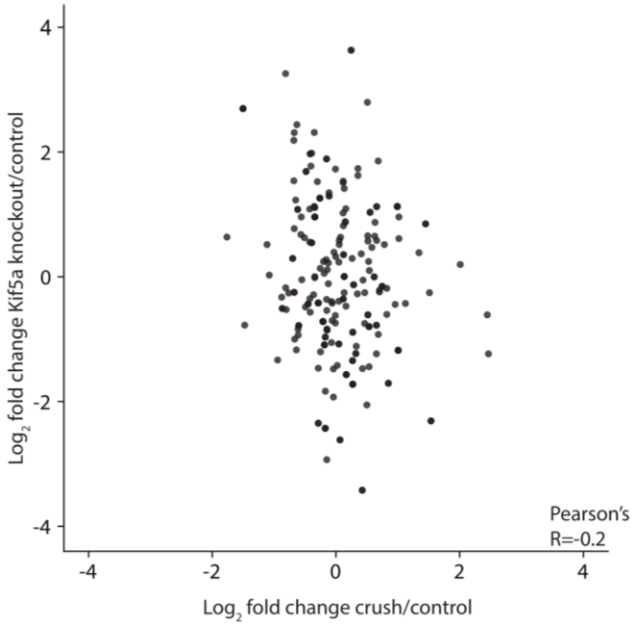

Supplemental Figure 2.3. Comparison of transport changes after ONC and after Kif5a KO a. Average log_2 fold change of each protein identity present in both proteomic samples were compared against each other. There was little correlation between the data sets (Pearson's R=-0.2), suggesting that Kif5a loss is only a part of the broader ONC response, and vice versa.

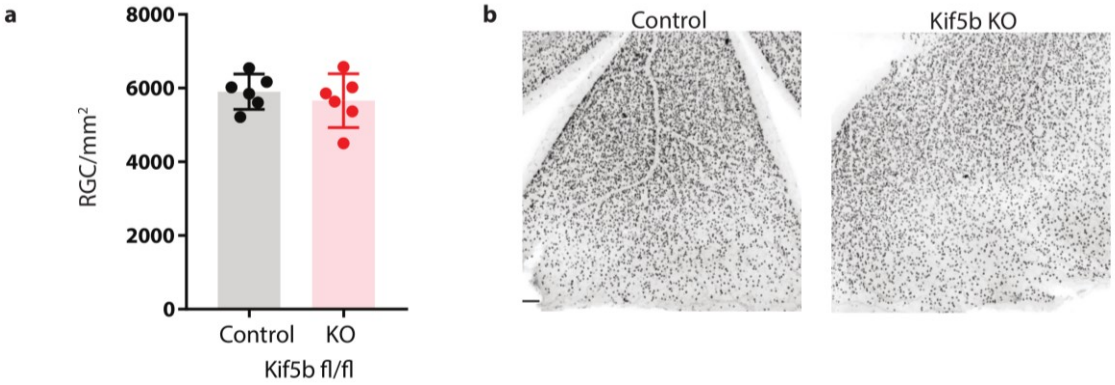

Supplemental Figure 2.4. Kif5b loss does not lead to RGC degeneration a. Quantification of Brn3a+ cell density across entire wholemount retinal surface. Each point represents one retina. Statistical comparison of homozygous Kif5b KO at 1 month after viral injection (control n=6, KO n=6) by two-sample, two-tailed t-test showed not significance. b. Representative image of wholemount retinas. Scale= 100 μm.

References

Belin, S., Nawabi, H., Wang, C., Tang, S., Latremoliere, A., Warren, P., Schorle, H., Uncu, C., Woolf, C.J., He, Z., and Steen, J.A. (2015). Injury-Induced Decline of Intrinsic Regenerative Ability Revealed by Quantitative Proteomics. Neuron *86*, 1000–1014.

Best, M.D. (2009). Click Chemistry and Bioorthogonal Reactions : Unprecedented Selectivity in the Labeling of Biological Molecules. Biochemistry *48*, 6571–6584.

Blair, M.A., Ma, S., and Hedera, P. (2006). Mutation in KIF5A can also cause adult-onset hereditary spastic paraplegia. Neurogenetics *7*, 47–50.

Brenner, D., Yilmaz, R., Muller, K., Grehl, T., Petri, S., Meyer, T., Grosskreutz, J., Weydt, P., Ruf, W., Neuwirth, C., Weber, M., Pinto, S., Claeys, K.G., Hu, A., Jablonka, S., Sendtner, M., Klopstock, T., Carvalho, M. De, Sperfeld, A., Borck, G., Volk, A.E., Dorst, J., Weis, J., Otto, M., Schuster, J., Tredici, K. Del, Braak, H., Danzer, K.M., Freischmidt, A., Meitinger, T., Strom, T.M., Ludolph, A.C., Andersen, P.M., and Weishaupt, J.H. (2018). Hot-spot KIF5A mutations cause familial ALS. Brain *141*, 688–697.

Butler, M.H., David, C., Ochoa, G.C., Freyberg, Z., Daniell, L., Grabs, D., Cremona, O., and De Camilli, P. (1997). Amphiphysin II (SH3p9; BIN1), a member of the amphiphysin/Rvs family, is concentrated in the cortical cytomatrix of axon initial segments and nodes of ranvier in brain and around T tubules in skeletal muscle. J. Cell Biol. *137*, 1355–1367.

Butowt, R., and Von Bartheld, C.S. (2007). Conventional kinesin-I motors participate in the anterograde axonal transport of neurotrophins in the visual system. J. Neurosci. Res. *85*, 2546–2556.

Cai, D., Yingjing, S., De Bellard, M.E., Tang, S., and Filbin, M.T. (1999). Prior exposure to neurotrophins blocks inhibition of axonal regeneration by MAG and myelin via a cAMP-dependent mechanism. Neuron *22*, 89–101.

Cai, D., Hoppe, A.D., Swanson, J.A., and Verhey, K.J. (2007). Kinesin-1 structural organization and conformational changes revealed by FRET stoichiometry in live cells. J. Cell Biol. *176*, 51–63.

Chevalier-Larsen, E., and Holzbaur, E.L.F. (2006). Axonal transport and neurodegenerative disease. Biochim. Biophys. Acta *1762*, 1094–1108.

Chou, T.-H., Toft-Nielsen, J., and Porciatti, V. (2018). High-Throughput Binocular Pattern Electroretinograms in the Mouse. In Glaucoma Methods and Protocols, pp. 63–68.

Cociorva, D., L. Tabb, D., and Yates, J.R. (2006). Validation of Tandem Mass Spectrometry Database Search Results Using DTASelect. In Current Protocols in Bioinformatics, p. 13.4.1-13.4.14.

Dieterich, D.C., Hodas, J.J.L., Gouzer, G., Shadrin, I.Y., Ngo, J.T., Triller, A., Tirrell, D.A., and Schuman, E.M. (2010). In situ visualization and dynamics of newly synthesized proteins in rat hippocampal neurons. Nat. Neurosci. *13*, 897–905.

Galvao, J., Iwao, K., Apara, A., Wang, Y., Ashouri, M., Shah, N., Blackmore, M., Kunzevitzky, N.J., Moore, D.L., and Goldberg, J.L. (2018). The Kruppel-Like Factor Gene Target Dusp14 Regulates Axon Growth and Regeneration. Investig. Ophthalmol. Vis. Sci. *59*.

Gilley, J., Orsomando, G., Nascimento-ferreira, I., Michael, P., Gilley, J., Orsomando, G., Nascimento-ferreira, I., and Coleman, M.P. (2015). Absence of SARM1 Rescues

Development and Survival of NMNAT2-Deficient Axons. Cell Rep. *10*, 1974–1981.

Hammond, J.W., Blasius, T.L., Soppina, V., Cai, D., and Verhey, K.J. (2010). Autoinhibition of the kinesin-2 motor KIF17 via dual intramolecular mechanisms. J. Cell Biol. *189*, 1013–1025.

Hendricks, A.G., Perlson, E., Ross, J.L., Iii, H.W.S., Tokito, M., and Holzbaur, E.L.F. (2010). Motor Coordination via a Tug-of-War Mechanism Drives Bidirectional Vesicle Transport. Curr. Biol. *20*, 697–702.

Hertzog, M., Heijenoort, C. Van, Didry, D., Gaudier, M., Pre, T., Knossow, M., Guittet, E., and Carlier, M. (2004). The B-Thymosin / WH2 Domain: Structural Basis for the Switch from Inhibition to Promotion of Actin Assembly. Cell *117*, 611–623.

Hinz, F.I., Dieterich, D.C., Tirrell, D.A., and Schuman, E.M. (2012). Noncanonical amino acid labeling in vivo to visualize and affinity purify newly synthesized proteins in larval zebrafish. ACS Chem. Neurosci. *3*, 40–49.

Hirokawa, N., Noda, Y., Tanaka, Y., and Niwa, S. (2009). Kinesin superfamily motor proteins and intracellular transport. Nat. Rev. Mol. Cell Biol. *10*, 682–696.

Homma, N., Takei, Y., Tanaka, Y., Nakata, T., Terada, S., Kikkawa, M., Noda, Y., and Hirokawa, N. (2003). Kinesin superfamily protein 2A (KIF2A) functions in suppression of collateral branch extension. Cell *114*, 229–239.

Huang, J., Brady, S.T., Richards, B.W., Stenoien, D., Resau, J.H., Copeland, N.G., and Jenkins, N.A. (1999). Direct interaction of microtubule- and actin-based transport motors. Nature *397*, 267–270.

Hulce, J.J., Cognetta, A.B., Niphakis, M.J., Tully, S.E., and Cravatt, B.F. (2013). Proteome-wide mapping of cholesterol-interacting proteins in mammalian cells. Nat. Methods *10*, 259–264.

Knoferle, J., Koch, J.C., Ostendorf, T., Michel, U., Planchamp, V., Vutova, P., Tonges, L., Stadelmann, C., Bruck, W., Bahr, M., and Lingor, P. (2010). Mechanisms of acute axonal degeneration in the optic nerve in vivo. Proc. Natl. Acad. Sci. *107*, 6064–6069.

Kolb, H.C., Finn, M.G., and Sharpless, K.B. (2001). Click Chemistry: Diverse Chemical Function from a Few Good Reactions. Angew. Chemie *40*, 2004–2021.

Leaver, S.G., Cui, Q., Plant, G.W., Arulpragasam, A., Hisheh, S., Verhaagen, J., and Harvey, a R. (2006). AAV-mediated expression of CNTF promotes long-term survival and regeneration of adult rat retinal ganglion cells. Gene Ther. *13*, 1328–1341.

Li, X., Zimmerman, A., Copeland, N.G., Gilbert, D.J., Jenkins, N.A., and Yin, H.L. (1996). The Mouse Thymosin B4 Gene: Structure, Promoter Identification, and Chromosome Localization. Genomics *394*, 388–394.

Liang, P., and MacRae, T.H. (1997). Molecular Chaperones and the Cytoskeleton. J. Cell Sci. *110*, 1431–1440.

Liddelow, S.A., Guttenplan, K.A., Clarke, L.E., Bennett, F.C., Bohlen, C.J., Schirmer, L., Bennett, M.L., Münch, A.E., Chung, W.S., Peterson, T.C., Wilton, D.K., Frouin, A., Napier, B.A., Panicker, N., Kumar, M., Buckwalter, M.S., Rowitch, D.H., Dawson, V.L., Dawson, T.M., Stevens, B., and Barres, B.A. (2017). Neurotoxic reactive astrocytes are induced by activated microglia. Nature *541*, 481–487.

Liu, Q., Zie, F., Alvarado-Diaz, A., Smith, M.A., Moreira, P.I., Zhu, X., and Perry, G. (2011). Neurofilamentopathy in Neurodegenerative Diseases. Open Neurol. J. *5*, 58–62.

McDonald, W.H., Tabb, D.L., Sadygov, R.G., MacCoss, M.J., Venable, J., Graumann, J., Johnson, J.R., Cociorva, D., and Yates, J.R. (2004). MS1, MS2, and SQT - Three unified, compact, and easily parsed file formats for the storage of shotgun proteomic spectra and identifications. Rapid Commun. Mass Spectrom. *18*, 2162–2168.

McKerracher, L., Vidal-Sanz, M., Essagian, C., and Aguayo, A.J. (1990a). Selective impairment of slow axonal transport after optic nerve injury in adult rats. J. Neurosci. *10*, 2834–2841.

McKerracher, L., Vidal-Sanz, M., and Aguayo, A.J. (1990b). Slow transport rates of cytoskeletal proteins change during regeneration of axotomized retinal neurons in adult rats. J. Neurosci. *10*, 641–648.

Michaelevski, I., Medzihradszky, K.F., Lynn, A., Burlingame, A.L., and Fainzilber, M. (2010). Axonal transport proteomics reveals mobilization of translation machinery to the lesion site in injured sciatic nerve. Mol. Cell. Proteomics *9*, 976–987.

Milosevic, I., Giovedi, S., Lou, X., Raimondi, A., Collesi, C., Shen, H., Paradise, S., O'Toole, E., Ferguson, S., Cremona, O., and De Camilli, P. (2011). Recruitment of endophilin to clathrin-coated pit necks is required for efficient vesicle uncoating after fission. Neuron *72*, 587–601.

Morfini, G., Szebenyi, G., Richards, B., and Brady, S.T. (2001). Regulation of kinesin: Implications for neuronal development. Dev. Neurosci. *23*, 364–376.

Morfini, G.A., Burns, M., Binder, L.I., Kanaan, N.M., LaPointe, N., Bosco, D.A., Brown, R.H., Brown, H., Tiwari, A., Hayward, L., Edgar, J., Nave, K.-A., Garberrn, J., Atagi, Y., Song, Y., Pigino, G., and Brady, S.T. (2009). Axonal transport defects in neurodegenerative diseases. J. Neurosci. *29*, 12776–12786.

Nakajima, K., Yin, X., Takei, Y., Seog, D., Homma, N., and Hirokawa, N. (2012). Article Molecular Motor KIF5A Is Essential for GABA A Receptor Transport, and KIF5A Deletion Causes Epilepsy. Neuron *76*, 945–961.

Nicolas, A., Kenna, K.P., Renton, A.E., Ticozzi, N., Faghri, F., Chia, R., Dominov, J.A., Kenna, B.J., Nalls, M.A., Keagle, P., Rivera, A.M., Rheenen, W. van, Murphy, N.A., Vugt, J.J.F.A. van, Geiger, J.T., Spek, R.A. Van der, Pliner, H.A., Shankaracharya, Smith, B.N., Marangi, G., Topp, S.D., Abramzon, Y., Gkazi, A.S., Eicher, J.D., Kenna, A., Logullo, F.O., Simone, I., Logroscino, G., Salvi, F., Bartolomei, I., Borghero, G., Murru, M.R., Costantino, E., Pani, C., Puddu, R., Caredda, C., Piras, V., Tranquilli, S., Cuccu, S., Corongiu, D., Melis, M., Milia, A., Marrosu, F., Marrosu, M.G., Floris, G., Cannas, A., Tranquilli, S., Capasso, M., Caponnetto, C., Mancardi, G., Origone, P., Mandich, P., Conforti, F.L., Cavallaro, S., Mora, G., Marinou, K., Sideri, R., Penco, S., Mosca, L., Lunetta, C., Pinter, G.L., Corbo, M., Riva, N., Carrera, P., Volanti, P., Mandrioli, J., Fini, N., Fasano, A., Tremolizzo, L., Arosio, A., Ferrarese, C., Trojsi, F., Tedeschi, G., Monsurrò, M.R., Piccirillo, G., Femiano, C., Ticca, A., Ortu, E., Bella, V. La, Spataro, R., Colletti, T., Sabatelli, M., Zollino, M., Conte, A., Luigetti, M., Lattante, S., Marangi, G., Santarelli, M., Petrucci, A., Pugliatti, M., Pirisi, A., Parish, L.D., Occhineri, P., Giannini, F., Battistini, S., Ricci, C., Benigni, M., Cau, T.B., Loi, D., Calvo, A., Moglia, C., Brunetti, M., Barberis, M., Restagno, G., Casale, F., Marrali, G., Fuda, G., Ossola, I., Cammarosano, S., Canosa, A., Ilardi, A., Manera, U., Grassano, M., Tanel, R., Pisano, F., Mora, G., Calvo, A., Mazzini, L., Riva, N., Mandrioli, J., Caponnetto, C., Battistini, S.,

Volanti, P., Bella, V. La, Conforti, F.L., Borghero, G., Messina, S., Simone, I.L., Trojsi, F., Salvi, F., Logullo, F.O., D'Alfonso, S., Corrado, L., Capasso, M., Ferrucci, L., Harms, M.B., Goldstein, D.B., Shneider, N.A., Goutman, S., Simmons, Z., Miller, T.M., Chandran, S., Pal, S., Manousakis, G., Appel, S.H., Simpson, E., Wang, L., Baloh, R.H., Gibson, S., Bedlack, R., Lacomis, D., Sareen, D., Sherman, A., Bruijn, L., Penny, M., Moreno, C. de A.M., Kamalakaran, S., Goldstein, D.B., Allen, A.S., Appel, S., Baloh, R.H., Bedlack, R.S., Boone, B.E., Brown, R., Carulli, J.P., Chesi, A., Chung, W.K., Cirulli, E.T., Cooper, G.M., Couthouis, J., Day-Williams, A.G., Dion, P.A., Gibson, S., Gitler, A.D., Glass, J.D., Goldstein, D.B., Han, Y., Harms, M.B., Harris, T., Hayes, S.D., Jones, A.L., Keebler, J., Krueger, B.J., Lasseigne, B.N., Levy, S.E., Lu, Y.-F., Maniatis, T., McKenna-Yasek, D., Miller, T.M., Myers, R.M., Petrovski, S., Pulst, S.M., Raphael, A.R., Ravits, J.M., Ren, Z., Rouleau, G.A., Sapp, P.C., Shneider, N.A., Simpson, E., Sims, K.B., Staropoli, J.F., Waite, L.L., Wang, Q., Wimbish, J.R., Xin, W.W., Gitler, A.D., Harris, T., Myers, R.M., Phatnani, H., Kwan, J., Sareen, D., Broach, J.R., Simmons, Z., Arcila-Londono, X., Lee, E.B., Deerlin, V.M. Van, Shneider, N.A., Fraenkel, E., Ostrow, L.W., Baas, F., Zaitlen, N., Berry, J.D., Malaspina, A., Fratta, P., Cox, G.A., Thompson, L.M., Finkbeiner, S., Dardiotis, E., Miller, T.M., Chandran, S., Pal, S., Hornstein, E., MacGowan, D.J., Heiman-Patterson, T., Hammell, M.G., Patsopoulos, N.A., Dubnau, J., Nath, A., Phatnani, H., Musunuri, R.L., Evani, U.S., Abhyankar, A., Zody, M.C., Kaye, J., Finkbeiner, S., Wyman, S., LeNail, A., Lima, L., Fraenkel, E., Rothstein, J.D., Svendsen, C.N., Thompson, L.M., Eyk, J. Van, Maragakis, N.J., Berry, J.D., Glass, J.D., Miller, T.M., Kolb, S.J., Baloh, R.H., Cudkowicz, M., Baxi, E., Kaye, J., Finkbeiner, S., Wyman, S.K., LeNail, A., Lima, L., Fraenkel, E., Svendsen, C.N., Thompson, L.M., Eyk, J.E. Van, Berry, J.D., Miller, T.M., Kolb, S.J., Cudkowicz, M., Baxi, E., Benatar, M., Taylor, J.P., Wu, G., Rampersaud, E., Wuu, J., Rademakers, R., Züchner, S., Schule, R., McCauley, J., Hussain, S., Cooley, A., Wallace, M., Clayman, C., Barohn, R., Statland, J., Ravits, J., Swenson, A., Jackson, C., Trivedi, J., Khan, S., Katz, J., Jenkins, L., Burns, T., Gwathmey, K., Caress, J., McMillan, C., Elman, L., Pioro, E., Heckmann, J., So, Y., Walk, D., Maiser, S., Zhang, J., Benatar, M., Taylor, J.P., Rampersaud, E., Wu, G., Wuu, J., Silani, V., Ticozzi, N., Gellera, C., Ratti, A., Taroni, F., Lauria, G., Verde, F., Fogh, I., Tiloca, C., Comi, G.P., Sorarù, G., Cereda, C., D'Alfonso, S., Corrado, L., Marchi, F. De, Corti, S., Ceroni, M., Mazzini, L., Siciliano, G., Filosto, M., Inghilleri, M., Peverelli, S., Colombrita, C., Poletti, B., Maderna, L., Bo, R. Del, Gagliardi, S., Querin, G., Bertolin, C., Pensato, V., Castellotti, B., Lauria, G., Verde, F., Fogh, I., Tiloca, C., Comi, G.P., Sorarù, G., Cereda, C., Camu, W., Mouzat, K., Lumbroso, S., Corcia, P., Meininger, V., Besson, G., Lagrange, E., Clavelou, P., Guy, N., Couratier, P., Vourch, P., Danel, V., Bernard, E., Lemasson, G., Corcia, P., Laaksovirta, H., Myllykangas, L., Jansson, L., Valori, M., Ealing, J., Hamdalla, H., Rollinson, S., Pickering-Brown, S., Orrell, R.W., Sidle, K.C., Malaspina, A., Hardy, J., Singleton, A.B., Johnson, J.O., Arepalli, S., Sapp, P.C., McKenna-Yasek, D., Polak, M., Asress, S., Al-Sarraj, S., King, A., Troakes, C., Vance, C., Belleroche, J. de, Baas, F., Asbroek, A.L.M.A. ten, Muñoz-Blanco, J.L., Hernandez, D.G., Ding, J., Gibbs, J.R., Scholz, S.W., Floeter, M.K., Campbell, R.H., Landi, F., Bowser, R., Pulst, S.M., Ravits, J.M., MacGowan, D.J.L., Kirby, J., Pioro, E.P., Pamphlett, R., Broach, J., Gerhard, G., Dunckley, T.L., Brady, C.B., Kowall, N.W., Troncoso, J.C., Ber, I. Le, Mouzat, K., Lumbroso, S., Heiman-Patterson, T.D., Kamel, F., Bosch, L. Van Den, Baloh, R.H., Strom, T.M., Meitinger, T., Shatunov, A., Eijk, K.R. Van, Carvalho, M. de, Kooyman, M., Middelkoop, B., Moisse, M., McLaughlin, R.L., Es, M.A. Van, Weber, M., Boylan, K.B., Blitterswijk, M. Van, Rademakers, R., Morrison, K.E., Basak, A.N., Mora, J.S., Drory, V.E., Shaw, P.J., Turner, M.R., Talbot, K., Hardiman, O., Williams, K.L., Fifita, J.A., Nicholson, G.A., Blair, I.P., Rouleau, G.A., Esteban-Pérez, J., García-Redondo, A., Al-Chalabi, A., Kheifat, A. Al, Al-Chalabi, A., Andersen, P., Basak,

A.N., Blair, I.P., Chio, A., Cooper-Knock, J., Corcia, P., Couratier, P., Carvalho, M. de, Dekker, A., Drory, V., Redondo, A.G., Gotkine, M., Hardiman, O., Hide, W., Iacoangeli, A., Glass, J., Kenna, K., Kiernan, M., Kooyman, M., Landers, J., McLaughlin, R., Middelkoop, B., Mill, J., Neto, M.M., Moisse, M., Pardina, J.M., Morrison, K., Newhouse, S., Pinto, S., Pulit, S., Robberecht, W., Shatunov, A., Shaw, P., Shaw, C., Silani, V., Sproviero, W., Tazelaar, G., Ticozzi, N., Damme, P. van, Berg, L. van den, Spek, R. van der, Eijk, K. van, Es, M. van, Rheenen, W. van, Vugt, J. van, Veldink, J., Weber, M., Williams, K.L., Zatz, M., Bauer, D.C., Twine, N.A., Rogaeva, E., Zinman, L., Ostrow, L.W., Maragakis, N.J., Rothstein, J.D., Simmons, Z., Cooper-Knock, J., Brice, A., Goutman, S.A., Feldman, E.L., Gibson, S.B., Taroni, F., Ratti, A., Gellera, C., Damme, P. Van, Robberecht, W., Fratta, P., Sabatelli, M., Lunetta, C., Ludolph, A.C., Andersen, P.M., Weishaupt, J.H., Camu, W., Trojanowski, J.Q., Deerlin, V.M. Van, Brown, R.H., Berg, L.H. van den, Veldink, J.H., Harms, M.B., Glass, J.D., Stone, D.J., Tienari, P., Silani, V., Chiò, A., Shaw, C.E., Traynor, B.J., and Landers, J.E. (2018). Genome-wide Analyses Identify KIF5A as a Novel ALS Gene. Neuron *97*, 1268–1283.e6.

Park, K.K., Liu, K., Hu, Y., Kanter, J.L., and He, Z. (2010). PTEN/mTOR and axon regeneration. Exp. Neurol. *223*, 45–50.

Pasinelli, P., and Brown, R.H. (2006). Molecular biology of amyotrophic lateral sclerosis: insights from genetics. Nat. Rev. Neurosci. *7*, 710–723.

Peng, J.M., Elias, J.E., Thoreen, C.C., Licklider, L.J., and Gygi, S.P. (2003). Evaluation of multidimensional chromatography coupled with tandem mass spectrometry (LC/LC-MS) for Large-Scale Protein Analyis: The Yeast Proteome. J. Proteome Res. *2*, 43–50.

Perry, G., Rizzuto, N., Autilio-Gambetti, L., and Gambetti, P. (1985). Paired helical filaments from Alzheimer disease patients contain cytoskeletal components. Proc. Natl. Acad. Sci. *82*, 3916–3920.

Quigley, H.A., Guy, J., and Anderson, D.R. (1979). Blockade of Rapid Axonal Transport: Effect of Intraocular Pressure Elevation in Primate Optic Nerve. Arch. Ophthalmol. *97*, 525–531.

Rahman, A., Kamal, A., Roberts, E.A., and Goldstein, L.S.B. (1999). Defective Kinesin Heavy Chain Behavior in Mouse Kinesin Light Chain Mutants. J. Cell Biol. *146*, 1277–1287.

Reid, E., Kloos, M., Ashley-koch, A., Hughes, L., Bevan, S., Svenson, I.K., Graham, F.L., Gaskell, P.C., Dearlove, A., Pericak-vance, M.A., Rubinsztein, D.C., and Marchuk, D.A. (2002). A Kinesin Heavy Chain (KIF5A) Mutation in Hereditary Spastic Paraplegia (SPG10). Am. J. Hum. Genet. 1189–1194.

Roffe, M., Hajj, G.N.M., Azevedo, H.F., Alves, V.S., and Castilho, B.A. (2013). IMPACT Is a Developmentally Regulated Protein in Neurons That Opposes the Eukaryotic Initiation Factor 2a Kinase GCN2 in the modulation of Neurite Outgrowth. J. Biol. Chem. *288*, 10860–10869.

Sadygov, R.G., Eng, J., Durr, E., Saraf, A., McDonald, H., MacCoss, M.J., and Yates, J.R. (2002). Code developments to improve the efficiency of automated MS/MS spectra interpretation. J. Proteome Res. *1*, 211–215.

Sánchez-Migallón, M.C., Valiente-Soriano, F.J., Nadal-Nicolás, F.M., Vidal-Sanz, M., and Agudo-Barriuso, M. (2016). Apoptotic retinal ganglion cell death after optic nerve transection or crush in mice: Delayed RGC loss with BDNF or a caspase 3 inhibitor.

Investig. Ophthalmol. Vis. Sci. *57*, 81–93.

Sato, K., Saigusa, D., Saito, R., Fujioka, A., Nakagawa, Y., Nishiguchi, K.M., Kokubun, T., Motoike, I.N., Maruyama, K., Omodaka, K., Shiga, Y., Uruno, A., Koshiba, S., Yamamoto, M., and Nakazawa, T. (2018). Metabolomic changes in the mouse retina after optic nerve injury. Sci. Rep. *8*, 1–13.

Schiapparelli, L.M., Mcclatchy, D.B., Liu, H., Sharma, P., Yates, J.R., and Cline, H.T. (2014). Direct Detection of Biotinylated Proteins by Mass Spectrometry. J. Proteome Res. *13*, 3966–3978.

Seshadri, S., Fitzpatrick, A.L., and et.al (2010). Genome-wide Analysis of Genetic Loci Associated with Alzheimer Disease. J. Am. Med. Assoc. *303*, 1832–1840.

Smith, P.D., Sun, F., Park, K.K., Cai, B., Wang, C., Kuwako, K., Martinez-Carrasco, I., Connolly, L., and He, Z. (2009). SOCS3 Deletion Promotes Optic Nerve Regeneration In Vivo. Neuron *64*, 617–623.

Soppina, V., Rai, A.K., Ramaiya, A.J., Barak, P., and Mallik, R. (2009). Tug-of-war between dissimilar teams of microtubule motors regulates transport and fission of endosomes. Proc. Natl. Acad. Sci. *106*.

Speers, A.E., and Cravatt, B.F. (2009). Activity-Based Protein Profiling (ABPP) and Click Chemistry (CC)-ABPP by MudPIT Mass Spectrometry. Curr. Protoc. Chem. Biol. *1*, 29–41.

Szklarczyk, D., Morris, J.H., Cook, H., Kuhn, M., Wyder, S., Simonovic, M., Santos, A., Doncheva, N.T., Roth, A., Bork, P., Jensen, L.J., and Mering, C. Von (2017). The STRING database in 2017: quality-controlled protein – protein association networks, made broadly accessible. Nucleic Acids Res. *45*, 362–368.

Tabb, D.L., McDonald, W.H., and Yates, J.R. (2002). DTASelect and contrast: Tools for assembling and comparing protein identifications from shotgun proteomics. J. Proteome Res. *1*, 21–26.

Tessa, A., Silvestri, G., Fulvia de Leva, M., Denora, P.S., Masciullo, M., Dotti, M.T., Casali, C., Melone, M.A.B., Federico, A., Filla, A., and Santorelli, F.M. (2008). A novel KIF5A/SPG10 mutation in spastic paraplegia associated with axonal neuropathy. J. Neurol. *255*, 1090–1092.

Toda, H., Mochizuki, H., Flores, R., Josowitz, R., Krasieva, T.B., Lamorte, V.J., Suzuki, E., Gindhart, J.G., Furukubo-Tokunaga, K., and Tomoda, T. (2008). UNC-51/ATG1 kinase regulates axonal transport by mediating motor-cargo assembly. Genes Dev. *22*, 3292–3307.

Verhey, K.J., and Hammond, J.W. (2009). Traffic control : regulation of kinesin motors. Nat. Rev. Mol. Cell Biol. *10*.

Wang, X., and Schwarz, T.L. (2009). The Mechanism of Ca2+-Dependent Regulation of Kinesin-Mediated Mitochondrial Motility. Cell *136*, 163–174.

Wang, Y., Cameron, E.G., Li, J., Stiles, T.L., Kritzer, M.D., Lodhavia, R., Hertz, J., Nguyen, T., Kapiloff, M.S., and Goldberg, J.L. (2015). Muscle A-Kinase Anchoring Protein-α is an Injury-Specific Signaling Scaffold Required for Neurotrophic- and Cyclic Adenosine Monophosphate-Mediated Survival. EBioMedicine *2*, 1880–1887.

Washburn, M.P., Wolters, D., and Yates, J.R. (2001). Large-scale analysis of the yeast proteome by multidimensional protein identification technology. Nat. Biotechnol. *19*.

Xia, C.-H., Roberts, E.A., Her, L.-S., Liu, X., Williams, D.S., Cleveland, D.W., and Goldstein, L.S.B. (2003). Abnormal neurofilament transport caused by targeted disruption of neuronal kinesin heavy chain KIF5A. J. Cell Biol. *161*, 55–66.

Xiao, S., McLean, J., and Robertson, J. (2006). Neuronal intermediate filaments and ALS: A new look at an old question. Biochim. Biophys. Acta *1762*, 1001–1012.

Xu, T., Park, S.K., Venable, J.D., Wohlschlegel, J.A., Diedrich, J.K., Cociorva, D., Lu, B., Liao, L., Hewel, J., Han, X., Wong, C.C.L., Fonslow, B., Delahunty, C., Gao, Y., Shah, H., and Yates, J.R. (2015). ProLuCID: An improved SEQUEST-like algorithm with enhanced sensitivity and specificity. J. Proteomics *129*, 16–24.

Yaffe, M.B., Farr, G.W., Miklos, D., Sternlicht, M.L., and Sternlicht, H. (1992). TCP1 complex is a molecular chaperone in tubulin biogenesis. Nature *358*.

Yang, R., Bentley, M., Huang, C., and Banker, G. (2016). Analyzing kinesin motor domain translocation in cultured hippocampal neurons. Methods Cell Biol. *131*, 217–232.

Yasuda, M., Tanaka, Y., Omodaka, K., Nishiguchi, K.M., Nakamura, O., Tsuda, S., and Nakazawa, T. (2016). Transcriptome profiling of the rat retina after optic nerve transection. Sci. Rep. *6*, 1–11.

Zhang, B., Higuchi, M., Yoshiyama, Y., Ishihara, T., Forman, M.S., Martinez, D., Joyce, S., Trojanowski, J.Q., and Lee, V.M.-Y. (2004). Retarded axonal transport of R406W mutant tau in transgenic mice with a neurodegenerative tauopathy. J. Neurosci. *24*, 4657–4667.

Zhao, C., Takita, J., Tanaka, Y., Setou, M., Nakagawa, T., Takeda, S., Yang, H.W., Terada, S., Nakata, T., Takei, Y., Saito, M., Tsuji, S., Hayashi, Y., and Hirokawa, N. (2001). Charcot-Marie-Tooth disease type 2A caused by mutation in a microtubule motor KIF1Bbeta. Cell *105*, 587–597.

Zhou, Y., Pernet, V., Hauswirth, W.W., and Di Polo, A. (2005). Activation of the extracellular signal-regulated kinase 1/2 pathway by AAV gene transfer protects retinal ganglion cells in glaucoma. Mol. Ther. *12*, 402–412.

CHAPTER 3: Dynamic protein synthesis following optic nerve injury

Abstract

Most retinal ganglion cells (RGCs) eventually die after injury or in disease. However, the protein changes underlying this process are not fully understood. Here we develop and apply *in vivo* quantitative mass spectrometry of newly synthesized proteins to isolate the cellular changes occurring in the retina after injury. Isolating protein synthesis at 1 day and 5 days after injury, both in the retina and the optic nerve, uncovers a dynamic translational response within broader proteostasis regulation which includes maintenance and degradation pathways. We identify and validate several protein candidates regulating axon outgrowth *in vitro*, which we successfully apply to regulation of RGC survival *in vivo*.

Introduction

Most adult central nervous system (CNS) neurons, such as retinal ganglion cells (RGCs), cannot regenerate their axons after injury. As a result, RGCs often undergo apoptotic cell death after traumatic injury or in diseases like glaucoma that affect the optic nerve. Preventing this death requires a detailed understanding of the dynamic cellular processes occurring from the time of injury until cell death is initiated. Optic nerve crush (ONC) is a reproducible model of retinal ganglion cell (RGC) degeneration. Although RGCs are the initial cells injured by optic nerve injury, other neurons like amacrine and bipolar cells, non-neuronal cells like Mueller glia, and invading immune cells all contribute to the overall retinal response to injury.

Labeling of newly synthesized proteins by incorporation of noncanonical amino acids (ncAAs) has been used to visualize and enrich nascent proteins through two closely related methods for identifying and isolating azide groups: fluorescent noncanonical amino acid tagging (FUNCAT) and bio-orthogonal noncanonical amino acid tagging (BONCAT) (Schiapparelli et al., 2014; Shen et al., 2014). Azidohomoalanine (AHA), one such ncAA, closely resembles methionine but has an azide-containing side group. Azide moieties are available for copper

catalyzed azide-alkyne cycloaddition, a set of reactions known as click chemistry (Alvarez-Castelao et al., 2017; Best, 2009; Dieterich et al., 2007; Schiapparelli et al., 2014; Shen et al., 2014; Speers and Cravatt, 2009). We have previously shown that intravitreal AHA injection efficiently labels proteins in the mammalian retina. By combining AHA with proteomics, we recovered AHA-labeled proteins from both retina and identified over 1000 AHA-labeled proteins that were synthesized over 24 hours, as well as shown that ncAA-labeling combined with western blotting can be used to identify newly synthesized candidate proteins (Schiapparelli et al., 2014; Shen et al., 2014). Here, we now establish quantitative BONCAT through isotopic variants of biotin, measuring early and sustained protein synthesis dynamics in the retina after ONC. We then determine the effects of manipulating these candidates through an *in vitro* neurite outgrowth assay and for *in vivo* RGC survival after ONC.

Results

Azidohomoalanine (AHA) labels retinal proteins for quantitative mass spectrometry

To label newly synthesized proteins, intravitreal injections of AHA were given to adult rats. AHA is charged onto methionine tRNAs by endogenous tRNA synthetase and incorporated into proteins in place of methionine (Yuet and Tirrell, 2014). After 1 day, nascent AHA-containing proteins accumulated in the retina and were transport down RGC axons (Figure 1a). Biotinylated AHA has a mass shift of 523.2749 compared to endogenous methionine (Figure 1b). In these experiments, we collect retinas and ONs 1 or 5 days after daily AHA injection and perform either FUNCAT for localization of newly synthesized proteins or BONCAT for western blot and mass spectrometry-based identification and quantification (Figure 1c).

We first asked if intravitreal injection of AHA would incorporate into retinal cells within 24 hours by FUNCAT imaging. After conjugation to a fluorescently tagged alkyne, we observed positive cells in the ganglion cell and inner nuclear layers only after AHA injection compared to control (Figure 1d). Previous work with AHA-injected retinas have shown efficient conjugation to a biotin-alkyne by western blot (Schiapparelli et al., 2014). We next asked if isotopic variants of

biotin, Biotin 351 (heavy biotin) and Biotin 347 (light biotin), would react equivalently with AHA. AHA-labeled proteins were isolated from 16 homogenized rat retinas and split into two groups. Two click chemistry reactions were performed in parallel with heavy and light biotin and probed on a western blot. We found equal expression of biotin in the retinal samples, suggesting these mass tags could be used for quantification of AHA-containing proteins from different samples (Figure 1e). However, we note that we recovered low signal of biotinylated proteins in the optic nerve samples at this time point.

DiDBiT coupled with MS/MS has been used for identification of ~1000 retinal proteins after AHA-injection. Here, we collected 8 AHA-injected retinas per either sham or ONC groups and conjugated those proteins with either heavy or light biotin. After MS, we identified over 1300 retina proteins in heavy and light groups combined, with over 800 proteins present in all three replicates (Figure 1f). Together, these data suggest AHA can reproducibly label retinal proteins after injury for quantitative mass spectrometry.

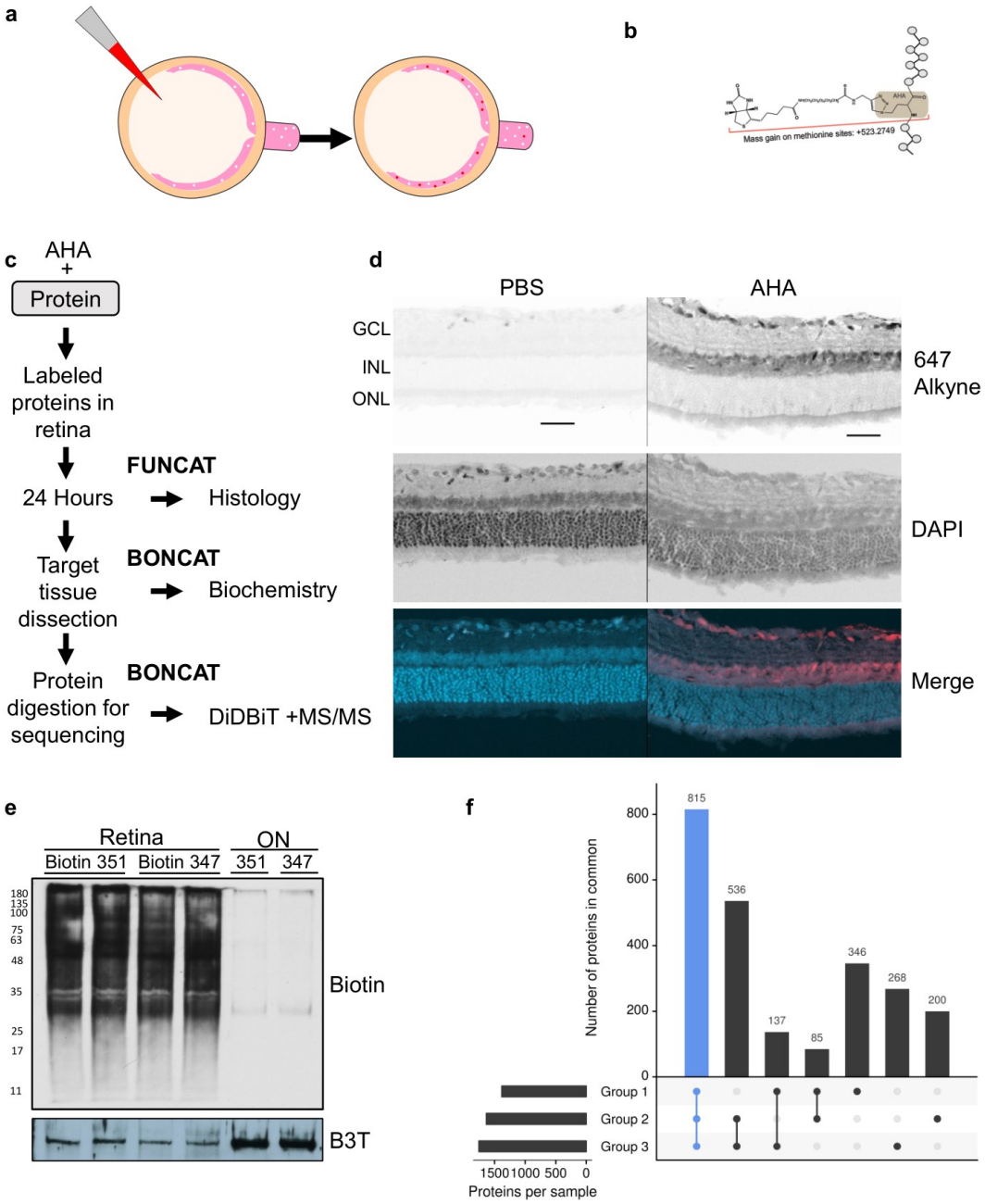

Figure 3.1. Azidohomoalanine (AHA) labeling detects newly synthesized proteins in the retina. a. AHA injected intravitreously incorporates into newly translating proteins. **b.** Biotinylated AHA has a mass shift of 523kD compared to methionine. **c.** Standard protocol for new protein visualization by FUNCAT or enrichment and quantification by BONCAT followed by mass spectrometry. **d.** Click reaction with Alexa 647 alkyne show distribution of new proteins in the ganglion cell layer (GLC) and inner nuclear layer (INL), with few AHA-labeled proteins in the outer nuclear layer (ONL). scale= 50 µm. **e.** Western blot of biotin after click chemistry with either heavy or light biotin alkyne. Equivalent labeling in retinal tissue with either isotope of biotin, but little to no labeling present in optic nerve samples after 24 hours. **f.** Comparison of protein identities in each replicate of AHA-labeled retinas, before separating peptides into heavy or light biotin groups. Each replicate consisted of 8 retinas from ONC samples, and 8 retinas from control samples.

Retinal protein synthesis dynamics over 1 and 5 days after ONC

Retinal cells are in flux in the days following ONC, with retraction of injured axons from the crush site occurring between 6 hours and 1 day after injury, and re-growth and initial axon sprouting in surviving RGCs occurring up to 1 week after ONC (Sellés-Navarro et al., 2001). To capture both phases of cellular response, we injected AHA in either the 24 hours after ONC or every day for the 5 days after ONC, and collected tissue for click chemistry, western blot, and proteomics. Western blot of the 5-day tissue showed strong labeling in the retina both with and without crush, similar to the 1-day samples, and also the presence of biotinylated proteins in the optic nerve (Figure 2a).

Although all proteins undergo synthesis, the rate of new protein translation depends on half-life and protein turnover. We therefore compared the protein identities detected in our uninjured 1 day and 5 day AHA retinas to total proteins in an un-injected retina (Figure 2b). As expected, more proteins were found in the total retina than newly synthesized in either 1 or 5 days. However, there were over 750 proteins in common between all 3 groups. These proteins could perhaps have a high turnover rate, allowing enough new synthesis for detection by mass spectrometry. Interestingly, there were 268 and 153 proteins found only in 1-day or 5-day retinas, respectively. A likely reason for the detection of these proteins in only AHA samples is that only measuring nascent proteins reduces the complexity of the total retinal tissue by removing highly abundant and long-lived proteins.

To compare individual proteins between control and ONC conditions, we used Stouffer's Z score on both 1-day and 5-day AHA retinal samples (Figure 2c-d). We isolated the proteins that decreased (left half) or increased (right half) the most in synthesis after injury across 3 proteomic replicates. At 1-day, the protein with the highest increase in synthesis after ONC is HNRNPA1, an RNA-binding protein associated with stress granules in neurodegenerative diseases like ALS(Kim et al., 2013). CTSL, a protein involved in protein degradation, is increased in synthesis 5 days after injury, coincident with increased degeneration of RGCs

(Sánchez-Migallón et al., 2016). Additionally, Rab11a and Rab11b were also upregulated in synthesis at 5 days. Not only does Rab11 regulate local protein turnover (Howes et al., 2010), its role in integrin trafficking and *in vitro* CNS regeneration (Eva et al., 2010; Koseki et al., 2017) correlate with the re-growth and sprouting seen at this time point. Quantification of newly synthesized proteins identifies temporally-relevant cellular changes after ONC injury.

We next asked how protein synthesis dynamics differ at 1 and 5 days after ONC. After filtering for proteins quantified in the retina at both time points, we graphed either those that increased or decreased relative to control over time (Figure 2e). WARS, tryptophanyl tRNA-synthetase, increased the most relative to control at 5 days compared to 1 day after injury. The family of aminoacyl-tRNA synthetases (AARS) play multiple roles beyond canonical translation including regulating cell proliferation, inflammation, and RNA processing (Park et al., 2005). In fact, at least two members of the AARs family affect peripheral nerve degeneration and regeneration (Park et al., 2015), positioning WARS as a candidate to manipulate in CNS injury response. In contrast, GRK1, rhodopsin kinase, decreases in synthesis in the retina over time. As GRK1 is part of the phototransduction cascade, we hypothesize that its decrease is due to the loss of functional vision after ONC.

Figure 3.2. Comparison of retinal protein synthesis 1 and 5 days after ONC. a. Western blot of biotin after click chemistry with AHA-labeled retinas and optic nerves, with and without ONC. There is extensive labeling in the retina, with detectable labeled proteins found in optic nerve fractions. Below is a Ponceau S stain of the samples showing equal loading and total protein presence. **b.** Protein identity comparison of retinas labeled with 1 day of AHA, 5 days of AHA, or total protein without injury. **c-d.** Largest differences in protein synthesis 1 day **(c)** or 5 days **(d)** after ONC, quantified by Stouffer's Z score across 3 replicates. **e.** Comparison of protein synthesis differences from 1 day to 5 days after injury. Largest increases labeled in progressively darker blue, with the largest increase labeled as Wars. Largest decreases labeled in progressively darker red, with the largest decrease labeled as Grk1.

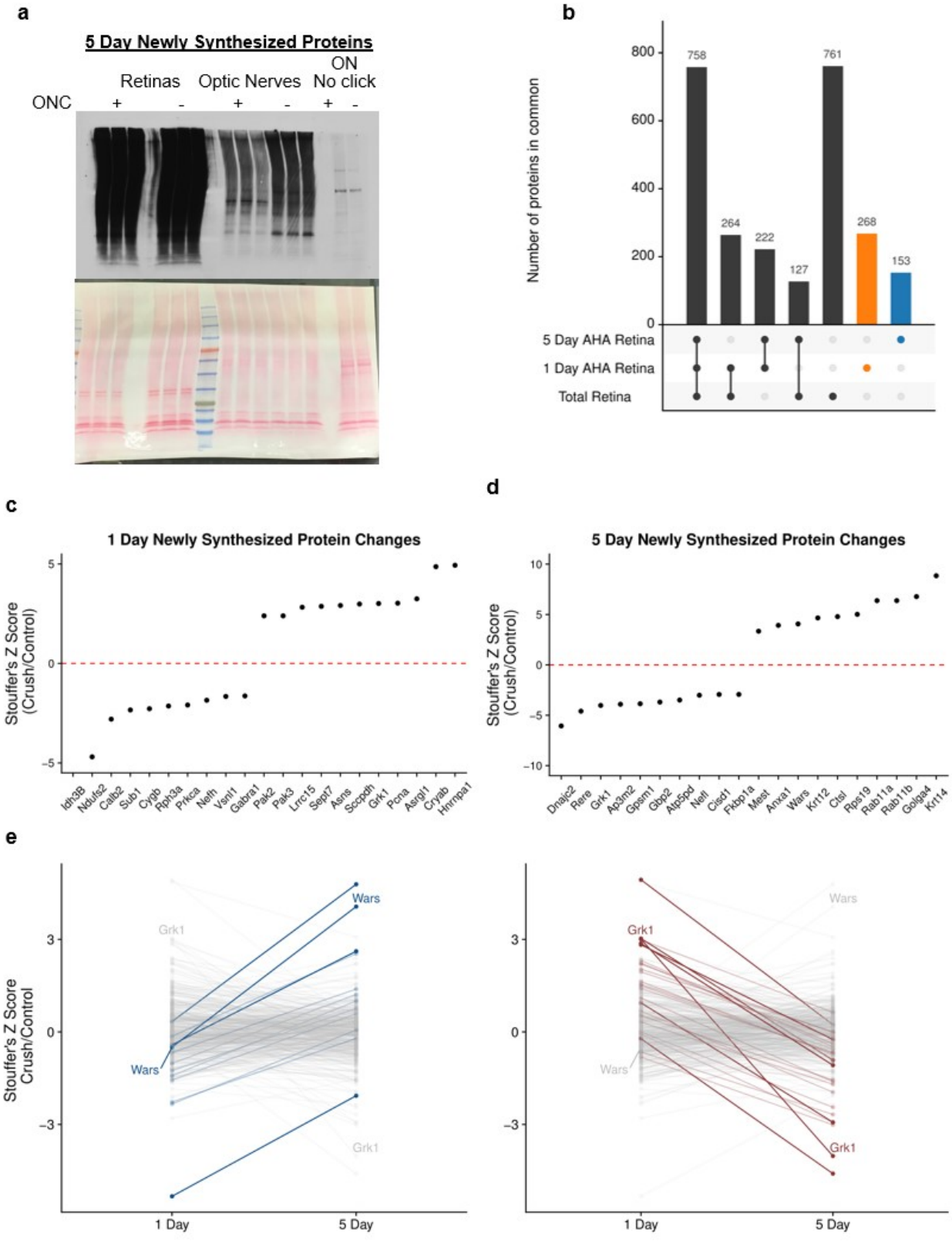
a
5 Day Newly Synthesized Proteins
Retinas
Optic Nerves
ON
No click
ONC
+ - + - + -
b
Number of proteins in common
800
600
400
200
0
758
264
222
127
761
268
153
5 Day AHA Retina
1 Day AHA Retina
Total Retina
c
1 Day Newly Synthesized Protein Changes
Stouffer's Z Score
(Crush/Control)
5
0
−5
Idh3B
Ndufs2
Calb2
Sub1
Cygb
Rph3a
Prkca
Nefh
Vsnl1
Gabra1
Pak2
Pak3
Lrrc15
Sept7
Asns
Sccpdh
Grk1
Pcna
Asrgl1
Cryab
Hnrnpa1
d
5 Day Newly Synthesized Protein Changes
Stouffer's Z Score
(Crush/Control)
10
5
0
−5
−10
Dnajc2
Rere
Grk1
Ap3m2
Gpsm1
Gbp2
Atp5pd
Nefl
Cisd1
Fkbp1a
Mest
Anxa1
Wars
Krt12
Ctsl
Rps19
Rab11a
Rab11b
Golga4
Krt14
e
Stouffer's Z Score
Crush/Control
3
0
−3
Grk1
Wars
Wars
Grk1
1 Day
5 Day
Wars
Grk1
Wars
Grk1
1 Day
5 Day

Protein synthesis and transport to the optic nerve after injury

In our 5 day AHA western blot tissue, we noted biotinylated proteins present in the optic nerve that decreased after ONC (Figure 2a). We next asked what proteins were synthesized then transported to the optic nerve and quantified how this changed after injury. From the same animals use for the 5-day retina experiments, we first compared replicates of the ON proteomes and found a high level of correlation between replicates (Pearson R=9.14, Figure 3a). However, we did note that proteomic yield and protein diversity was more variable than in the retina, most likely due to technical difficulties in enrichment of low signal in the high background environment of the optic nerve (Figure 3b). Nonetheless, comparison of the two replicates at the protein level indicated several large changes 5 days after injury. Surprisingly, we found the presence histone proteins that increased in the ON after injury. While histone proteins are synthesized in the cytoplasm, the presence of them in the axonal compartment *in vivo* has not been previously seen. Further validation and manipulation of axonal histones will provide insight into their non-canonical roles in injury response.

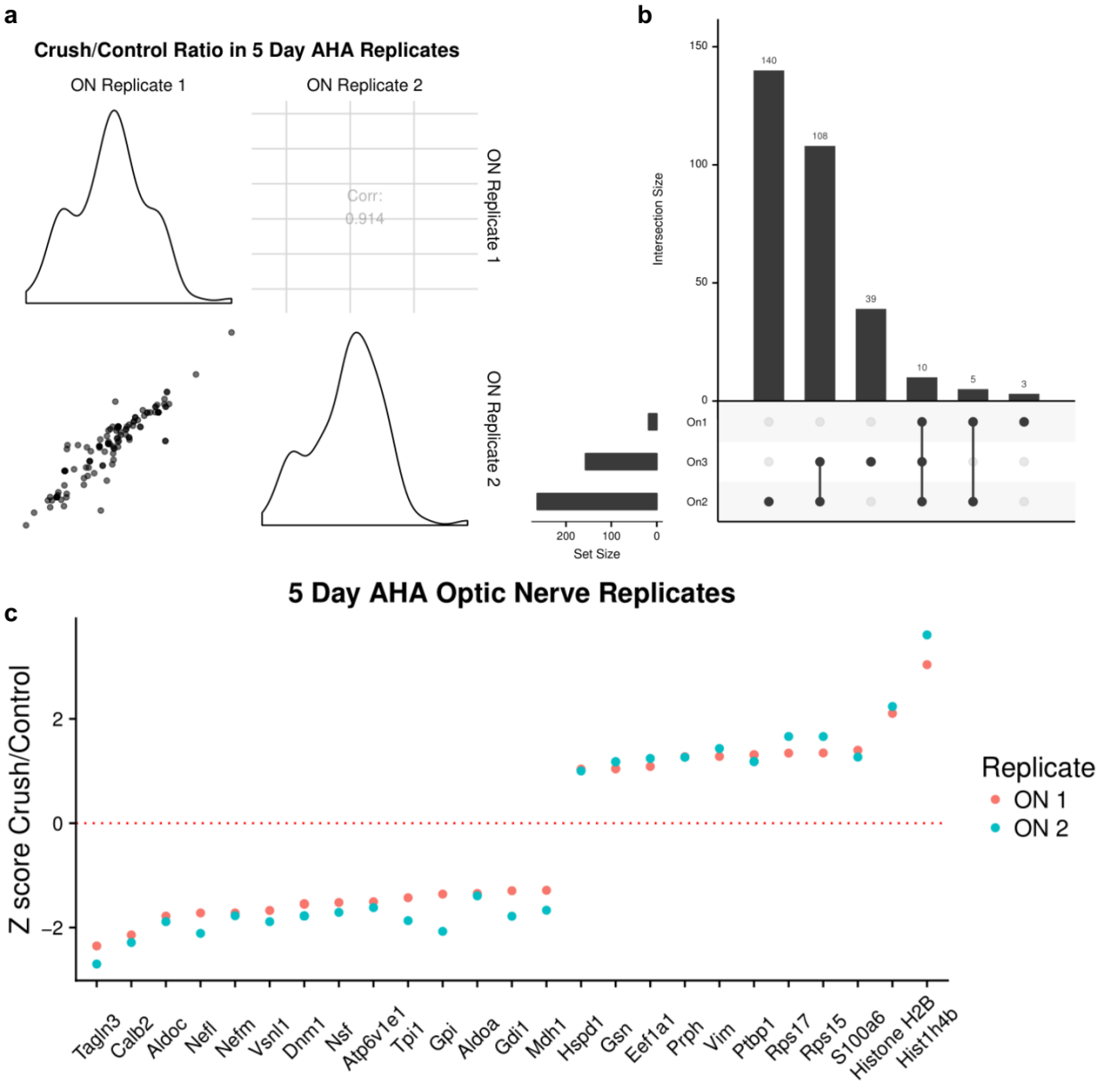

Figure 3.3. Changes in protein synthesis and transport to the ON 5 days after injury. a. Pearson's correlation between ON proteomic replicates, comparing the crush/control protein synthesis ratio. R=0.914. **b.** Comparison of protein IDs in optic nerve replicates. There is increased variability in mass spectrometry detection due to the decreased signal in the ON compared to the retina. ON1 was excluded from further analyses. **c.** Z score comparison of crush compared to control, highlighting the largest changes in synthesis and transport into the optic nerve 5 days after injury.

Quantification of neurite outgrowth of proteomic candidates *in vitro*

Changes in rates of protein synthesis after injury suggest a role in injury response, but not necessarily an intrinsic cellular survival or growth-related protein. We next asked if any of our candidate proteins from 1-day AHA retinal proteomics affected neurite growth through a hippocampal outgrowth assay. We selected candidate proteins based on either Stouffer's Z score, presence or absence in all replicates, or a large fold change difference in at least one replicate. As it was unclear if all early retinal responses to injury are pro-survival or pro-apoptosis, we generated overexpression and shRNA vectors for all candidates, along with KLF9 plasmids as positive controls for outgrowth promotion or inhibition (Moore et al., 2009).

Cultured hippocampal neurons were transfected with plasmids 3 days after plating and imaged for neurite quantification 3 days later (Figure 4a). To quantify the longest neurite length distribution, we compared the median of the overexpression or knockdown control plasmid to all candidate gene medians (Figure 4b). We found significant outgrowth differences in 4 of the 15 candidate gene manipulations, with two candidates extending neurites further than our positive control (Figure 4c-d). Knockdown of GTF2I, PNCA and ASRGL1 increased neurite outgrowth significantly, while overexpression of HNRNPA1 decreased neurite outgrowth significantly. These data demonstrate the power of quantifying changes in protein synthesis for candidate selection of relevant survival and outgrowth regulators.

Figure 3.4. Quantification of neurite outgrowth with manipulation of proteomic candidates. a. Timeline of *in vitro* experimental protocol. Embryonic day 17 mouse hippocampi were harvested and grown in defined media. 3 days later, overexpression or knockdown plasmids were transfected with Lipofectamine LTX. On day 6, all wells were imaged, and positive cells were traced by a blinded investigator. **b.** Legend for neurite outgrowth graph. Red rectangle defines the 25% and 75% interquartile range, with center red line as the median. Notches on the rectangle define the 95% confidence interval. Dotted black line is the extended GFP median to aid in visual comparison. **c.** Comparison of longest neurite lengths with each transfection condition. GFP used as an overexpression control, and scramble used as a knockdown control. KLF9 overexpression and knockdown were used as positive controls. Data points above 1100um excluded from graph but included in summary statistics and comparisons. Overexpression plasmids were compared using Kruskal-Wallis test with two-stage linear step-up procedure of Benjamini, Krieger, and Yekutieli controlling the false discovery rate to 0.05. Knockdown plasmids were similarly compared to the scramble control. HNRNPA1 OE $p<0.01$. GTF2I KD $p<0.01$, PCNA KD $p<0.01$, ASRGL1 KD $p=0.02$. **d.** Representative images of neurite length. As shown, scramble= 357 μm, GTF2I KD= 532 μm, PCNA KD= 486 μm. Scale=100 μm.

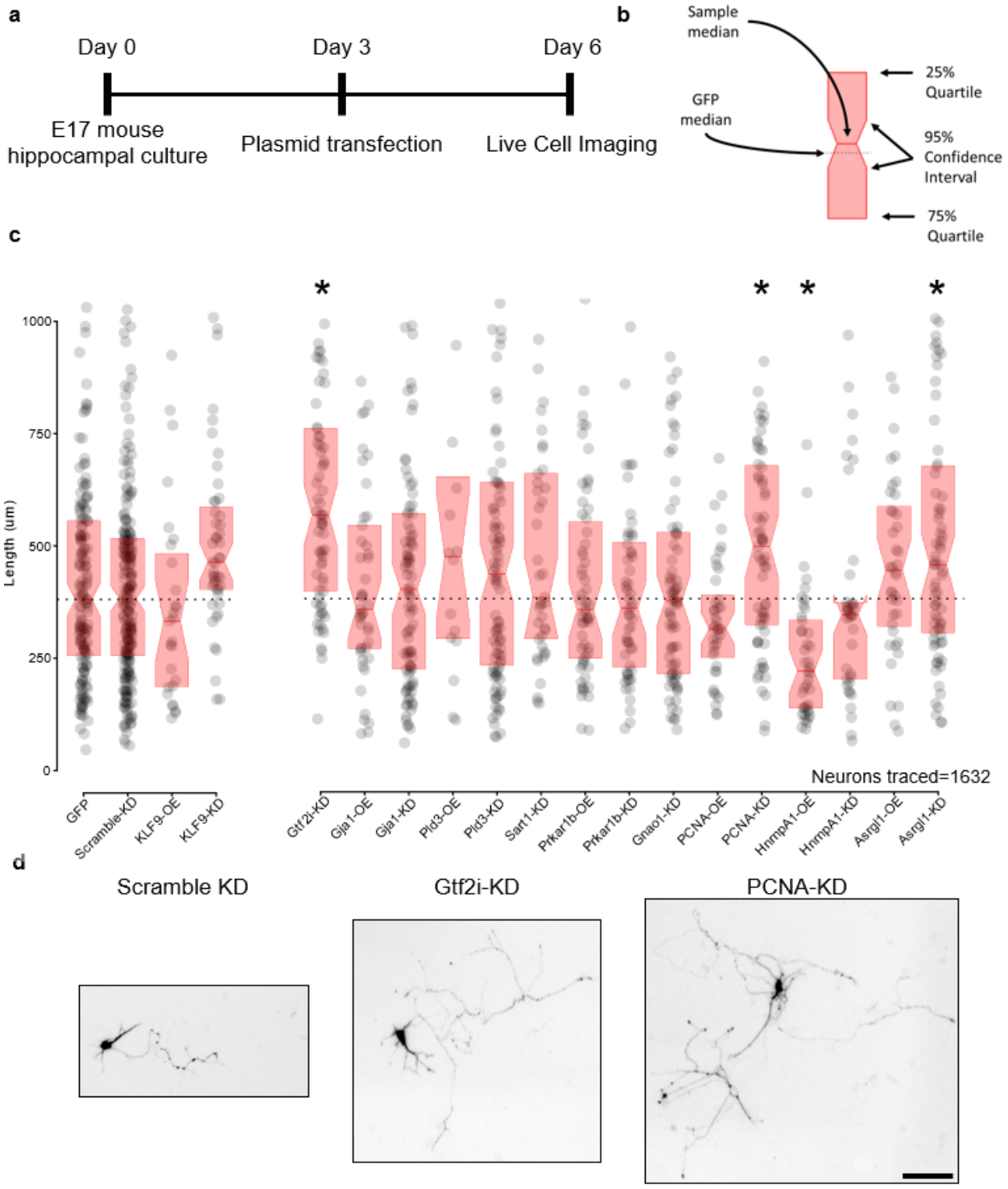
a
Day 0
Day 3
Day 6
E17 mouse hippocampal culture
Plasmid transfection
Live Cell Imaging
b
Sample median
GFP median
25% Quartile
95% Confidence Interval
75% Quartile
c
Length (um)
1000
750
500
250
0
Neurons traced=1632
GFP
Scramble-KD
KLF9-OE
KLF9-KD
Gtf2i-KD
Gja1-OE
Gja1-KD
Pld3-OE
Pld3-KD
Sart1-KD
Prkar1b-OE
Prkar1b-KD
Gnao1-KD
PCNA-OE
PCNA-KD
HnrnpA1-OE
HnrnpA1-KD
Asrgl1-OE
Asrgl1-KD
d
Scramble KD
Gtf2i-KD
PCNA-KD

Quantification of RGC survival *in vivo*

As overexpression decreased neurite outgrowth, we hypothesized that HNRPNA1 was detrimental to survival after injury, similar to its role in concentration-dependent stress granule formation in other neurodegenerative diseases like ALS (Deshaies et al., 2018; Kim et al., 2013; Molliex et al., 2015). Our previous works demonstrated that proteins in the HNRNP family transport to the ON and presynaptic terminals from RGC cell bodies (Chapter 11). We also demonstrated that transport of KIF5A, a kinesin motor protein, was inhibited after ONC (Chapter 12). Based these findings, we hypothesized that HNRNPA1 was a cargo of KIF5A, and accumulated in the cell body after ONC forming stress granules, a prediction supported by previous studies of HNRNP and kinesin interactions (Kanai et al., 2004). Indeed we were able to pull down a myc-tagged HNRNPA1, but not a myc-tagged GFP, through co-immunoprecipitation with a FLAG-tagged GFP *in vitro* (Figure 5a).

We next asked if proteins that changed in synthesis after ONC, validated through the *in vitro* neurite outgrowth screen, could affect RGC survival *in vivo*. We injected viral vectors 2 weeks prior to ONC, and retinas collected 2 weeks after (Figure 5b). We first developed an AAV viral vector of HNRNPA1 knockdown. HNRNPA1 knockdown significantly decreased RGC survival after injury (Figure 5c). We next knocked down GTF2I *in vivo* using an AAV virus, which increased RGC survival 21% compared to control (Figure 5d). Based on our *in vitro* and *in vivo* findings, quantifying new protein synthesis in response to *in vivo* injury isolates relevant candidates for neuron survival and outgrowth.

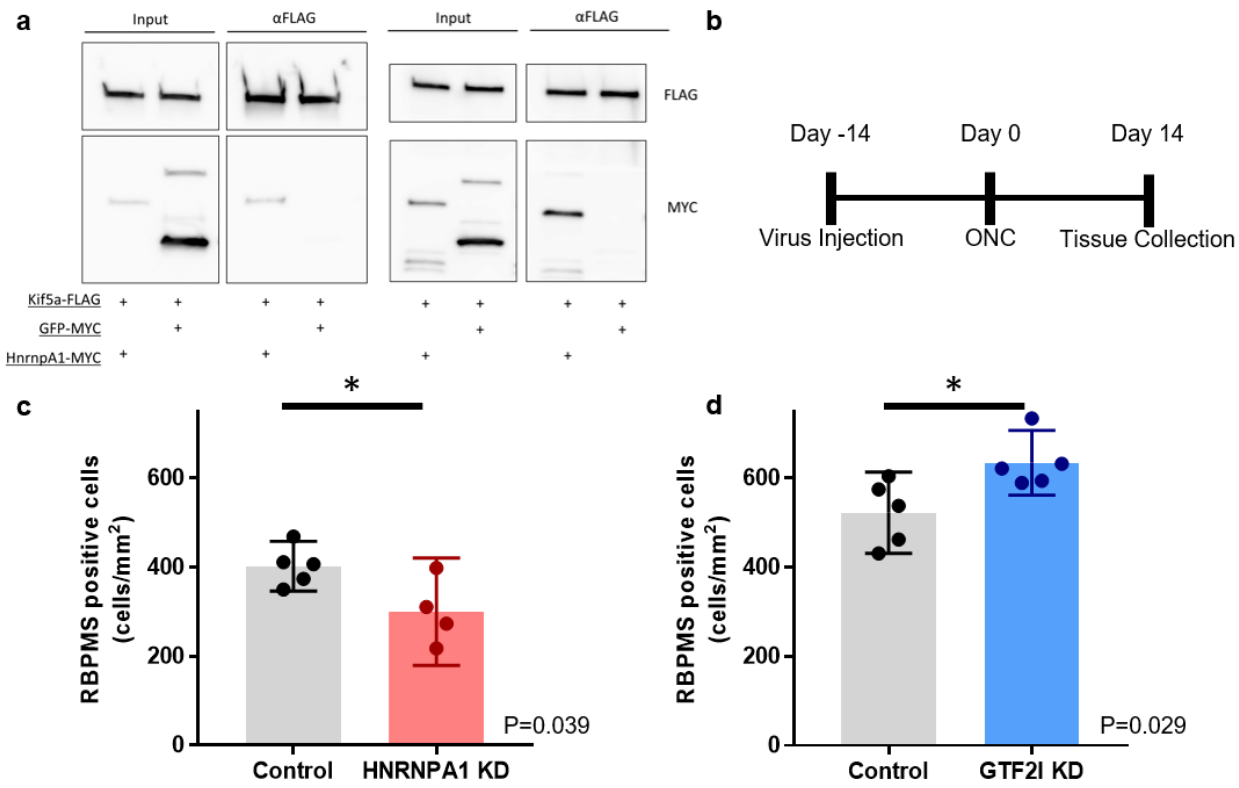

Figure 3.5. Quantification of RGC survival *in vivo*. a. Co-immunoprecipitation of HnrnpA1 by Kif5a pulldown in COS7 cells. Top panels show FLAG expression at 125kD in inputs and IPs. Bottom panels show MYC bound to either GFP or HNRNPA1 in the inputs, and only HNRNPA1 after FLAG IP. **b.** Timeline of *in vivo* RGC survival experiments. Two weeks before ONC, eyes were injected intravitreously with AAV viruses. Two weeks after crush, retinas were collected for RGC counting. **c.** HNRNPA1 knockdown decreased RGC survival compared to mCherry control. Two-sample, two-tailed T-test. **d.** GTF2I KD increased survival compared to mCherry control. Two-sample, two-tailed T-test.

Discussion

Previous studies have detailed transcriptomic changes in the retina after injury, but these remain a proxy for the protein-level changes in the cell (Yasuda et al., 2014). Tandem mass tagging (TMT) or iTRAQ (Hollander et al., 2012) for quantitative proteomics can provide protein abundance changes in RGCs after axonal injury, as used to identify c-myc as a regulator of survival and regeneration after injury (Belin et al., 2015), but has several limitations. First, total protein abundance does not directly measure translational responses to an injury, but instead the net of protein synthesis and degradation. Isolating changes in translation requires removing the impact of homeostatic mechanisms, themselves dynamic after cellular manipulation (Savitski et al., 2018), from proteomic analysis. Second, changes in abundance operate at a slower time course than protein synthesis due to protein turnover rates, limiting temporal resolution of existing proteomic strategies. To overcome these barriers understanding the cellular response to injury, we adapted nascent proteomics with ncAAs to quantify acute changes in protein synthesis across multiple time points *in vivo*.

Part of the difficulty in dissecting the neurodegenerative process after injury is due to the dynamically evolving response by damaged neurons. Proteomic analysis of retinal cells using iTRAQ at time points after injury correlated to axon dieback, regrowth, sprouting, and eventual apoptosis, yet only detected 214 proteins for quantification limiting interpretative power (Magharious et al., 2011; Sellés-Navarro et al., 2001). In contrast, using AHA we were able to quantify over 1000 retinal proteins at 1 day and 5 days after injury (Figure 2b). This improved depth of detection permitted selection of multiple injury-responsive protein candidates, both at individual time points and those dynamically shifting during the degenerative process.

The increased transport of nuclear proteins, such as HIST1H4B and HIST1H2B, into the optic nerve 5 days after injury was an unexpected, but not unprecedented, finding. *In vitro* neuronal proteomics localized several nuclear proteins to the growth cone, including histone proteins as well as PCNA (Estrada-Bernal et al., 2012), a time point where retracted axons re-

grow to the injury site (Sellés-Navarro et al., 2001). Exploration of novel functions of canonical nuclear proteins will be a focus of future work.

A limitation of retinal proteomics is the inclusion of non-RGCs, although histology suggests an enrichment of GCL and INL cells above photoreceptors (Figure 1d). We are therefore unable to directly determine if changing protein synthesis is from RGCs, non-neuronal cells, or a mixed response from multiple cells. Manipulating our prominent candidate proteins in a neuronal culture identifies cell-autonomous effectors of neurite growth, increasing the likelihood of conserved effects in the different environment of the adult retina after injury. Both candidate pro-growth regulators tested *in vivo* affected RGC survival after ONC, with GTF2I knockdown as a candidate protective therapeutic.

GTF2I- regulated calcium entry affected outgrowth in developing cortical cultured neurons (Deurloo et al., 2018). Since calcium-mediated activity regulates RGC axon extension *in vitro* (Corredor et al., 2012; Goldberg et al., 2002), increasing calcium entry by knocking down GTF2I is a plausible mechanism for the protective effects seen after ONC.

Proteomic analysis of new synthesis highlights the dynamic injury response with better than global proteomics or transcriptomics. Combining translation with protein degradation changes through the time course of neurodegeneration or regeneration will greatly increase our understanding of disease and expand the pool of potential therapies.

Methods

Animal surgeries

Animal experiments were conducted in accordance with the guidelines of the Institutional Animal Care and Use Committee (IACUC) and the Institutional Biosafety Committee of University of California, San Diego, Scripps Research, and Stanford University, and complied with the ARVO Statement for the Use of Animals in Ophthalmic and Vision Research.

Animal lines

C57BL/6 mice or Sprague Dawley rats were used for all wildtype experiments.

Intravitreal Injection

Sprague Dawley rats or mice (30-45 day old) were used for all experiments. A microinjector pressure system (Picosprizer II) with a pulled glass micropipette in a micromanipulator was used to inject reagents intravitreally. For viral injections, mice were injected intravitreally with 1.5 µl volume of AAV2-mCherry, AAV7m8-shRNA HnrnpA1, or AAV7m8-shRNA Gtf2i (titers ranged from 0.5 to 1 × 10^{13} genome copies/ml). For *in vivo* AHA experiments, we injected each eye with ~5 µL of 400 mM AHA in PBS, as described previously (Schiapparelli et al., 2014). The injections were given twice over 24 hours or once a day for 5 days under deep anesthesia with either 0.5 mg/kg Medetomidine and 75mg/kg ketamine *ip* or 2% isofluorane under nose cone. The eyes were treated with topical antibiotics and analgesics.

Optic nerve crush

Under deep anesthesia, the optic nerve was exposed and crushed using fine forceps (Dumont #5) at 1.5 mm behind the optic nerve head for 5 seconds. Care was taken to avoid damaging the blood supply to the retina. Sham surgeries exposed the optic nerve, but no crush was given. All optic nerve crush procedures were performed by a surgeon blinded to the viral treatment. Postoperatively, animals were allowed to recover on a heating pad and were given

subcutaneous injections of buprenorphine hydrochloride, 0.1 mg/kg, twice a day for 3 consecutive days to minimize discomfort.

Fresh tissue collection

Rats or mice were euthanized with CO_2 and decapitated for brain removal. The tissue was frozen immediately in isopentane in dry ice and stored at -80°C for biochemistry studies. Co-immunoprecipitation studies continued directly without freezing.

Immunohistochemistry

At different time points after surgeries, animals were deeply anesthetized and transcardially perfused with 4% PFA in PBS. Retinas were dissected and fixed in 4% PFA for 1 hour and subsequently washed in PBS. Retinas were kept in PBS at 4°C until ready for antibody staining. They were incubated with anti-RBPMS (1:300; PhosphoSolutions, 1830-RBPMS). Secondary antibodies were Alexa Fluor 647-conjugated, highly cross-adsorbed antibodies (1:500; Invitrogen). Wholemount retinal images were acquired using a laser scanning confocal microscope (Carl Zeiss 880) and quantified by a researcher blinded to the experimental condition.

Fluorescent noncanonical amino acid tagging (FUNCAT)

AHA-injected samples were processed for click chemistry according to the following protocol, modified from previous studies (Dieterich et al., 2010; Hinz et al., 2012). Sections were transferred to Eppendorf tubes or six-well plates with reaction mixture composed of 100 μm Tris [(1-benzyl-1H-1,2,3-triazol-4-yl)methyl]amine (TBTA, Sigma) dissolved in 4:1 tBuOH/DMSO (Sigma), 100 μm CuSO4 (Sigma), 1.25 μm Alexa Fluor 647 alkyne (Invitrogen), and 250 μm Tris(2-carboxyethyl)phosphine (TCEP, Sigma). The reaction proceeded overnight at room temperature.

RGC quantification

The RBPMS quantification were performed in a masked fashion as previously described (Wang et al., 2015). Briefly, the retinas were divided into 4 quadrants, and one digital

micrograph was taken from a fixed distance from the periphery of each of the 4 fields. These were then counted using ImageJ object counter by a blinded investigator.

Co-Immunoprecipitation

For co-immunoprecipitation, COS7 cells were homogenized in buffer (20 mmol/L HEPES, pH 7.4, 150 mmol/L NaCl, 5 mmol/L EDTA, 0.5% Triton, 50 mmol/L NaF, 1 mmol/L sodium orthovanadate, 1 mmol/L DTT, and protease inhibitors). After centrifugation at 10,000 x g for 10 minutes at 4°C, the clarified extracts were used for immunoprecipitation using appropriate antibodies (2µg rabbit anti-FLAG, CST, 14793S) and 20 µL protein G sepharose (Millipore, Fastflow) for 3 hours to at 4°C. The beads were washed 3-5 times with lysis buffer, and the immunoprecipitated proteins were eluted with 2x Laemmli buffer for western blotting.

For all electrophoresis, 5-20ug of protein was loaded on a 4-20% Tris-Glycine Gel (Thermo Fisher Scientific XP04202) and transferred to an activated 0.2 um PVDF membrane for immunoblotting. The membranes were saturated with Ponceau S stain for 5 minutes and imaged, before washing with ddH20. The membranes were saturated with TBS 1x, 0.05% Tween-20, and 5% nonfat dry milk for 1 hour at room temperature, then incubated overnight at 4°C with rabbit anti-FLAG (1:2000, CST, 14793S), and mouse anti-myc (1:1000, EMD Millipore, 05-724). All membranes were washed with TBS-Tween between incubations. The membranes were then saturated with peroxidase-conjugated goat anti-mouse, anti-rabbit, or anti-goat (1:2000, Abcam, ab6789, ab6721, and ab97110) secondary antibodies for 3 hours at room temperature and revealed with SuperSignal West Femto Chemiluminescent Substrate using ImageQuant LAS4000. Stripping to ensure equal loading was done with ReBlot Plus Strong Antibody Stripping Solution (EMD Millipore 2504).

Click reaction for biotinylation of AHA-labeled proteins

Neuronal tissue (optic nerves or retinas) were lysed in 0.5% SDS in PBS plus a cocktail of endogenous protease inhibitors (Complete Protease Inhibitor Cocktail Tablets, Roche) by homogenizing and sonicating with 10 pulses using a tip sonicator (Sonic Dismembrator model

100, Fisher Scientific). Samples were boiled for 10 min and cooled to room temperature. Any remaining insoluble material was resuspended with additional sonication pulses. We measure protein concentration using a protein assay kit (Bio-Rad), and aliquots of 1.5 mg of protein suspension were transferred to eppendorf tubes. AHA that was incorporated into proteins was labeled with PEG4 carboxamide-Propargyl Biotin (biotin-alkyne) (Invitrogen) by click chemistry reaction performed in the total protein suspension as described previously. For quantitative MS analysis click reactions were done using biotin-alkyne labeled with heavy stable Carbon and Nitrogen isotopes: Biotin-β-Alanine-13C3,15N-Alkyne [Biotin Propargyl amide] or the light isotope form of the alkyne (Setareh Biotech) to the different experimental groups (McClatchy et al., 2015). For each reaction, we used an aliquot of 1.5 mg of protein lysate, and brought the reaction volume to 346 µl with PBS before adding the click reaction reagents. We added the following reagents in sequence, vigorously vortexing after each addition: 30 µL of 1.7 mM tris[(1-benzyl-1H-1,2,3-triazol-4-yl)methyl]amine (TBTA) (Sigma) dissolved in 4:1 tert-butanol/DMSO (Sigma), 8 µL of 50 mM CuSO4 dissolved in ultrapure water (Sigma), 8 µL of 5 mM of biotin-alkyne (in light or heavy form) dissolved in DMSO, and 8 µL of 50 mM TCEP (Sigma) dissolved in water. The click reactions were vortexed and incubated at room temperature for 1–2 h or overnight with gentle rotation at 4 °C. After the completion of the cycloaddition reaction, 10 µl of each click reaction were separated for analyzing biotin-alkyne incorporation to proteins by western blot using anti-biotin antibody (Pierce). The click reactions of both experimental groups were mixed 1:1, vortexed and proteins were precipitated with methanol/chloroform. Proteins were precipitated by adding three volumes of methanol, one volume of chloroform, and three volumes of water, vortexed, and centrifuged at 15,000g for 2 min at room temperature. The aqueous and organic phases were removed carefully from the tube without disturbing the protein disc at the interface. Protein pellets were washed once by adding three volumes of methanol and centrifuging at 15,000g for 2 min. Pellets containing biotinylated proteins were air-dried for 10 min. Protein precipitates were resuspended by adding 200 µl 8 M Urea and 200 µl

0.2 % ProteaseMax surfactant (Promega) dissolved in 50 mM NH_4HCO_3. The protein suspension was reduced by adding tris(2-carboxyethyl)phosphine (TCEP, Sigma) to 5 mM final concentration and incubated at 55 °C with vigorous orbital shaking using a Thermomixer (Eppendorf). Protein alkylation was done by adding iodoacetamide (Sigma) to 10 mM final concentration and incubating with vigorous shaking in the dark for 20 min. To digest the proteins, we added in the following order: 150 µL of 50 mM NH4HCO3, 2.5 µL of 1% ProteaseMAX dissolved in 50 mM NH4HCO3, and 1:100 (enzyme/protein, w/w) sequencing grade trypsin (Promega) to a final reaction volume of 500 µL. The digestion reactions were incubated for 3.5 h at 37 °C with vigorous orbital shaking. The protein digestion reactions from biotin-AHA labeled proteins were stopped by adding trifluoroacetic acid (TFA) (Sigma) to 0.1% final concentration. Samples were centrifuged at 20,000g for 20 min at room temperature to remove undigested insoluble material and supernatant containing the peptide mixture was collected in an eppendorf tube. Any remaining peptides in the insoluble pellet were extracted by adding 0.5 mL of 0.1% TFA in water, resuspending the pellet by pipetting and centrifuging again for 20 min. The supernatant was pooled with the previous one before desalting using Sep-Pak tC18 solid-phase extraction cartridges (Waters). Prior to loading the mixture of peptides, the cartridges were washed sequentially with 3 mL of acetonitrile, 3 mL of 0.5% acetic acid, 50% acetonitrile in water, and 3 mL of 0.1% TFA in water. After loading the peptide mixtures, the cartridges were washed with 3 mL of 0.1% TFA and then with 0.250 mL of 0.5% acetic acid in water. The peptides were eluted into a clean tube with 1 mL of 0.5% acetic acid, 80% acetonitrile in water, and dried in eppendorf tubes in a Speed Vac (Thermo). Ten milligrams of dried peptide pellet was solubilized in 1 mL of PBS and incubated with a 200 µL slurry of NeutrAvidin beads (Pierce) for 1 h at room temperature. The beads were precipitated by centrifugation at 1000g for 5 min and flow through was collected for MS analysis of unbound peptides. Beads were washed three times by adding 1 mL of PBS with 1 mL of 5% acetonitrile in PBS, and a last wash in ultrapure water. Excess liquid was completely removed from the

beads using a micropipette, and biotinylated peptides were eluted by adding 0.3 mL of solution containing 0.2% TFA, 0.1% formic acid, and 80% acetonitrile in water. The beads were centrifuged at 1000g and the first elution of biotinylated peptides was transferred to an eppendorf tube. A second elution of 0.3 mL was boiled for 5 min for maximum release of peptides from the beads.

Mass Spectrometry

Dried peptides were resolubilized in Buffer A (5% ACN, 95% water, 0.1% formic acid) and then were pressure-loaded onto a 250-μm i.d. capillary with a kasil frit. The capillary contained 2 cm of 10 μm Jupiter C18-A material (Phenomenex, Ventura, CA), followed by 2 cm 5 μm Partisphere strong cation exchanger (Whatman, Clifton, NJ). This loading column was washed with buffer A. After washing, a 100 μm i.d. capillary with a 5 μm pulled tip packed with 15 cm 4 μm Jupiter C18 material (Phenomenex, Ventura, CA) was attached to the loading column with a union, and the entire split-column (loading column−union−analytical column) was placed inline with an Agilent 1100 quaternary HPLC (Palo Alto, CA). The sample was analyzed using MudPIT, which is a modified 12- step separation previously described. The buffer solutions used were buffer A, 80% acetonitrile/0.1% formic acid (buffer B), and 500 mM ammonium acetate/5% acetonitrile/0.1% formic acid (buffer C). Step 1 consisted of a 60 min gradient from 0 to 100% buffer B. Steps 2−11 had the following profile: 3 min of 100% buffer A, 5 min of X% buffer C, a 10 min gradient from 0 to 10% buffer B, and a 105 min gradient from 15 to 45% buffer B. The buffer C percentages (X) were 10, 15, 20, 30, 35, 40, 50, 60, and 100%, respectively, for the 12-step analysis. In the final two steps, the gradient contained: 5 min of 100% buffer A, 5 min of 90% buffer C plus 10% B, a 10 min gradient from 0 to 15% buffer B, and a 105 min gradient from 15 to 100% buffer B. As peptides eluted from the microcapillary column, they were electrosprayed directly into a Velos mass spectrometer (ThermoFisher, Palo Alto, CA) with the application of a distal 2.4 kV spray voltage. A cycle of one full-scan FT mass spectrum (300−1600 m/z) at 60 000 resolution followed by 20 data-dependent IT MS/MS

spectra at a 35% normalized collision energy was repeated continuously throughout each step of the multidimensional separation. Application of mass spectrometer scan functions and HPLC solvent gradients was controlled by the Xcalibur data system. Analysis of Mass Spectra Each MudPIT analysis was analyzed separately. Both MS1 and MS2 (tandem mass spectra) were extracted from the XCalibur data system format (.RAW) into MS1 and MS2 formats using in house software (RAW_Xtractor). MS/MS spectra remaining after filtering were searched with the Prolucid Software against the UniProt_rat_03-25-2014 concatenated to a decoy database in which the sequence for each entry in the original database was reversed. All searches were parallelized and performed on a Beowulf computer cluster consisting of 100 1.2 GHz Athlon CPUs. No enzyme specificity was considered for any search. The following modifications were searched for a static modification of 57.02146 on cysteine for all analyses, a differential modification of 523.2749 on methionine for AHA using the Life Technologies biotin-alkyne, and a differential modification of 351.1774 (heavy) and 347.1702 (light) on methionine for AHA using the Seterah Biotech biotin-alkynes. Prolucid results were assembled and filtered using the DTASelect (version 2.0) program. DTASelect 2.0 uses a linear discriminant analysis to dynamically set XCorr and DeltaCN thresholds for the entire data set to achieve a user-specified false discovery rate (FDR). In addition, the modified peptides were required to be fully tryptic, <5 ppm deviation from peptide match, and an FDR at the spectra level of 0.01. The FDRs are estimated by the program from the number and quality of spectral matches to the decoy database. For all datasets, the protein FDR was <1% and the peptide FDR was <0.5%.

***In vitro* neurite assay**

Hippocampus cells were seeded at a density of 200,000 cells/well in 6 well culture dishes (Falcon) that were coated with poly-d-lysine (0.1mg/mL, Sigma-Aldrich) and were cultured in defined medium (Neurobasal; ThermoFIsher), L-glutamine (Thermofisher), Penicillin-Streptomycin (ThermoFisher), and B27 supplement (ThermoFisher). After 3 days *in vitro*, the candidate gene plasmid vectors were transfected into hippocampus neurons with Lipofectamine

LTX (Invitrogen). The amount of DNA used for each well was initially 0.5μg, and gradually increased to 2.0μg at maximum depending on transfection efficiency. After 6 days *in vitro* (on the day3 after transfection), the series of images were obtained using the 10x objectives of an inverted microscope and tiled with the integrated software in microscope (Zeiss).

Neurite Quantification

Images were converted into a .tif file and then quantified through ImageJ with the Simple Neurite Tracer plugin. For each image, the scale was set to 1.5385 micrometers per pixel. Neurons were traced from the center of the cell body to the end of the longest neurite. Neurons were not traced if they were less than 50 micrometers or were dead. Dead neurons were identified as a cluster of small bright spots. A neuron was still traced if the bright spots were in the shape of a branch and were still connected. Some neurons were too faded to trace because it was not possible to identify where the branch ended.

Chapter 3, in part, is currently being prepared for submission for publication of the material. Shah SH, Schiapparelli LM, Yakota S, Ma Y, Xia X, Saturday S, Sun C, Yates III JR, Cline HT, Goldberg JL. “Quantitative protein synthesis changes in the visual system after optic nerve injury”. The dissertation author was a primary investigator and author of this paper.

References

Alvarez-Castelao, B., Schanzenbächer, C.T., Hanus, C., Glock, C., tom Dieck, S., Dörrbaum, A.R., Bartnik, I., Nassim-Assir, B., Ciirdaeva, E., Mueller, A., Dieterich, D.C., Tirrell, D.A., Langer, J.D., and Schuman, E.M. (2017). Cell-type-specific metabolic labeling of nascent proteomes in vivo. Nat. Biotechnol. *35*, 1196–1201.

Belin, S., Nawabi, H., Wang, C., Tang, S., Latremoliere, A., Warren, P., Schorle, H., Uncu, C., Woolf, C.J., He, Z., and Steen, J.A. (2015). Injury-Induced Decline of Intrinsic Regenerative Ability Revealed by Quantitative Proteomics. Neuron *86*, 1000–1014.

Best, M.D. (2009). Click Chemistry and Bioorthogonal Reactions : Unprecedented Selectivity in the Labeling of Biological Molecules. Biochemistry *48*, 6571–6584.

Corredor, R.G., Trakhtenberg, E.F., Pita-Thomas, W., Jin, X., Hu, Y., and Goldberg, J.L. (2012). Soluble Adenylyl Cyclase Activity Is Necessary for Retinal Ganglion Cell Survival and Axon Growth. J. Neurosci. *32*, 7734–7744.

Deshaies, J.E., Shkreta, L., Moszczynski, A.J., Sidibé, H., Semmler, S., Fouillen, A., Bennett, E.R., Bekenstein, U., Destroismaisons, L., Toutant, J., Delmotte, Q., Volkening, K., Stabile, S., Aulas, A., Khalfallah, Y., Soreq, H., Nanci, A., Strong, M.J., Chabot, B., and Vande Velde, C. (2018). TDP-43 regulates the alternative splicing of hnRNP A1 to yield an aggregation-prone variant in amyotrophic lateral sclerosis. Brain *141*, 1320–1333.

Deurloo, M.H.S., Turlova, E., Chen, W.L., Lin, Y.W., Tam, E., Tassew, N.G., Wu, M., Huang, Y.C., Crawley, J.N., Monnier, P.P., Groffen, A.J.A., Sun, H.S., Osborne, L.R., and Feng, Z.P. (2018). Transcription Factor 2I Regulates Neuronal Development via TRPC3 in 7q11.23 Disorder Models. Mol. Neurobiol.

Dieterich, D.C., Lee, J.J., Link, A.J., Graumann, J., Tirrell, D.A., and Schuman, E.M. (2007). Labeling, detection and identification of newly synthesized proteomes with bioorthogonal non-canonical amino-acid tagging. Nat. Protoc. *2*, 532–540.

Dieterich, D.C., Hodas, J.J.L., Gouzer, G., Shadrin, I.Y., Ngo, J.T., Triller, A., Tirrell, D.A., and Schuman, E.M. (2010). In situ visualization and dynamics of newly synthesized proteins in rat hippocampal neurons. Nat. Neurosci. *13*, 897–905.

Estrada-Bernal, A., Sanford, S.D., Sosa, L.J., Simon, G.C., Hansen, K.C., and Pfenninger, K.H. (2012). Functional complexity of the axonal growth cone: A proteomic analysis. PLoS One *7*.

Eva, R., Dassie, E., Caswell, P.T., Dick, G., ffrench-Constant, C., Norman, J.C., and Fawcett, J.W. (2010). Rab11 and Its Effector Rab Coupling Protein Contribute to the Trafficking of 1 Integrins during Axon Growth in Adult Dorsal Root Ganglion Neurons and PC12 Cells. J. Neurosci. *30*, 11654–11669.

Goldberg, J.L., Espinosa, J.S., Xu, Y., Davidson, N., Kovacs, G.T., and Barres, B.A. (2002). Retinal Ganglion Cells Do Not Extend Axons by Default. Neuron *33*, 689–702.

Hinz, F.I., Dieterich, D.C., Tirrell, D.A., and Schuman, E.M. (2012). Noncanonical amino acid labeling in vivo to visualize and affinity purify newly synthesized proteins in larval zebrafish. ACS Chem. Neurosci. *3*, 40–49.

Hollander, A., D'Onofrio, P.M., Magharious, M.M., Lysko, M.D., and Koeberle, P.D. (2012). Quantitative retinal protein analysis after optic nerve transection reveals a neuroprotective role for hepatoma-derived growth factor on injured retinal ganglion cell.

Investig. Ophthalmol. Vis. Sci. *53*, 3973–3989.

Howes, M.T., Kirkham, M., Riches, J., Cortese, K., Walser, P.J., Simpson, F., Hill, M.M., Jones, A., Lundmark, R., Lindsay, M.R., Hernandez-Deviez, D.J., Hadzic, G., McCluskey, A., Bashir, R., Liu, L., Pilch, P., McMahon, H., Robinson, P.J., Hancock, J.F., Mayor, S., and Parton, R.G. (2010). Clathrin-independent carriers form a high capacity endocytic sorting system at the leading edge of migrating cells. J. Cell Biol. *190*, 675–691.

Kanai, Y., Dohmae, N., and Hirokawa, N. (2004). Kinesin transports RNA: Isolation and characterization of an RNA-transporting granule. Neuron *43*, 513–525.

Kim, H.J., Kim, N.C., Wang, Y.-D., Scarborough, E. a, Moore, J., Diaz, Z., MacLea, K.S., Freibaum, B., Li, S., Molliex, A., Kanagaraj, A.P., Carter, R., Boylan, K.B., Wojtas, A.M., Rademakers, R., Pinkus, J.L., Greenberg, S. a, Trojanowski, J.Q., Traynor, B.J., Smith, B.N., Topp, S., Gkazi, A.-S., Miller, J., Shaw, C.E., Kottlors, M., Kirschner, J., Pestronk, A., Li, Y.R., Ford, A.F., Gitler, A.D., Benatar, M., King, O.D., Kimonis, V.E., Ross, E.D., Weihl, C.C., Shorter, J., and Taylor, J.P. (2013). Mutations in prion-like domains in hnRNPA2B1 and hnRNPA1 cause multisystem proteinopathy and ALS. Nature *495*, 467–473.

Koseki, H., Donegá, M., Lam, B.Y.H., Petrova, V., van Erp, S., Yeo, G.S.H., Kwok, J.C.F., Ffrench-Constant, C., Eva, R., and Fawcett, J.W. (2017). Selective rab11 transport and the intrinsic regenerative ability of CNS axons. Elife *6*, 1–25.

Magharious, M., D'Onofrio, P.M., Hollander, A., Zhu, P., Chen, J., and Koeberle, P.D. (2011). Quantitative iTRAQ analysis of retinal ganglion cell degeneration after optic nerve crush. J. Proteome Res. *10*, 3344–3362.

McClatchy, D.B., Ma, Y., Liu, C., Stein, B.D., Martínez-Bartolomé, S., Vasquez, D., Hellberg, K., Shaw, R.J., and Yates, J.R. (2015). Pulsed azidohomoalanine labeling in mammals (PALM) detects changes in liver-specific LKB1 knockout mice. J. Proteome Res. *14*, 4815–4822.

Molliex, A., Temirov, J., Lee, J., Coughlin, M., Kanagaraj, A.P., Kim, H.J., Mittag, T., and Taylor, J.P. (2015). Phase Separation by Low Complexity Domains Promotes Stress Granule Assembly and Drives Pathological Fibrillization. Cell *163*, 123–133.

Moore, D.L., Blackmore, M.G., Hu, Y., Kaestner, K.H., Bixby, J.L., Lemmon, V.P., and Goldberg, J.L. (2009). KLF Family Members Regulate Intrinsic Axon Regeneration Ability. Science (80-.). *326*, 298–301.

Park, B.S., Jo, H.W., and Jung, J. (2015). Expression profile of aminoacyl-tRNA synthetases in dorsal root ganglion neurons after peripheral nerve injury. J. Mol. Histol. *46*, 115–122.

Park, S.G., Ewalt, K.L., and Kim, S. (2005). Functional expansion of aminoacyl-tRNA synthetases and their interacting factors: New perspectives on housekeepers. Trends Biochem. Sci. *30*, 569–574.

Sánchez-Migallón, M.C., Valiente-Soriano, F.J., Nadal-Nicolás, F.M., Vidal-Sanz, M., and Agudo-Barriuso, M. (2016). Apoptotic retinal ganglion cell death after optic nerve transection or crush in mice: Delayed RGC loss with BDNF or a caspase 3 inhibitor. Investig. Ophthalmol. Vis. Sci. *57*, 81–93.

Savitski, M.M., Zinn, N., Faelth-savitski, M., Grandi, P., Bergamini, G., Bantscheff, M., Savitski, M.M., Zinn, N., Faelth-savitski, M., Poeckel, D., Gade, S., and Becher, I. (2018).

Multiplexed Proteome Dynamics Profiling Reveals Mechanisms Controlling Protein Homeostasis Resource Multiplexed Proteome Dynamics Profiling Reveals Mechanisms Controlling Protein Homeostasis. Cell *173*, 260–274.e25.

Schiapparelli, L.M., Mcclatchy, D.B., Liu, H., Sharma, P., Yates, J.R., and Cline, H.T. (2014). Direct Detection of Biotinylated Proteins by Mass Spectrometry. J. Proteome Res. *13*, 3966–3978.

Sellés-Navarro, I., Ellezam, B., Fajardo, R., Latour, M., and McKerracher, L. (2001). Retinal ganglion cell and nonneuronal cell responses to a microcrush lesion of adult rat optic nerve. Exp. Neurol. *167*, 282–289.

Shen, W., Liu, H.H., Schiapparelli, L., McClatchy, D., He, H. yan, Yates, J.R., and Cline, H.T. (2014). Acute Synthesis of CPEB Is Required for Plasticity of Visual Avoidance Behavior in Xenopus. Cell Rep. *6*, 737–747.

Speers, A.E., and Cravatt, B.F. (2009). Activity-Based Protein Profiling (ABPP) and Click Chemistry (CC)-ABPP by MudPIT Mass Spectrometry. Curr. Protoc. Chem. Biol. *1*, 29–41.

Wang, Y., Cameron, E.G., Li, J., Stiles, T.L., Kritzer, M.D., Lodhavia, R., Hertz, J., Nguyen, T., Kapiloff, M.S., and Goldberg, J.L. (2015). Muscle A-Kinase Anchoring Protein-α is an Injury-Specific Signaling Scaffold Required for Neurotrophic- and Cyclic Adenosine Monophosphate-Mediated Survival. EBioMedicine *2*, 1880–1887.

Yasuda, M., Tanaka, Y., Ryu, M., Tsuda, S., and Nakazawa, T. (2014). RNA sequence reveals mouse retinal transcriptome changes early after axonal injury. PLoS One *9*, 1–11.

Yuet, K.P., and Tirrell, D.A. (2014). Chemical tools for temporally and spatially resolved mass spectrometry-based proteomics. Ann. Biomed. Eng. *42*, 299–311.

CONCLUSION

In diseases like glaucoma, vision loss results from the death of retinal ganglion cells (RGCs). Current therapeutic strategies do not adequately prevent or restore visual function for patients afflicted with these neurodegenerative diseases, partially due to the complexity of the neural circuits involved. Previous studies of the degenerative process and regenerative therapies have used genetic or transcriptomic approaches as a proxy for proteins, the effectors of cellular dynamics. While some recent studies have investigated the proteomic component of RGCs and the whole retina, tools have been lacking to capture all dimensions of protein dynamics *in vivo*, especially after injury. Over the course of this thesis work, I sought to improve our understanding of two aspects of the cellular response in projection neurons like RGCs; changes in protein synthesis and protein transport within intracellular compartments acutely after injury in the central nervous system.

As discussed in chapter 1 our understanding of protein transport in the brain was incomplete and limited to protein-by-protein biochemical and radioactive tagging approaches. We developed a mass spectrometry compatible technique and proceeded with NHS-biotin for unbiased proteomic surveys of the optic nerve (ON), and presynaptic compartments of the superior colliculus (SC) and lateral geniculate nucleus of the thalamus (LGN). Beyond establishment of a novel platform for analysis of protein transport in all projection neurons in the central and peripheral nervous systems, we created the first database of the transportome in RGCs.

We adapted this methodology in Chapter 2 to quantitatively measure how the transportome is changed after injury, uncovering protein transport deficits of a specific kinesin isoform, Kif5a, at a timepoint where measurements of protein accumulation could not detect a significant difference. In fact, the early detection of transport deficits for several proteins known to be affected in optic nerve injury should change our understanding of the time-course in neurodegeneration.

We next focused on dissecting the homeostatic protein response in the retina after injury across two time points in Chapter 3. We developed a quantitative mass spectrometry reagent to isolate the synthesis of new proteins from the protein maintenance and degradation, which accurately reflected the early and intermediate phenotypes of the retina after optic nerve crush. We used *in vitro* and *in vivo* assays of axon growth and neuron survival to confirm that changes in protein translation reflect probable regulators of the degenerative and regenerative response.

While these strategies have led to important biological conclusions and tools for further research in many areas of neuroscience, there are still limitations to overcome. The visual system is ideal for both methodologies as the cell bodies of RGCs, the projection neurons of the retina, are spatially separated from their axons in the optic nerve and their presynaptic regions in the brain. To isolate newly synthesized proteins in the RGC cell bodies, and even in specific subtypes of RGCs, we need to leverage genetic approaches to target cells. One such method is the use of non-canonical amino acids (ncAAs) that are only charged by mutant tRNA synthetases, such as the azidonorleucine (ANL) incorporated by pMARS (Mahdavi et al., 2016). As only cells that express this mutant enzyme will replace methionine with ANL, we can either use conditional transgenic mouse line (Alvarez-Castelao et al., 2017) or viral delivery specific to RGCs as used throughout this thesis, followed by temporally-restricted ANL injection. While the data are still preliminary, early results indicate genetically-defined protein tagging as a viable approach for cell-type specific proteomic studies.

Insights gained from such proteomic analysis must still be put into context based on molecular interaction. For example, many cellular events are regulated by post-translation modifications (PTMs) like phosphorylation. In glaucoma both c-jun (Levkovitch-Verbin et al., 2005) and 14-3-3 proteins (Yang et al., 2008) are phosphorylated in RGCs, which would require unbiased phosphoproteomic methods to detect accurately. Similarly, negative regulation from microRNAs cannot be directly detected by proteomic methods, although their effects may be inferred based on bioinformatic predictions. Finally, dissecting the role of transcription factors in

injury response requires accurate ChIP-sequencing and RNA-sequencing to uncover regulatory events at the genomic level. It is the successful integration of these various techniques that will lead to a full understanding of *in vivo* neurodegeneration and subsequent identification of regenerative candidates.

References

Alvarez-Castelao, B., Schanzenbächer, C.T., Hanus, C., Glock, C., tom Dieck, S., Dörrbaum, A.R., Bartnik, I., Nassim-Assir, B., Ciirdaeva, E., Mueller, A., Dieterich, D.C., Tirrell, D.A., Langer, J.D., and Schuman, E.M. (2017). Cell-type-specific metabolic labeling of nascent proteomes in vivo. Nat. Biotechnol. *35*, 1196–1201.

Levkovitch-Verbin, H., Quigley, H.A., Martin, K.R.G., Harizman, N., Valenta, D.F., Pease, M.E., and Melamed, S. (2005). The transcription factor c-jun is activated in retinal ganglion cells in experimental rat glaucoma. Exp. Eye Res. *80*, 663–670.

Mahdavi, A., Hamblin, G.D., Jindal, G.A., Bagert, J.D., Dong, C., Sweredoski, M.J., Hess, S., Schuman, E.M., and Tirrell, D.A. (2016). Engineered Aminoacyl-tRNA Synthetase for Cell-Selective Analysis of Mammalian Protein Synthesis. J. Am. Chem. Soc. *138*, 4278–4281.

Yang, X., Luo, C., Cai, J., Pierce, W.M., and Tezel, G. (2008). Phosphorylation-dependent interaction with 14-3-3 in the regulation of bad trafficking in retinal ganglion cells. Investig. Ophthalmol. Vis. Sci. *49*, 2483–2494.